

THE UNIVERSITY OF CALGARY

AQUEOUS CORROSION OF SELECT MATERIALS IN  
SIMULATED COAL GASIFICATION ENVIRONMENTS

BY

DEMUNI MUDITHA JAYASINGHE

A THESIS

SUBMITTED TO THE FACULTY OF GRADUATE STUDIES  
IN PARTIAL FULFILLMENT OF THE REQUIREMENTS FOR THE  
DEGREE OF MASTER OF SCIENCE

DEPARTMENT OF MECHANICAL ENGINEERING

CALGARY, ALBERTA

AUGUST, 1988



DEMUNI MUDITHA JAYASINGHE 1988

Permission has been granted to the National Library of Canada to microfilm this thesis and to lend or sell copies of the film.

The author (copyright owner) has reserved other publication rights, and neither the thesis nor extensive extracts from it may be printed or otherwise reproduced without his/her written permission.

L'autorisation a été accordée à la Bibliothèque nationale du Canada de microfilmer cette thèse et de prêter ou de vendre des exemplaires du film.


L'auteur (titulaire du droit d'auteur) se réserve les autres droits de publication; ni la thèse ni de longs extraits de celle-ci ne doivent être imprimés ou autrement reproduits sans son autorisation écrite.

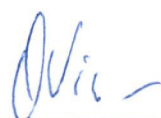
ISBN 0-315-46614-6


THE UNIVERSITY OF CALGARY


FACULTY OF GRADUATE STUDIES

The undersigned certify that they have read, and recommend to the Faculty of Graduate Studies for acceptance, a thesis entitled "Aqueous Corrosion of Select Materials in a Simulated Coal Gasification Environment," submitted by Demuni Muditha Jayasinghe in partial fulfillment of the requirements for the degree of Master of Science in Mechanical Engineering.

  
Chairman, Dr. W.J.D. Shaw  
Department of Mechanical  
Engineering

  
Dr. O.G. Vinogradov  
Department of Mechanical  
Engineering

  
Dr. E.C. Mikulcik  
Department of Mechanical  
Engineering

  
Dr. V.I. Birss  
Department of Chemistry

Date August 29, 1988.

## ABSTRACT

The objective of this work was to investigate the aqueous corrosion behaviour of 11 selected alloys and to identify the best corrosion resistant material among them for use in a coal gasification environment. Previous studies have concentrated on high temperature corrosion. However, this work is concerned with the aqueous corrosion that occurs during start up and shut down procedures.

The aqueous corrosion behaviour was studied under a simulated condition that is similar to the actual coal gasification environment. The behaviour of the materials in various gas concentrations were explored using electrochemical corrosion techniques. Corrosion was correlated to the alloy composition of the material.

The data was analyzed using the Tafel extrapolation method. This method was used to analyze all the results of this thesis and a computer program was developed to aid in this analysis.

A rating of materials tested shows the Fe-Mn-Al stainless steel to be the best in terms of corrosion

resistance and that it was also found to exhibit the least amount of sensitivity to variations in changes of gaseous component mixtures. Other materials that closely follow Fe-Mn-Al material are duplex alloy F255 and AISI 316 stainless steel. None of these materials showed any possible pitting corrosion in the environment in which they were tested.

The theoretical analysis of the mild steel under deaerated condition showed that, corrosion was due to the simultaneous occurrence of several partial anodic and cathodic reactions. These reactions are identified and examined in this work.

The effect of the alloy content shows that a high nickel content is not a desirable condition. Both cobalt and molybdenum are detrimental to aqueous corrosion of the high nickel alloys. The chromium content should be maintained around 20% to 25%, which is in keeping with that found for high temperature gaseous corrosion. These results suggest directions in which specific alloy development could be made.

## ACKNOWLEDGMENTS

The author wishes to express sincere gratitude to his supervisor, Dr. William J.D. Shaw, for his guidance, support and encouragement throughout this program.

Special thanks are due to the Mr. Larry Jensen for his excellent support for designing a computer program "CORRLOT" and Mr. R. Rowell for the laboratory assistance. Sincere thanks are also owed to the technical staff of the Department of Mechanical Engineering for their invaluable help, especially Mr. R. Bechold.

Finally, the author gratefully acknowledges the financial support provided by the Department of Mechanical Engineering and the Alberta Energy and Natural Resources office of Coal Research & Technology, grant # 2835-RG-85/19.

This work is dedicated to my wife Shamani, without whose patience and support and encouragement this work would not have been completed; and to my mother as a testimony of gratitude.

## TABLE OF CONTENTS

	PAGE
ABSTRACT .....	iii
ACKNOWLEDGMENTS .....	v
DEDICATION .....	vi
TABLE OF CONTENTS .....	vii
LIST OF TABLES .....	xi
LIST OF FIGURES .....	xiii
 CHAPTER 1 INTRODUCTION .....	 1
1.1 Objective of this Investigation.....	3
 CHAPTER 2 AQUEOUS CORROSION OF MATERIALS IN COAL	
GASIFICATION: A LITERATURE SURVEY.....	5
 CHAPTER 3 RELEVANT THEORY IN ELECTROCHEMISTRY.....	 13
3.1 Introduction.....	13
3.2 Thermodynamics of Aqueous Corrosion..	14
3.2.1 Electrode Processes.....	14
3.2.2 Electrode Potentials.....	17
3.2.3 Potentials vs. pH (Pourbaix)	
Diagrams.....	22
3.3 Kinetics of the Aqueous Corrosion....	24
3.3.1 Activation Polarization ( $\eta_A$ )..	26
3.3.2 Concentration Polarization ( $\eta_T$ )	27
3.3.3 Combined Polarization.....	31
3.3.4 Resistance Polarization.....	31



	PAGE
3.3.5 Kinetic Properties of the Single and Dual Exchange Reactions.....	33
3.4 Passivity of Corrosion Resistant Alloys.....	36
CHAPTER 4 EXPERIMENTAL STUDY.....	47
4.1 Introduction.....	47
4.2 Description of Test Materials.....	47
4.3 Description of Experimental Set-Up...	56
4.3.1 EG & G Potentiostat.....	56
4.3.2 The Old Potentiostat.....	59
4.3.3 The Standard Polarization Cell	59
4.3.4 The Salt Bridge.....	59
4.3.5 The Reference Electrode.....	60
4.3.6 The Auxiliary Electrodes.....	60
4.4 General Experimental Techniques.....	60
4.4.1 Preparation of the Working Electrode.....	60
4.4.2 Solution Preparation.....	61
4.4.3 Experimental Procedure.....	61
CHAPTER 5 TEST RESULTS AND DISCUSSION.....	65
5.1 Introduction.....	65
5.2 Techniques Used to Determine Tafel Slopes and Corrosion Current Density.	65

	PAGE
5.2.1 Linear Polarization Method....	65
5.2.2 Tafel Extrapolation Method....	66
5.3 Comparison of Linear Polarization Method with Tafel Extrapolation.....	71
5.4 Comparison of Material Corrosiveness under Different Gaseous Environments.	72
CHAPTER 6 GENERAL DISCUSSION AND ANALYSIS.....	90
6.1 Introduction.....	90
6.2 Kinetics of the Corrosion Process....	90
6.2.1 Corrosion Kinetics in the Nitrogen Environment.....	90
6.2.2 Total Cathodic and Anodic Polarization Curves.....	94
6.3 Corrosion Resistance of Materials under Variable Concentration of Gas Composition in Coal Gasification Environment.....	94
6.4 Effect of Anion Concentration on the Corrosion Rate in Coal Gasification Environment.....	99
6.5 Pitting Tendency of the Materials....	101
CHAPTER 7 EFFECT OF ALLOY COMPOSITION ON CORROSION..	102
7.1 Introduction.....	102

	PAGE
7.2 Methods for Developing Corrosion	
Resistant Alloys.....	102
7.3 Effect of Alloying on the Corrosion	
Resistance of Materials.....	103
CHAPTER 8 CONCLUSIONS.....	118
CHAPTER 9 RECOMMENDATIONS FOR FUTURE WORK.....	121
REFERENCES.....	123

## LIST OF TABLES

<u>TABLE</u>	<u>TITLE</u>	<u>PAGE</u>
4.1	CHEMICAL COMPOSITION OF MILD STEEL.....	48
4.2	CHEMICAL COMPOSITION OF Fe-Mn-Al STAINLESS STEEL	48
4.3	CHEMICAL COMPOSITION OF 316 STAINLESS STEEL....	49
4.4	CHEMICAL COMPOSITION OF PYROMET 31.....	49
4.5	CHEMICAL COMPOSITION OF PYROMET 751.....	50
4.6	CHEMICAL COMPOSITION OF HASTALLOY C22.....	50
4.7	CHEMICAL COMPOSITION OF HASTALLOY C276.....	51
4.8	CHEMICAL COMPOSITION OF CUSTOM 450.....	51
4.9	CHEMICAL COMPOSITION OF FERRALIUM 255.....	52
4.10	CHEMICAL COMPOSITION OF UDIMET 700.....	52
4.11	CHEMICAL COMPOSITION OF 446 STAINLESS STEEL....	53
4.12	CHEMICAL COMPOSITION OF THE TEST SOLUTION	54
4.13	SIMULATED GAS MIXTURE TEST CONDITIONS.....	55
4.14	TOTAL GAS MIXTURE.....	55
4.15	CONCENTRATION OF THE TEST SOLUTION.....	61
4.16	pH VALUES OF THE SOLUTION WITH DIFFERENT GAS MIXTURES.....	63
4.17	ABBREVIATIONS FOR THE TEST MATERIALS.....	64
5.1	LINEAR POLARIZATION VERSUS TAFEL EXTRAPOLATION.	71
5.2	CORROSION BEHAVIOUR OF MATERIALS IN DIFFERENT GASEOUS ENVIRONMENTS.....	77

<u>TABLE</u>	<u>TITLE</u>	<u>PAGE</u>
5.3	CORROSION BEHAVIOUR OF MATERIALS IN AERATED, DEAERATED AND HYDROGEN ENVIRONMENTS.....	78
5.4	ELECTROCHEMICAL CORROSION DATA FOR PMS MATERIAL IN DIFFERENT GASEOUS ENVIRONMENTS.....	79
7.1	CHARACTERISTIC PASSIVATION VALUES OF MATERIALS TESTED IN THE TOTAL GAS MIXTURE.....	106

## LIST OF FIGURES

<u>FIGURE</u>	<u>TITLE</u>	<u>PAGE</u>
3.1	THE STRUCTURE OF THE ELECTRICAL DOUBLE LAYER...	16
3.2	SCHEMATIC OF THE PRIMARY AND SECONDARY SOLVENT MOLECULES FOR CATIONS IN WATER.....	18
3.3	CONCENTRATION POLARIZATION FOR CATHODIC REACTION .....	30
3.4	COMBINED POLARIZATION FOR CATHODIC REACTION...	32
3.5	TAFEL SLOPES AND OVERPOTENTIALS FOR A SINGLE EXCHANGE PROCESS.....	34
3.6	EVANS DIAGRAM FOR DUAL EXCHANGE PROCESS.....	37
3.7	HYPOTHETICAL ANODIC AND CATHODIC POLARIZATION BEHAVIOUR FOR MATERIAL EXHIBITING PASSIVE ANODIC BEHAVIOUR.....	38
3.8	EFFECT OF CATHODIC EXCHANGE CURRENT DENSITY ON THE STABILITY OF THE PASSIVE STATE.....	40
3.9	BEHAVIOUR OF ACTIVE-PASSIVE ALLOYS IN A SYSTEM CONTAINING ACTIVATION CONTROLLED CATHODIC REDUCTION PROCESS.....	44
3.10	BEHAVIOUR OF ACTIVE-PASSIVE ALLOYS IN A SYSTEM CONTAINING A DIFFUSION-CONTROLLED CATHODIC REDUCTION PROCESS.....	45
4.1	EXPERIMENTAL SET UP.....	57

<u>FIGURE</u>	<u>TITLE</u>	<u>PAGE</u>
4.2	EG & G POTENTIOSTAT.....	58
5.1	POTENTIODYNAMIC SCAN OF 316 STAINLESS STEEL IN TOTAL GAS MIXTURE.....	68
5.2	POTENTIODYNAMIC SCAN OF PYROMET 751 IN AMMONIA ENVIRONMENT.....	69
5.3	DETERMINATION OF CORROSION CURRENT DENSITY OF MILD STEEL IN TOTAL GAS MIXTURE.....	73
5.4	DETERMINATION OF CORROSION CURRENT DENSITY OF 316 STAINLESS STEEL IN CARBON MONOXIDE ENVIRONMENT.....	74
5.5	DETERMINATION OF CORROSION CURRENT DENSITY OF FERRALIUM 255 IN CARBON DIOXIDE/CARBON MONOXIDE ENVIRONMENT.....	75
5.6	POTENTIODYNAMIC SCAN OF Fe-Mn-Al STAINLESS STEEL IN AMMONIA ENVIRONMENT.....	87
5.7	POTENTIODYNAMIC SCAN OF FERRALIUM 255 IN HYDROGEN SULFIDE ENVIRONMENT.....	88
5.8	POTENTIODYNAMIC SCAN OF PYROMET 751 IN HYDROGEN GAS COMBINATION ENVIRONMENT.....	89
6.1	THEORETICAL ANODIC AND CATHODIC POLARIZATION CHARACTERISTICS FOR MILD STEEL IN NITROGEN SATURATED SOLUTION.....	95
6.2	THEORETICAL AND EXPERIMENTAL POLARIZATION CURVES FOR MILD STEEL IN NITROGEN SATURATED SOLUTION.....	96

<u>FIGURE</u>	<u>TITLE</u>	<u>PAGE</u>
7.1	PASSIVATION CHARACTERISTICS OF 446 STAINLESS STEEL IN TOTAL GAS MIXTURE.....	105
7.2	PASSIVATION CHARACTERISTICS OF FERRALIUM 255 IN TOTAL GAS MIXTURE.....	106
7.3	PASSIVATION CHARACTERISTICS OF CUSTOM 450 IN TOTAL GAS MIXTURE.....	108
7.4	PASSIVATION CHARACTERISTICS OF 316 STAINLESS STEEL IN TOTAL GAS MIXTURE.....	109
7.5	PASSIVATION CHARACTERISTICS OF PYROMET 31 IN TOTAL GAS MIXTURE.....	110
7.6	PASSIVATION CHARACTERISTICS OF PYROMET 751 IN TOTAL GAS MIXTURE.....	112
7.7	PASSIVATION CHARACTERISTICS OF UDIMET 700 IN TOTAL GAS MIXTURE.....	113
7.8	PASSIVATION CHARACTERISTICS OF HASTALLOY C22 IN TOTAL GAS MIXTURE.....	114
7.9	PASSIVATION CHARACTERISTICS OF HASTALLOY C276 IN TOTAL GAS MIXTURE.....	115
7.10	PASSIVATION CHARACTERISTICS OF Fe-Mn-Al STAINLESS STEEL IN TOTAL GAS MIXTURE.....	116



## CHAPTER 1

### 1 INTRODUCTION

At present a major limitation in building and operating coal gasification plants is being able to find an economical material selection that performs satisfactorily. Coal gasification environments are normally much more severe than the corrosive environments experienced in the oil and gas industries. The material must perform under high temperature in corrosive environments as well as at low temperature under aqueous conditions. Therefore normally expensive, alloy materials are required in the construction of coal gasification plants. The use of highly exotic superalloys does not always guarantee long component life. Thus the major problem, that must be overcome in order for these plants to become economical is that of identifying the best types of alloy materials that will give adequate service lives at reasonable cost.

Prior to this research work very little, information has been generated regarding the aqueous corrosion problem. Back in the early 1970's a task force was set up for evaluation of materials exposed to coal gasification processes. The evaluation was directed at corrosion/erosion/creep and stress corrosion behaviour.

This task force evolved into the Metal Properties Council (MPC) and has been active in pursuing and screening various materials for gasification plants [1,2]. Initially it was thought that only high temperature corrosion was important. Aqueous corrosion only occurred upon start up and shut down and because of the short time period was deemed unimportant. However experience, in pilot plants soon indicated that aqueous corrosion was a major problem. These studies have identified that the most common types of failures in gasification plants are either corrosion or stress corrosion cracking [3,4]. Many material screening tests have been conducted during actual pilot plant operation by utilizing coupons or fabrication of components out of various types of materials [5,6]. However all of the work, to date has been limited to determining the corrosion rate of coupons based either on a weight loss or a weight gain. There has not been any work directed towards the investigation of fundamental mechanisms that are occurring. Electrochemical corrosion investigations are required in order to obtain this fundamental information.

The information obtained from an electrochemical corrosion study of the material interaction in an aqueous environment will help to identify directions of material

development. This in turn will lead to the production of economical materials that give adequate service lives.

The information needed for material selection in coal gasification plants is only now becoming available. Extrapolation using other types of plant designs cannot be made since these are normally based on high oxygen atmospheres and more simple and less severe corrosion conditions. Coal gasification conditions have low oxygen atmospheres and quite complex gas mixtures often containing  $\text{H}_2\text{S}$ ,  $\text{NH}_3$ ,  $\text{CO}_2$ ,  $\text{CO}$  and ionic salts with high anion contents such as  $\text{SO}_4^{-2}$ ,  $\text{Cl}^-$ , and  $\text{HCO}_3^-$ .

#### 1.1 Objectives of this Investigation

The main objective of this investigation was to identify the best corrosion resistant material from a selected group for use in a coal gasification environment. In the process of identifying the best material an evaluation, of the corrosion behaviour of all the materials was undertaken. An analysis of the electrochemical corrosion behaviour should lead to an understanding of the reactions that govern the corrosion processes. By selecting a wide range of alloys with varying chemical compositions it was thought that the analysis may indicate how alloy composition may affect the corrosion process.

The general corrosion behaviour of eleven materials ranging from a common material such as mild steel to an expensive material like udimet-700 (high nickel content) were explored under complex gas mixture and high ionic strength produced water conditions using electrochemical techniques.

Since cost is the major factor in selecting materials for a coal gasification environment, testing materials for this investigation included one very economical material, Fe-Mn-Al stainless steel. Fe-Mn-Al is an austenitic steel and is often referred to as poorman's stainless steel due to the absence of high cost refractory elements. The composition of the gas mixture and ionic concentration of the test solution were duplicated as close as possible to actual field condition. This should result in close simulation (laboratory tests) to field conditions and should result in accurate corrosion behaviour.

## CHAPTER 2

### AQUEOUS CORROSION OF MATERIALS IN COAL GASIFICATION

#### ENVIRONMENT:

#### A LITERATURE REVIEW

Material degradation in coal gasification environments can occur by two different corrosion processes. These are high temperature gaseous corrosion (sometimes referred to as oxidation) and aqueous corrosion. Since 1971 the research emphasis for coal gasification systems has been on high temperature corrosion. Presently very little, information exists regarding aqueous corrosion in these environments.

Hebsur [3] investigated the gaseous corrosion testing of a few selected alloys in an environment with  $H_2S$  contents up to 1.5 v/o (volume %) and at temperatures as high as  $982^{\circ}C$  for 1000 hours. The results showed that the most severe sulfidation attack occurred in alloys that experienced the high  $H_2S$  concentrations or high temperature. Recent studies on long term tests by the same researchers revealed that scale breakaway attack can be obtained in the temperature range of  $870 - 982^{\circ}C$  with  $H_2S$  levels of 1.0 and 0.5 v/o, respectively. Also data obtained, from short term tests showed unrealistically low

values of corrosive attack. From these tests it was concluded that,

1. Chromium concentrations of at least 20% and preferably 25% are required for long term corrosion resistance under the test conditions.
2. Limited corrosion at 900<sup>o</sup> C was shown by alloys Incolloy 671 and Strellite 6B after 10,000 hours.

It appears that commercially available alloys have the potential to provide corrosion rates of less than 20 mil/year based on 100,000 hour tests.

Further extensive work on high temperature corrosion/erosion in coal gasification by Bhattacharyya et al. [7] revealed that aluminized 310 stainless steel and Incoloy 800 samples were the least affected under both atmospheric and high pressure operations whereas Inconel 601 and unprotected Incoloy 800 suffered the greatest damage. Significantly greater damage resulted from an increase in temperature, pressure, H<sub>2</sub>S content and velocity of gases.

Baxter et al. [8], in their investigation of the corrosion behaviour of model alloys based on Fe-25 w/o (weight %) Cr-20 w/o Ni, and Fe-12 w/o Cr-12 w/o Ni in an

environment containing oxygen and sulfur at 650°C and 875°C showed that alloy composition plays an important role in preventing rapid degradation. A minimum Cr content of 14 w/o should allow a protective scale to be formed on austenitic Fe-base alloys in a CO<sub>2</sub>/CO environment at 850° C. Significantly higher levels are usually considered necessary for long term scale stability and for protection at higher temperatures. Also it was found that small additions of Zr (1-6% by weight) promote protective oxide scale formation and enhance scale stability.

The work of Natesan [9] showed that alloys with Fe:Cr ~ 1.6 to 2.0 and Ni:Cr ~ 1.0 will exhibit acceptable corrosion behaviour in high temperature mixed gas atmospheres in coal gasification systems and could be used as a base alloy for development/modification to improve the sulfidation resistance of materials. The mixed-gas environments of various coal gasification system have, in general, low oxygen partial pressures and moderate-to-high sulfur partial pressures, a combination that leads to severe materials degradation via corrosion. The available information on the behaviour of commercial engineering alloys and advanced materials exposed to these environments showed a viable alloy should develop protective oxide scale upon exposure to mixed gas atmospheres. Further extensive

work related to materials selection in high temperature coal gasification can be found in the literature [5,10-16].

In the early 1970's MacNab et al. [2] carried out an experimental program to identify the principal corrodents in aqueous coal gasification environments and to determine the effects of concentration of each species. The test solution (recirculating quench water) was saturated with gas of a composition corresponding to a gas analysis used in a pilot plant. This represented conditions in the bottom of a quench tower. The gas composition consisted of gases such as  $\text{CO}_2$ ,  $\text{H}_2\text{S}$ ,  $\text{NH}_3$ ,  $\text{H}_2$ ,  $\text{CO}$ ,  $\text{CH}_4$ ,  $\text{N}_2$  and  $\text{HCN}$ . The corrosiveness depended on the relative concentration of the various components and the temperature. This program was not successful because it did not take into account the complexity of the problem. Overlooked were such things as accumulated corrosion product, blow down, particulate matter entrained in the gas, and components introduced by the water itself.

Even with the above simplifications a large number of tests were necessary to evaluate each environment. At this point the Energy and the Gas Research Institute of the Technology Research Institute ,EGRIT, introduced a



satisfactory planned experimental program that offered the following:

1. A reduced number of tests without sacrificing information.
2. An increase in the quantity of data obtained.
3. A means of analyzing and interpreting the large number of results.

At the conclusion of this program it was established that austenitic stainless steels were satisfactory for all quench tower operating conditions that were examined. Carbon steel showed variable behaviour depending on the particular environment. It was known that factors which accelerated corrosion were cyanide, phenol and chlorides. The data obtained in this program was intended to provide guidance for building pilot plants until actual operating experience was available. Prior to this program, MacNab [2] mentioned that corrosivity may be accelerated by the formation of formic acid from reaction of carbon monoxide and steam at high pressure.

The work of Bakker et al. [5] indicated that the laboratory corrosion rates were considerably lower than those found in pilot plants. Therefore, a project was implemented to determine how variables were affecting the

corrosion rate of the materials in a Syngas Cooler environment. These variables were identified as follows;

1. Cyclic operation in product formation.
2. System pressure and  $H_2S$  partial pressure.
3.  $HCl$  in raw Syngas.
4. Corrosion during shutdowns and startups.
5. Temperature differential between heat exchanger tubes and Syngas.
6. Stress.

The corrosion associated with shut down and start up was found to be a major problem and critical in terms of corrosion rates.

Bakker et al. [5] revealed that this corrosion occurred mainly because of the formation of scale during exposure to a gaseous high temperature  $H_2S$  environment. The hypothesis that was the scale formation attracted and trapped moisture and also promoted the formation of Polythionic and Sulfuric acid. This formation may result in general acidic corrosion of low alloy steels and pitting or stress corrosion of stainless steels. All these corrosion processes can be enhanced by the presence of chloride.

According to Bakker et al. [5], there was a noticeable increase in the corrosion of low alloy steel when it was exposed to moist air. Exposure to dry air did not result in any measurable corrosion. In addition, alloy samples exposed to an HCl environment showed consistent weight loss. While in an HCl-free environment they experienced a weight gain. The  $\text{FeCl}_2$  corrosion product formed during exposure to a Syngas environment causes breakaway of the scale when moist air and chloride are present. Moreover it was, determined that acidic conditions during shut down cause pitting of austenitic stainless steels. High pressure appears to accelerate intergranular corrosion after acidic conditions have initiated attack. In order to design against corrosion during shut down further work, needs to be conducted.

Keiser et al. [4] found that AISI 304 stainless steel cracked intergranularly. This occurred when polythionic acid contacted a sensitized stressed component in a pilot plant. Later it was found that pitting corrosion occurred in mild steels when exposed to sour aqueous environments.

Only by conducting electrochemical corrosion investigations can the mechanisms of the corrosion behaviour be obtained. This in turn leads to an

understanding of the type of corrosion control, such as cathodic control, anodic control etc. Once the controlling corrosion reactions and control mechanism have been identified then suggestions, for improvement can be made. Unfortunately none of this information has been obtained to date.

CHAPTER 3  
RELEVANT THEORY IN ELECTROCHEMISTRY

3.1 Introduction

Corrosion is the destructive attack of a metal by chemical or electrochemical reaction with its environment. The product of this reaction may be solid, liquid or gaseous. The phenomena of this corrosion mechanism is extensively explained in the literature [17-23]. Therefore in this, section only theory relevant to aqueous corrosion will be covered.

A metal surface can be attacked by aqueous corrosion either generally or selectively. Such features of selective attack include grain boundaries, precipitates and metal/inclusion interfaces. In order for aqueous corrosion to occur, four conditions needed to be met. These are as follows;

1. A conducting environment.
2. An anode.
3. A cathode.
4. Return conducting path from anode to cathode.

Additionally, the aqueous corrosion is strongly affected by such factors as the electrode potential and acidity of the solution.

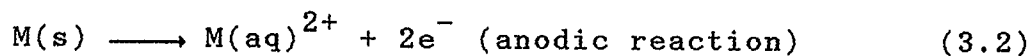
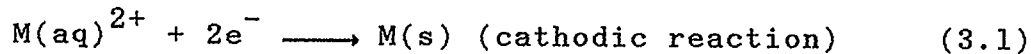
Thermodynamics provides a means of predicting the equilibrium state of a system of specified components, but provides no information on the detailed course of the reaction nor of the rate at which the system proceeds to equilibrium. Reactions can be predicted and an idea obtained with regard to the strength of the driving force. The kinetic laws of the reactions are fundamentally related to the activation energies of the electrode process, mass transport and basic properties of the metal/environment interface.

The kinetics of the corrosion process are directly related to the electrochemical reactions that are occurring simultaneously in the system. The corrosion potential, reaction rates and other kinetic data can be predicted from the basis of mixed potential theory. The actual corrosion rates are strongly affected by environmental factors and metallurgical variables.

### 3.2 Thermodynamics of Aqueous Corrosion

#### 3.2.1 Electrode Processes

In many aqueous corrosion situations oxidation reactions occur at one electrode and reduction reactions at the other electrode. These are usually defined as anodic and cathodic reactions.



During the course of normal electrochemical reactions a balance between oxidation and reduction reactions will occur. A complex mechanism occurs at the metal/aqueous interface. Because of the oxidation and reduction reactions involve species in the electrolyte reacting at or near the metal interface, the surface of the electrode is charged relative to the solution and the reactions are associated with specific electrode potentials [17]. If water is the primary solvent, then it can be visualized as dipolar molecules such that a positive side (hydrogen atoms) and a negative side (oxygen atoms) exist. These molecules align themselves in the direction of the electric field (see figure 3.1). This is called an inner layer of the Helmholtz double layer (HDL).

Moreover, because the electric field is strongest close to the ion, some water molecules reside very close to an ionic species in solution. The attraction is great enough that these water molecules are referred to as the primary water sheath of the ion. The electric field is weaker at distances outside the primary water sheath, but

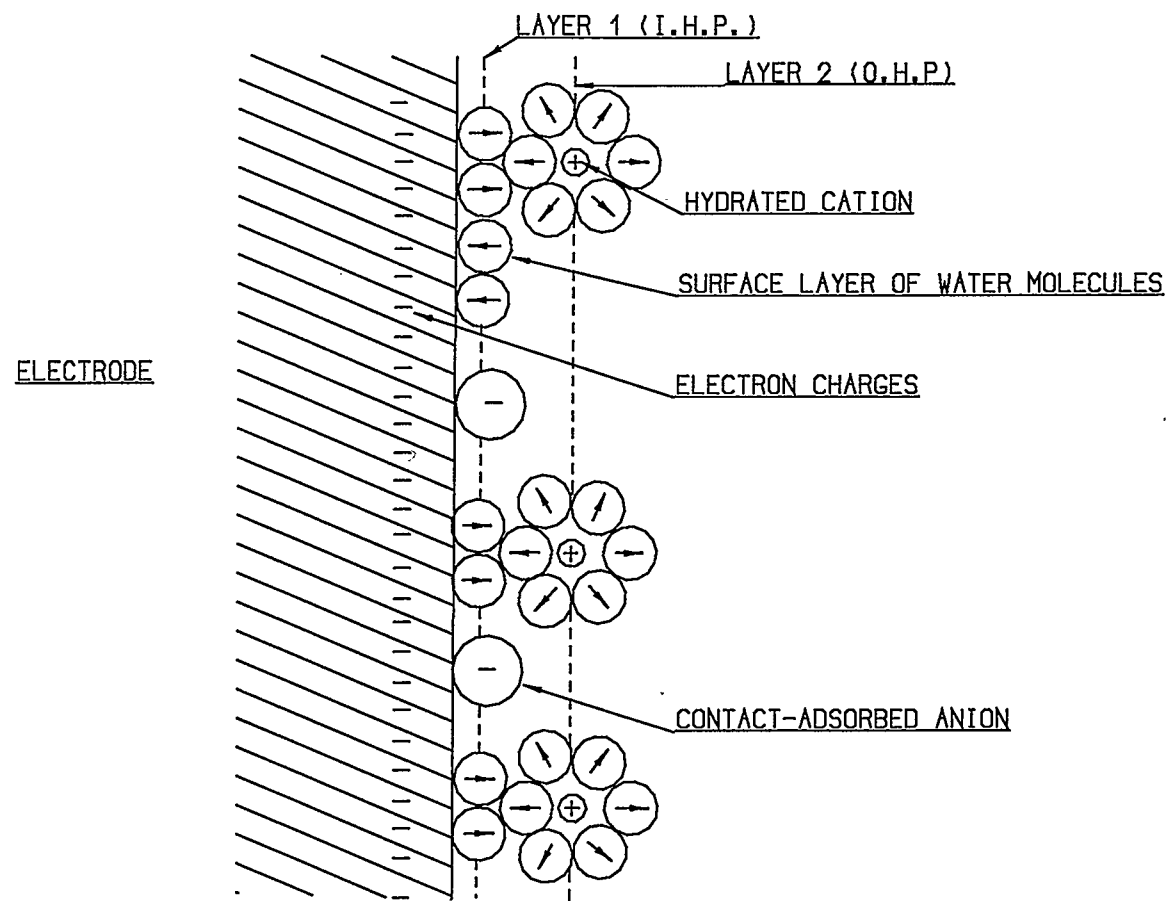


FIGURE 3.1 THE STRUCTURE OF THE ELECTRICAL DOUBLE LAYER (REF. 46)



it still disturbs polar molecules as the ion passes through the solution. The water molecules that are disturbed as the ion passes, but do not move with the ion are usually referred to as the secondary water sheath (figure 3.2). The first row of the double layer formed with water molecules limits the distance that hydrated ions can approach the interface. Outside the HDL there is usually a diffuse region referred to as the Gouy Chapman Layer [32]. This region is not usually considered when modelling the electrode/solution interface. HDL can be represented as a charged capacitor with a potential drop across the layer. It is usually simplified as a linear change in potential from the metal surface to the outer Helmholtz plane.

### 3.2.2 Electrode Potentials

At constant temperature, the free energy of a reaction can be expressed as,

$$\Delta G = \Delta H - T\Delta S \quad (3.3)$$

where,

$\Delta G$  = change of free energy (Gibbs free energy)

$\Delta H$  = change of enthalpy

$\Delta S$  = change of entropy

$T$  = absolute temperature

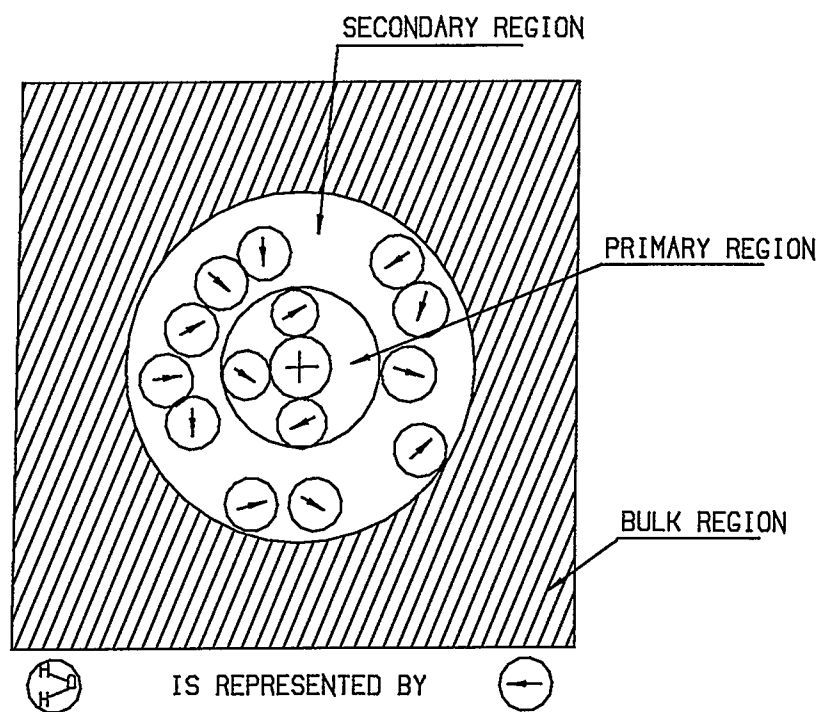


FIGURE 3.2 SCHEMATIC OF THE PRIMARY AND SECONDARY SOLVENT MOLECULES FOR CATIONS IN WATER (REF. 17)

if  $\Delta G > 0$ , the reaction will not take place under the particular conditions described.

if  $\Delta G < 0$  the reaction will occur, moving towards an equilibrium condition.

When all reactants and products are in standard conditions ( $P = 1$  atmosphere,  $T = 273^{\circ}$  K) the free energy can be expressed as,

$$\Delta G^{\circ} = -RT \ln K \quad (3.4)$$

where,

R is the gas constant, 8.314 Joule/deg-mole

K is the equilibrium constant.

The tendency for metal to corrode can also be expressed in terms of the electromotive force (e.m.f) of the corrosion cell. If the extent of reaction is small, such that the activities of reactants and products do not change, then the potential remains constant and can be expressed as,

$$\Delta G = -nFE \quad (3.5)$$

If the reaction occurs under standard conditions, then equation (3.5) becomes,

$$\Delta G^{\circ} = -nFE^{\circ} \quad (3.6)$$

where,

$n$  is the number of electrons per atom of species involved in the reaction

$F$  is the charge of one mole of electron, being 96,480 coulombs/mole

$E$  is the cell potential

Substituting equation (3.6) into equation (3.4) yields,

$$\ln K = - \frac{nFE^{\circ}}{RT} \quad (3.7)$$

By using eq. (3.7), equilibrium data for electrochemical reactions can be predicted,

$$\Delta G^{\circ} = \sum_L \nu_L G_L^{\circ} - \sum_M \nu_M G_M^{\circ} \quad (3.8)$$

where, subscripts  $L$  and  $M$  represents the product and reactant, respectively, and  $\nu_L$  and  $\nu_M$  are the corresponding stoichiometric coefficients.  $G^{\circ}$  is the free energy at standard condition. For the general equation,



If  $A$  is the equilibrium constant for the overall reaction (3.9), then it can be expressed as [18],

$$A = \frac{[a_Y]^y \cdot [a_Z]^z}{[a_W]^w \cdot [a_X]^x} \quad (3.10)$$

where,

$y$  is the moles of substance  $Y$ .

$a_Y$  is the activity coefficient of substance  $Y$ .

From the Van't Hoff isotherm,

$$\Delta G = -RT \ln K + RT \ln A \quad (3.11)$$

substituting eq. (3.5) into eq. (3.11) yields,

$$E = \frac{RT}{nF} \ln K - \frac{RT}{nF} \ln A \quad (3.12)$$

substituting eq.(3.4), (3.5) and (3.10) into eq.(3.12) yields,

$$E = E^0 - \frac{RT}{nF} \ln \frac{[a_Y]^y \cdot [a_Z]^z}{[a_W]^w \cdot [a_X]^x} \quad (3.13)$$

Moreover eq.(3.13) can be simplified to as,

$$E = E^{\circ} - \frac{2.3RT}{nF} \log \frac{[a_{\text{products}}]}{[a_{\text{reactants}}]} \quad (3.14)$$

Eq.(3.14) is called the Nernst equation. Electrode potentials as described above are always measured when no current is flowing between the electrode and some reference such as the Standard Hydrogen Electrode (SHE).

### 3.2.3 Potential versus pH (Pourbaix) Diagrams

Potential - pH diagrams are graphical representations of the domain of stability of metals, ions, oxides and other species in the solution. These diagrams are also a graphical representation of the Nernst equation. These diagrams were first made by M. Pourbaix [19,20] and have proved to be very useful in the study of corrosion systems.

These diagrams are based on thermodynamic computations for a number of selected chemical species and the equilibrium conditions between them. It is possible to predict from an E - pH diagram, if a metal will corrode. These diagrams do not provide precise information on the corrosion rate.

It is important to note that E - pH diagrams can also be constructed from experimental cyclic polarization

curves. These diagrams have more practical significance than the equilibrium  $E - pH$  diagrams constructed from thermodynamic data. They show how a metal in a natural environment may give rise to general corrosion, pitting, perfect or imperfect passivity or to immunity depending on the potential.

The Pourbaix diagrams have some limitations. These are as follows;

1.  $E - pH$  diagrams which are constructed for specific chemical species cannot be used, if an alteration of species occurs in the solution. This alteration can result in a change such as going from a corrosion state to a state of passivity.
2. Most  $E - pH$  diagrams are constructed at  $25^{\circ}\text{C}$  and 1 atmospheric pressure and must be modified for other conditions [22].
3. Activities of  $10^{-6}$  g-ion are not appropriate for toxic elements such as  $\text{Pb} \longrightarrow \text{Pb}^{2+}$ .
4. In a low corrosion or passivation region a condition of stress corrosion cracking may occur.

5. The tendency to pit cannot be made from these diagrams.

6. Oxides and hydroxides often exist as metastable products which can modify equilibrium boundaries on the diagram.

### 3.3 Kinetics of the Aqueous Corrosion

For most engineering applications of corrosion the kinetics or rate of corrosion is often the most important aspect. Since a corroding system is not at equilibrium, the corrosion rate can not be determined from thermodynamics calculations. Several useful terms should be defined. These are polarization (overpotential) and exchange current density.

Overpotential ( $\eta$ ): The displacement of the potential of an electrode from its reversible value is the overpotential  $\eta$ , given by,

$$\eta = E_p - E_r \quad (3.15)$$

where  $E_p$  is the polarized potential and  $E_r$  is the reversible or equilibrium potential. Cathodic overpotential



$(\eta_c)$  is always negative and given by,

$$\eta_c = E_{p,c} - E_{r,c} < 0 \quad (3.16)$$

Anodic overpotential is always positive and given by,

$$\eta_a = E_{r,a} - E_{p,a} > 0 \quad (3.17)$$

Exchange Current Density ( $i_o$ ): Exchange current density is the rate of the oxidation and reduction reaction occurring at an equilibrium electrode expressed in terms of current density. The exchange reaction rate and exchange current density can be interrelated as,

$$r_{\text{oxid}} = r_{\text{red}} = \frac{i_o}{nF} \quad (3.18)$$

where  $r_{\text{oxid}}$  and  $r_{\text{red}}$  are the equilibrium oxidation and reduction rates. Exchange current densities are influenced by the ratio of oxidized and reduced species which are present and by the temperature. There is no accurate theoretical way of determining  $i_o$  for a given system. Hence, it must be determined experimentally (21).

There are four types of polarization to be considered,

these being Activation, Concentration, Combined and Resistance polarization.

### 3.3.1 Activation Polarization ( $\eta_A$ ):

In most of the electrode processes charge transfer at a finite rate will involve an activation overpotential  $\eta_A$ . This overpotential occurs when activation energy is required to maintain the rate of the reaction. Activation polarization is determined by the electrochemical reactions and the overall reaction is controlled by the slowest step of a partial reaction in the sequence. The relationship between activation polarization and reaction rate can be derived as;

$$\eta_A = \pm \beta \log (i/i_o) \quad (3.19)$$

where  $\beta$  is the Tafel slope. It is constant for a given environment and dependant on temperature (21). It can be expressed as,

$$\beta = \frac{2.3RT}{\alpha nF} \quad (3.20)$$

where  $\alpha$  is the transfer coefficient which describes the shape of the rate controlling energy barrier. Substituting

eq. (3.20) into eq. (3.19) yields the Tafel equation for anodic process,

$$\eta_{A,a} = - \frac{2.3RT}{\alpha_a nF} \log(i_o) + \frac{2.3RT}{\alpha_a nF} \log(i) \quad (3.21)$$

Similary, for the cathodic process,

$$\eta_{A,c} = \frac{2.3RT}{\alpha_c nF} \log(i_o) - \frac{2.3RT}{\alpha_c nF} \log(i) \quad (3.22)$$

In general form eq. (3.21) and eq. (3.22) can be expressed as,

$$\beta_a = a + b \log(i) \quad (3.23)$$

limitation: Tafel equation behaves linearly when overpotential is greater than  $\pm 50$  mv [21].

### 3.3.2 Concentration Polarization ( $\eta_T$ ):

This refers to an electrochemical reaction which is controlled by the diffusion of ions in the electrolyte. The rate of an electrode reaction also depend on mass transfer, i.e. the rate at which the reactant is transported to the surface of the electrode and the rate at which the product is transported away from the electrode.

Concentration polarization normally occurs with the reduction reaction. At very high reduction rates, the region adjacent to the electrode surface will become depleted of hydrogen ions (hydrogen evolution reaction). If the reduction rate is increased further, limiting rate will be reached which is determined by the diffusion rate of ions to the electrode surface. This limiting rate is called the limiting diffusion current density,  $i_L$  and it is the maximum rate of reduction possible in a given system.  $i_L$  can be expressed as,

$$i_L = \frac{DnFC_b}{x} \quad (3.24)$$

where,

- D     is the diffusion coefficient of the reacting ion
- $C_b$    is the concentration of the reacting ion in the  
         bulk solution
- x     is the thickness of the diffusion layer

If  $C$  is ionic concentration at the electrode surface, then from the Nernst equation, overpotential of the cathodic reaction can be written as,

$$\eta_{T,c} = - \frac{RT}{nF} \ln \left( \frac{C}{C_b} \right) \quad (3.25)$$

since,

$$C_b = C - \frac{ix}{DnF} \quad (3.26)$$

Substituting eq. (3.26) into eq. (3.25) yields,

$$\eta_{T,c} = - \frac{RT}{nF} \log \left( \frac{1}{1 - \frac{ix}{CDnF}} \right) \quad (3.27)$$

Combining equations (3.24) and (3.27) yields the concentration polarization in a cathodic process as (figure 3.3),

$$\eta_{T,c} = \frac{2.3}{nF} \log \left( 1 - \frac{i}{i_L} \right) \quad (3.28)$$

It is important to note that any factor which causes an increased  $i_L$  (eq. 3.24) will result in an increase in corrosion rate, assuming the latter is solely determined by the kinetics of the cathodic process [22]. Furthermore,  $\eta_{T,c}$  depends on velocity (stirring effect), temperature and concentration of the solution.

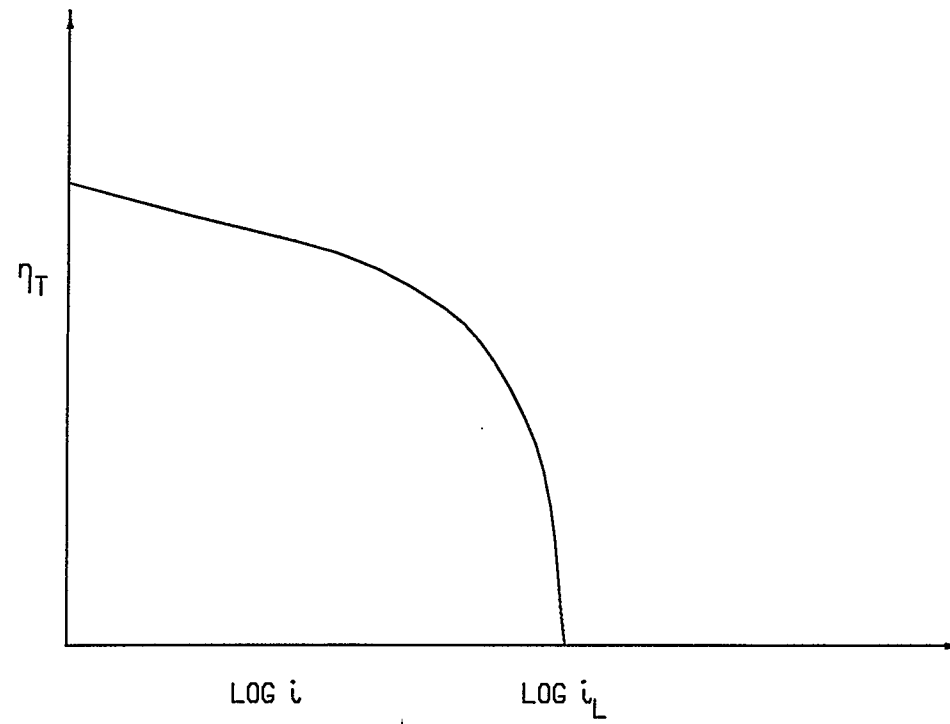


FIGURE 3.3 CONCENTRATION POLARIZATION FOR CATHODIC REACTION

### 3.3.3 Combined Polarization

Combined polarization will occur when both activation and concentration polarization take place in an anodic or cathodic process. Thus total polarization is given by (figure 3.4),

$$\eta_{\text{Total}} = \eta_{A,c} + \eta_{T,c} \quad (3.29)$$

From eq. (3.19) for cathodic process,

$$\eta_{A,c} = -\beta \log (i/i_o) \quad (3.30)$$

Hence,

$$\eta_{\text{Total}} = -\beta \log (i/i_o) + \frac{2.3 RT}{nF} \log \left(1 - \frac{i}{i_L}\right) \quad (3.31)$$

### 3.3.4 Resistance Polarization

When the electrochemical cell contains a low conductivity solution or a highly resistant film layer on the surface of the electrode, polarization rises due to resistance and is often referred to as polarization resistance ( $\eta_R$ ). It can be defined as,

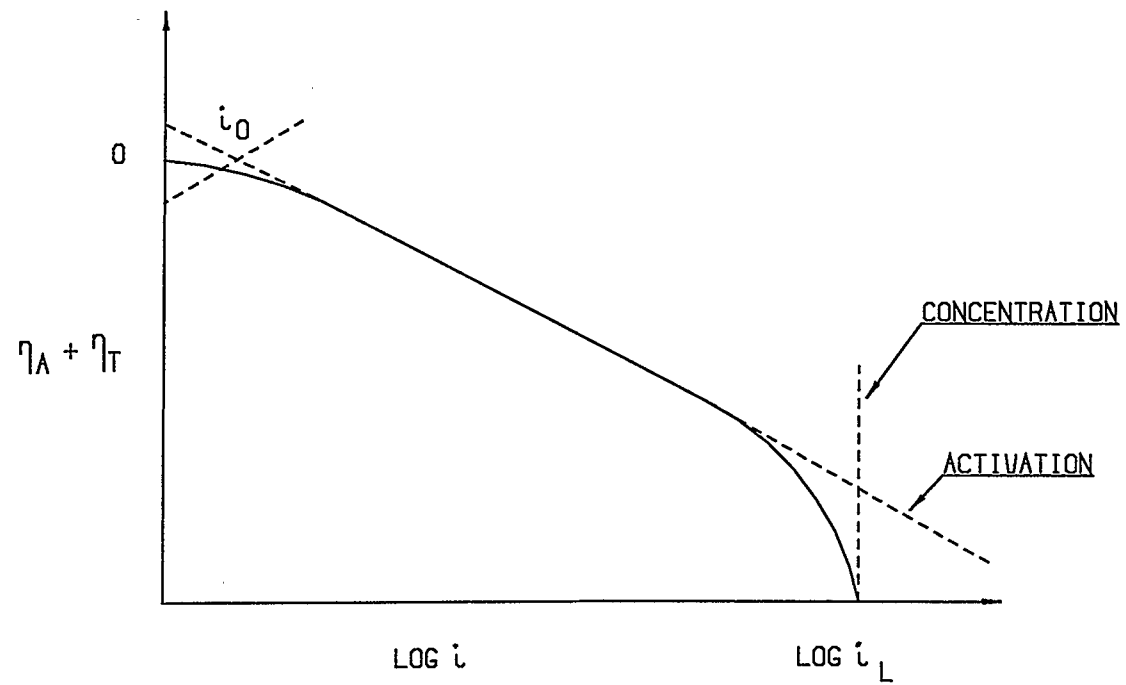


FIGURE 3.4 COMBINED POLARIZATION FOR CATHODIC REACTION



$$\eta_R = I (R_{\text{solu}} + R_f) \quad (3.32)$$

where,

$R_{\text{solu}}$  is the electrical resistivity of the solution, which is also dependant on the distance separating the electrodes or more generally on the geometry of the corroding system.

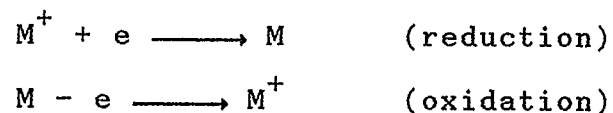
$R_f$  is the resistance produced by films or coatings formed on the electrode surface.

If the solution has good conductivity, then  $R_{\text{solu}}$  is negligible, and eq. (3.32) becomes,

$$\eta_R = IR_f \quad (3.33)$$

### 3.3.5 Kinetic Properties of the Single and Dual Exchange Reactions

As shown in figure 3.5, the Evans diagram is used to illustrate the single exchange reaction which occurs at a metal surface.



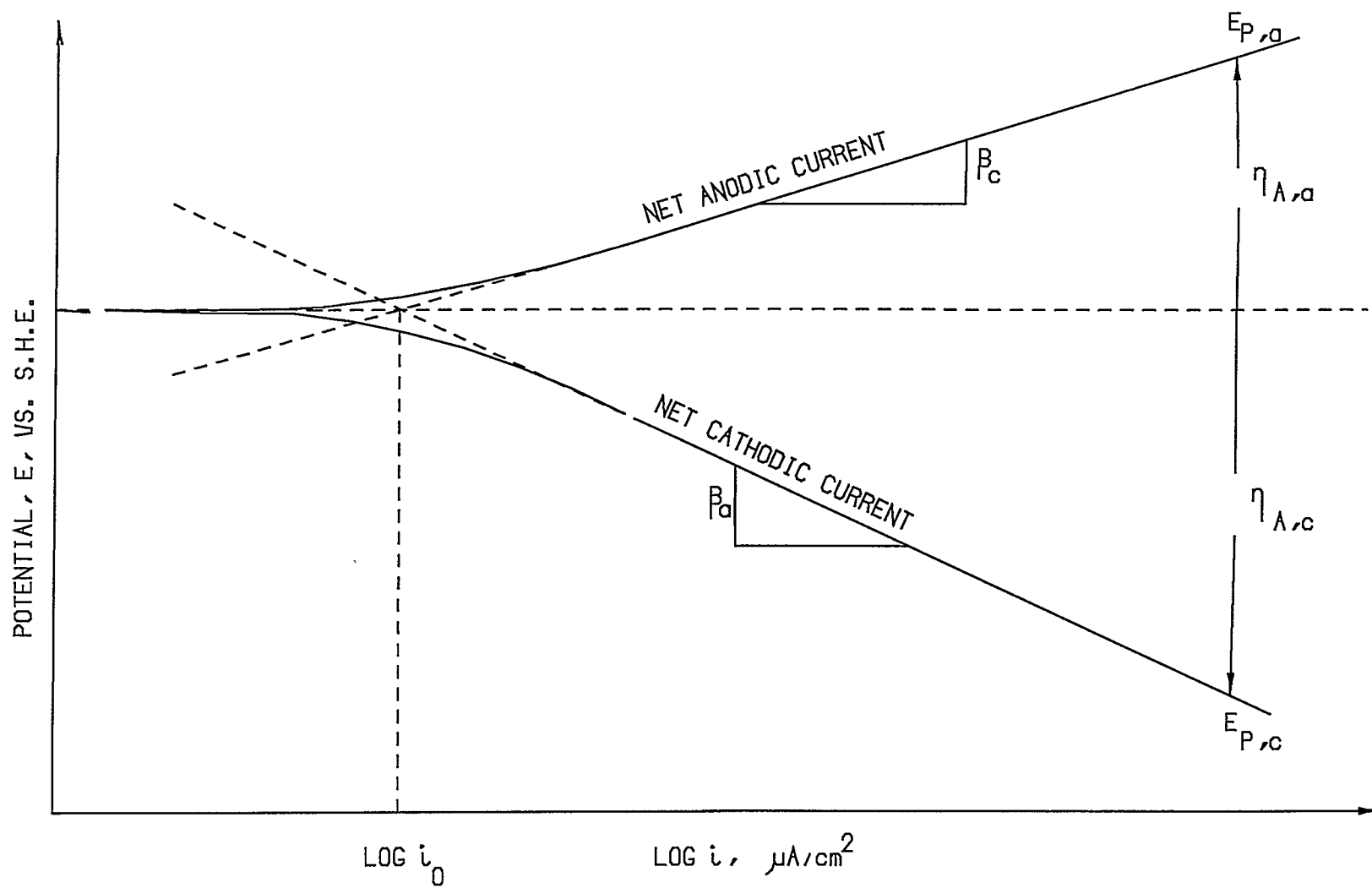


FIGURE 3.5 TAFEL SLOPES AND OVERPOTENTIALS FOR A SINGLE EXCHANGE PROCESS

For anodic process, eq.(3.21) can be expressed in the form of,

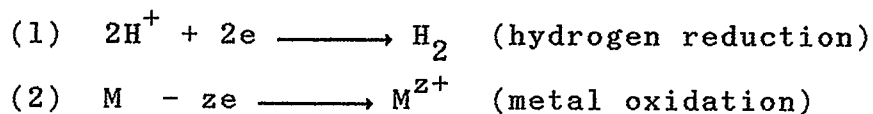
$$\eta_{A,a} = A_a + B_a \log(i) \quad (3.34)$$

Similary, for cathodic process,

$$\eta_{A,c} = A_c + B_c \log(i) \quad (3.35)$$

$B_a$  and  $B_c$  are constants and equal to the Tafel slopes in the linear region. Extrapolation of these linear regions to the reversible potential ( $E_r$ ) would give the log value of the exchange current density for that specific reaction.

The previous discussion has been concerned with the processes of oxidation and reduction of the metal. In a system where additional reactions take place, the Evans diagram displays the mixed characteristics of the total process.



Each reaction has a characteristic value of  $i_o$  and  $E_r$ . If

coupled interactively, reaction (1) is polarized away from its equilibrium position to be reduced to  $H_2$  gas, whereas reaction (2) is anodically polarized to give metal dissolution. The surface consequently assumes a resulting mixed potential,  $E_{\text{corr}}$ , with net corrosion current,

$$i_{\text{corr}} = i_{\text{a}}(M/M^{z+}) = i_{\text{c}}(H^+/H_2)$$

The shape of the mixed characteristic takes up the slope of the dominant Tafel curve in each region, this is displayed in figure 3.6. Corrosion rate ( $i_{\text{corr}}$ ) can be determined by the Tafel extrapolation or linear polarization method. These methods are discussed in chapter 5.

### 3.4 Passivity of Corrosion Resistant Alloys

On the basis of previous discussions it is evident that the rate of an activation controlled reaction should increase with increase in potential according to the Tafel relationship. But in many metal alloys, the metal dissolution rate decreases when the potential is raised above a critical value where the metal is said to have become passive.

As shown in figure 3.7, the behaviour of the active - passive metal can be divided into three different regions;

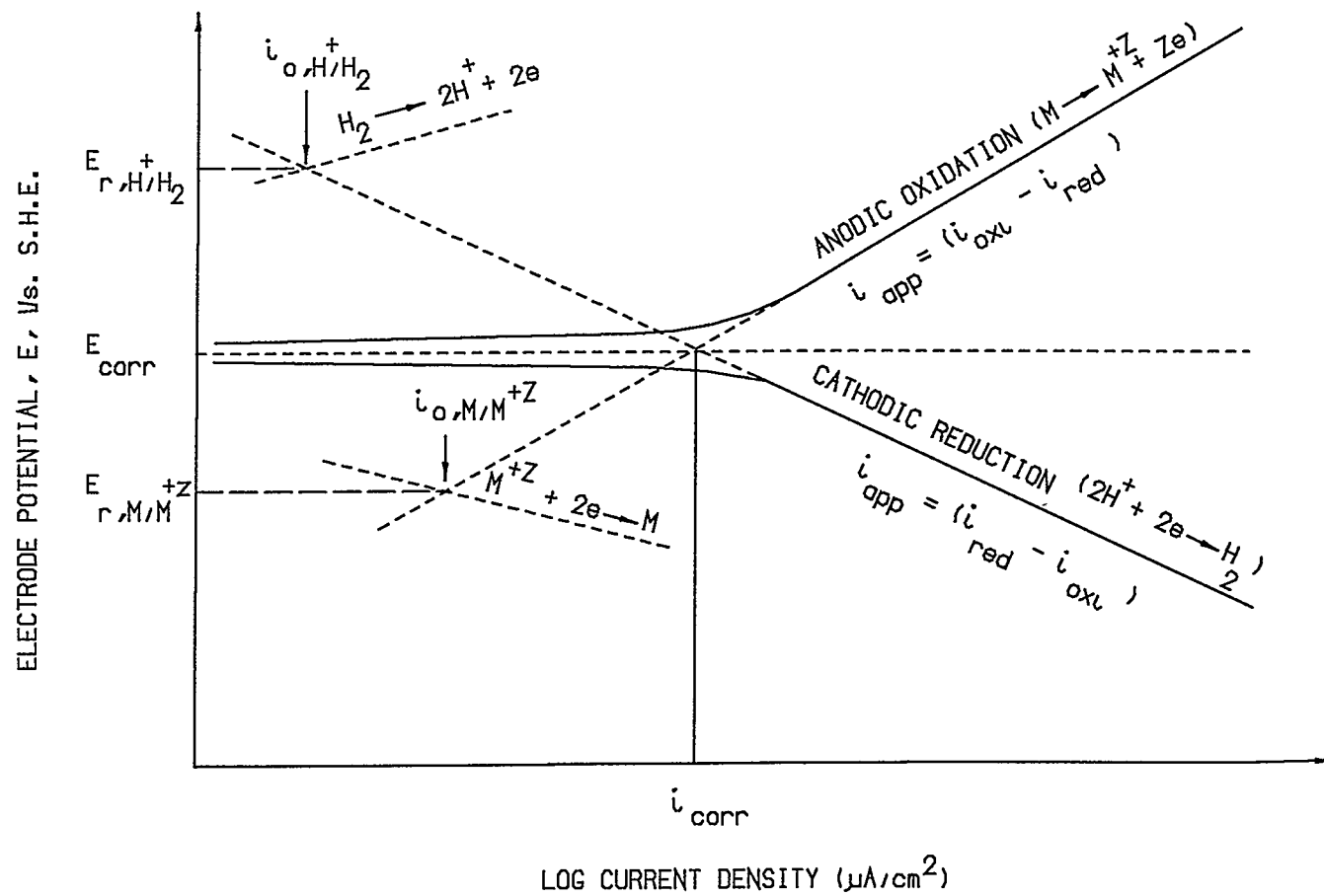


FIGURE 3.6 EVANS DIAGRAM FOR DUAL EXCHANGE PROCESS

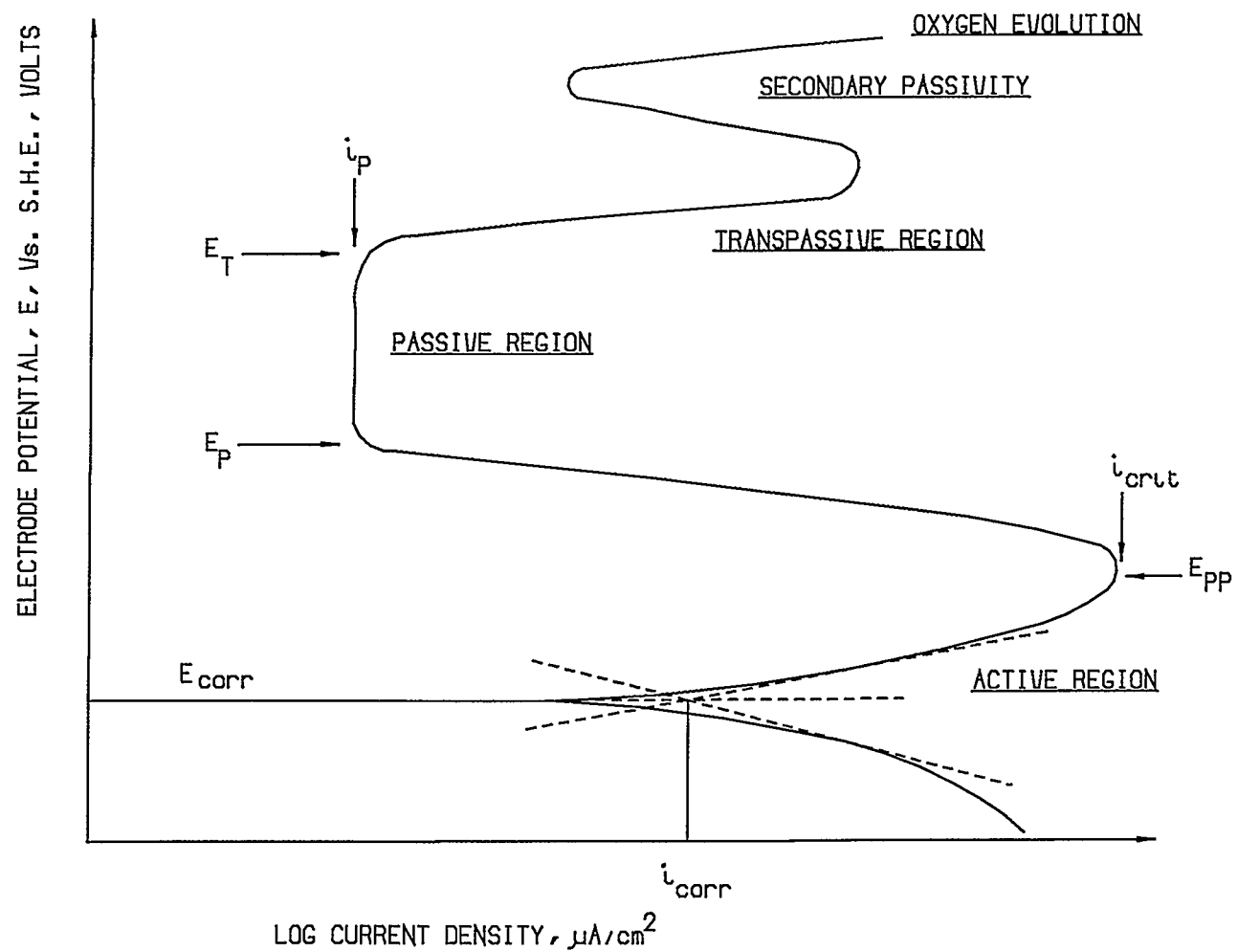


FIGURE 3.7 HYPOTHETICAL ANODIC AND CATHODIC POLARIZATION BEHAVIOUR FOR MATERIAL EXHIBITING PASSIVE ANODIC BEHAVIOUR

active, passive and trans - passive. The most important parameters describing the behaviour of an active - passive metal are the potential and current corresponding to the maximum current. They are called primary passive potential,  $E_{pp}$ , and critical current density,  $i_c$ . From figure 3.7 it is possible to determine,

1. The passive potential ( $E_{pp}$ )
2. The passive corrosion rate ( $i_p$ )
3. The breakdown potential ( $E_T$ )
4. The conditions necessary to achieve passivity
5. The relative stability of the passive state.

Furthermore, it is possible to compare the behaviour of two different alloys on the basis of these properties. From figure 3.8, it can be seen that the phenomenon of spontaneous passivation is dependent upon the relative positions of the cathodic reduction curve and the anodic dissolution curve. For a given reduction curve, the values of  $E_{pp}$  and  $i_c$  determine whether or not the metal will spontaneously passivate. Passivity index  $P$  may be defined as [24],

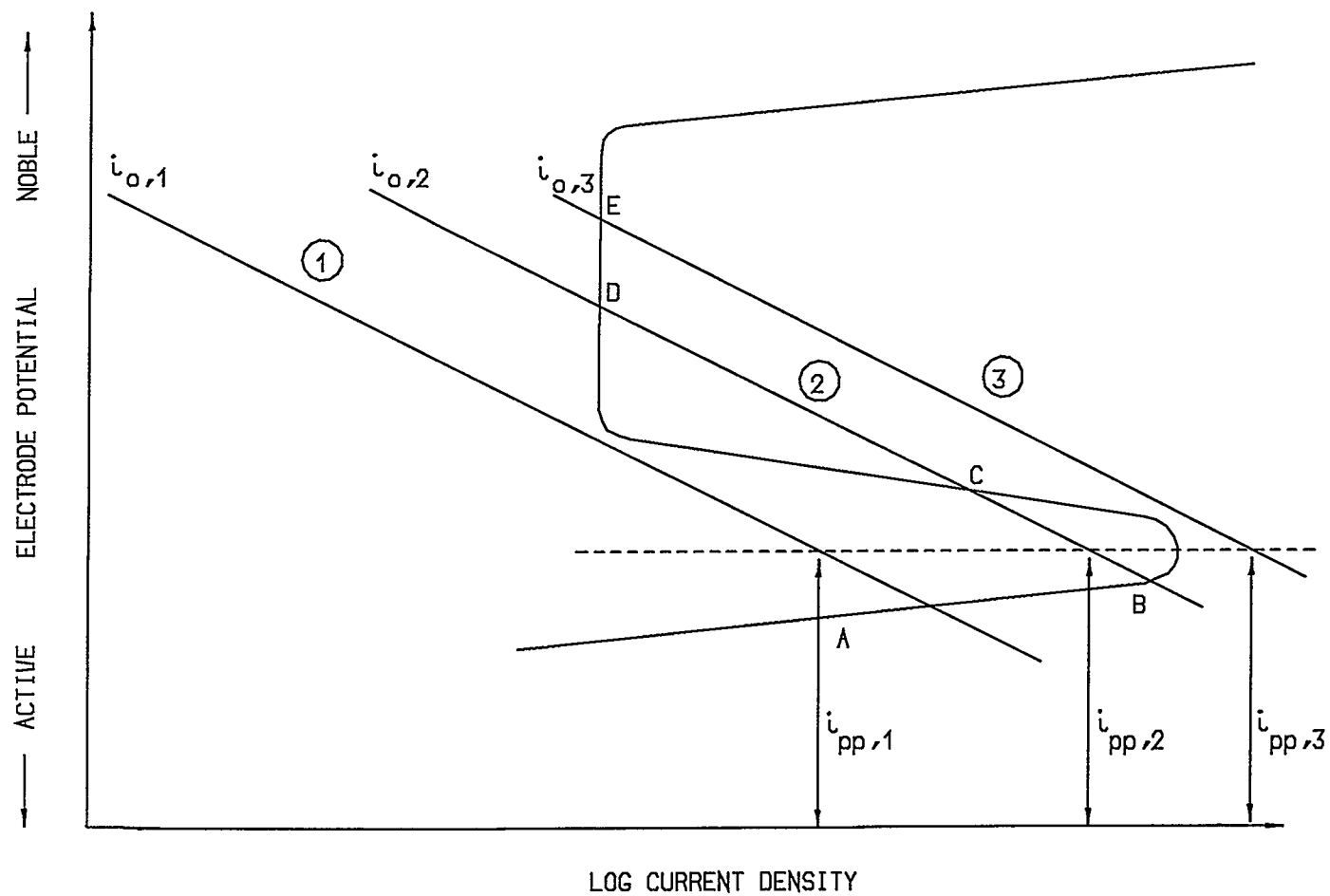


FIGURE 3.8 EFFECT OF CATHODIC EXCHANGE CURRENT DENSITY ON THE STABILITY OF THE PASSIVE STATE



$$P = \frac{i_{pp}}{i_c} \quad (3.36)$$

where,

$i_{pp}$  Cathodic partial current density at  $E_{pp}$   
 $i_c$  Critical anodic current density of the metal

1. If  $P \geq 1$  then alloy spontaneously passivates (case 3, figure 3.8)
2. If  $P < 1$ , the system cannot spontaneously transform from active to passive state, although a stable passive region may exist (case 2, figure 3.8)

As  $P$  increases from 0 to 1, the tendency toward spontaneous passivation increases proportionately. Hence  $P$  may, be used as a quantitative measure of the passivating tendency of a given metal in a corrosive medium.

- (A) For a system containing a single activation controlled cathodic reduction process, cathodic partial current density may be expressed as,

$$i_c = i_{o,c} \{ \exp(-\eta/\overleftarrow{\beta}) - \exp(\eta/\overrightarrow{\beta}) \} \quad (3.37)$$

where,

$i_{o,c}$  = exchange current density of the cathode process

$\eta$  = cathodic overvoltage

$\overleftarrow{\beta}$  and  $\overrightarrow{\beta}$  are Tafel constants for the reduction and oxidation reactions of the cathodic process respectively.

For an overvoltage of 50 mv or more, eq.(3.36) becomes,

$$p = \frac{i_{o,c} \exp(-\eta_{pp}/\overleftarrow{\beta})}{i_c} \quad (3.38)$$

where,

$\eta_{pp}$  cathodic overpotential corresponding to  $E_{pp}$

(B) The cathodic overvoltage of system under complete diffusion control, from eq.(3.28),

$$\eta_{T,c} = \frac{RT}{nF} \ln \left( 1 - \frac{i_c}{i_L} \right) \quad (3.39)$$

Rearranging eq.(3.39) and substituting into eq.(3.36) yields,

$$P = \frac{i_L \{1 - \exp(\eta_{PP}/K)\}}{i_c} \quad (3.40)$$

where,

$$K = \frac{RT}{nF} ,$$

For high cathodic overpotentials eq.(3.40) may be approximated by,

$$P = i_L/i_c \quad (3.41)$$

From equations (3.38) and (3.41) it can be seen that the passivating tendency of a given metal or alloy is dependent on the type of cathodic control existing within the system. Figures 3.9 and 3.10 illustrate behaviour of two different alloys in a system containing an activation controlled cathodic process and diffusion controlled cathodic process respectively.

Where,

- $i_{crit,1}$  = critical anodic current density of the alloy 1.
- $i_{crit,2}$  = critical anodic current density of the alloy 2.
- $E_{pp,1}$  = primary passive potential of the alloy 1.
- $E_{pp,2}$  = primary passive potential of the alloy 2.
- $i_{o,c}$  = exchange current density of the cathodic reaction.

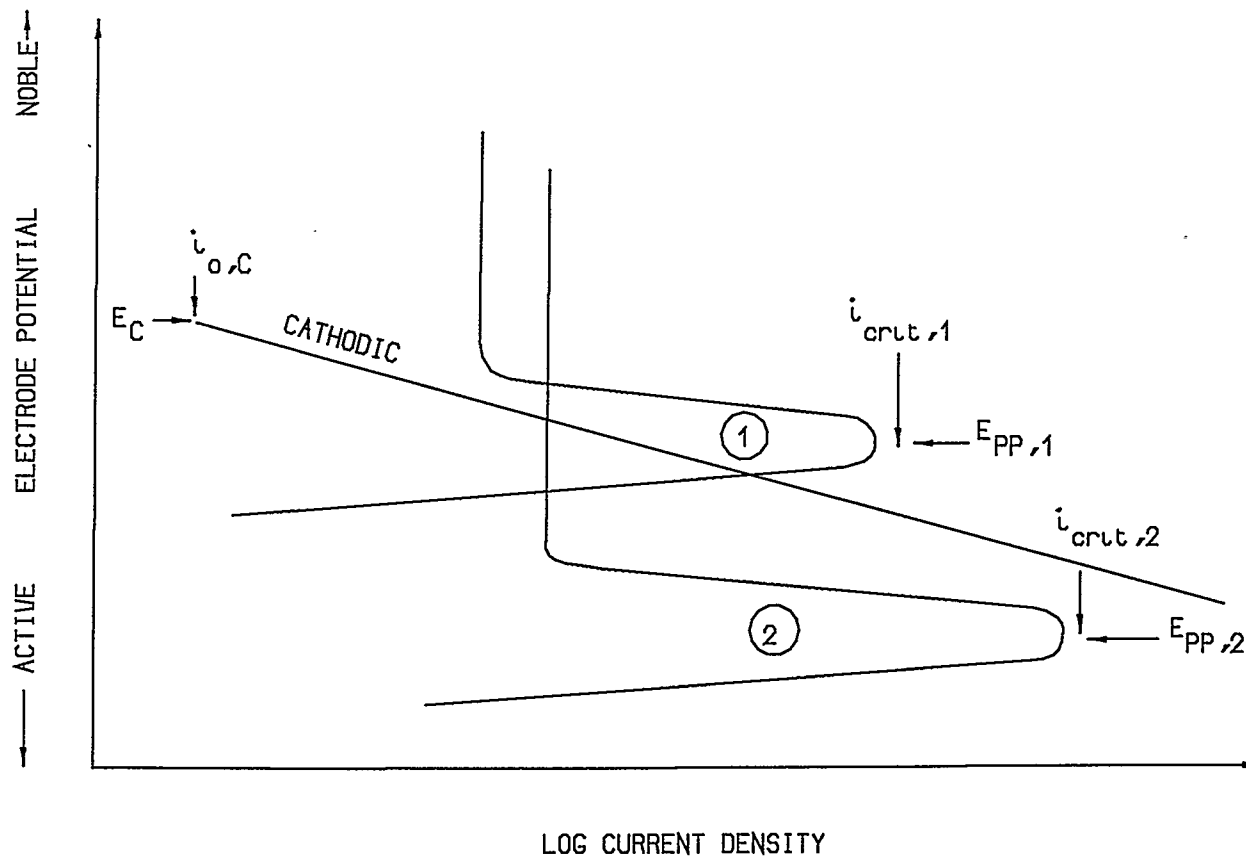


FIGURE 3.9 BEHAVIOUR OF ACTIVE-PASSIVE ALLOYS IN A SYSTEM CONTAINING AN ACTIVATION CONTROLLED CATHODIC REDUCTION PROCESS

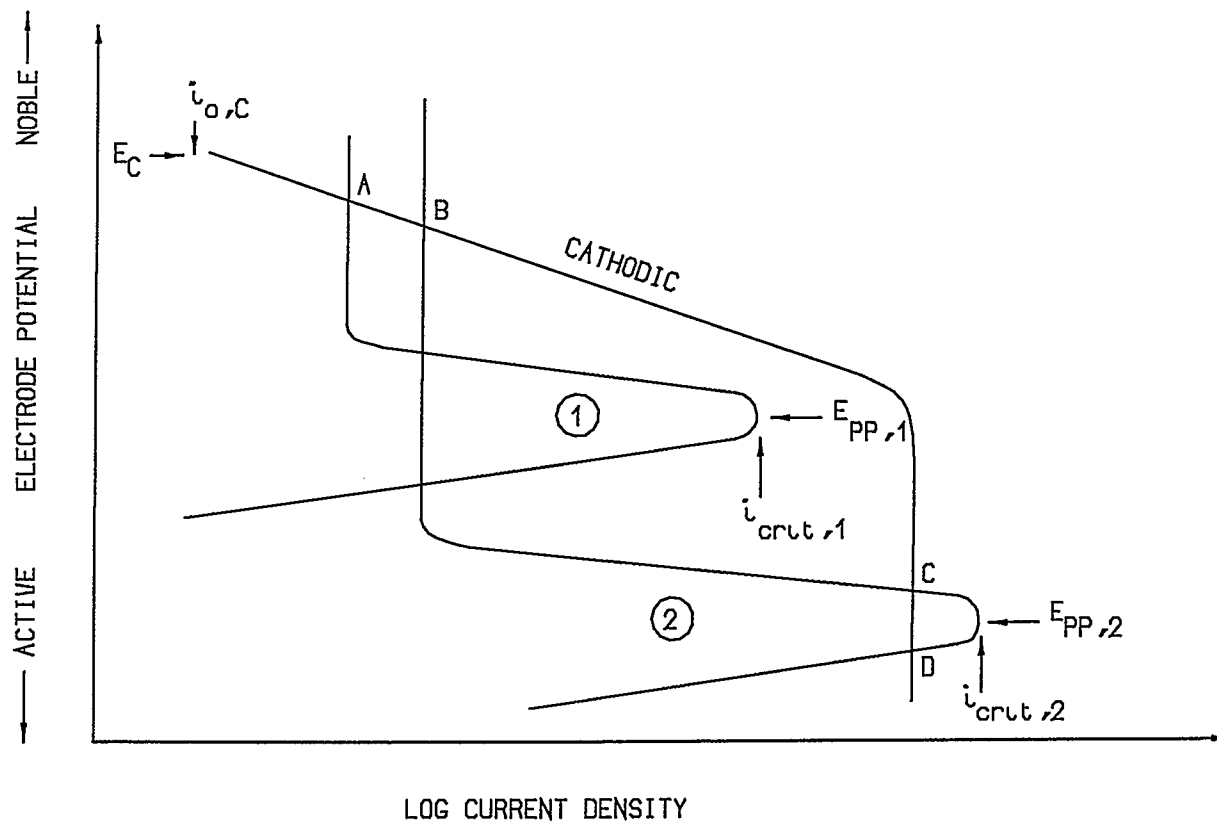


FIGURE 3.10 BEHAVIOUR OF ACTIVE-PASSIVE ALLOYS IN A SYSTEM CONTAINING DIFFUSION-CONTROLLED CATHODIC REDUCTION PROCESS

$E_c$  = reversible potential of the cathodic reaction.

From the above discussion and figures 3.9 and 3.10 two general rules concerning the case of passivation of a given metal or alloy can be stated:

1. To find a better corrosion resistant metal or alloy in a system where the cathodic process is activation controlled the metal or alloy with very active  $E_{pp}$  is usually superior as indicated in figure 3.9.
2. However, for a corrosive medium where the reduction process is diffusion controlled, a metal or alloy with a small critical anodic current will passivate easier as shown in figure 3.10

## CHAPTER 4

### EXPERIMENTAL STUDY

#### 4.1 Introduction

The purpose of this experimental work was to determine, evaluate and compare different materials for their resistance to corrosion in aqueous coal gasification environments. Electrochemical corrosion techniques were used for this study. The cyclic polarization method was used because it gives an overall understanding of the corrosion behaviour in a relatively short period of time.

#### 4.2 Description of the Test Materials

A total of 11 different alloy materials ranging from mild steel to fairly expensive high nickel alloys were selected. These materials were selected based on wide range of chemical composition, to check the effect of alloy elements on the corrosion. Also some of these materials have been used in pilot plant studies and found to be high temperature sulfidation resistant. The chemical composition of these materials, in weight percent, is given in tables 4.1 to 4.11.













TABLE 4.11  
CHEMICAL COMPOSITION OF 446 STAINLESS STEEL

Fe	Mg	Al	Si	C	P	S	Cr
	-	-	0.46	0.11	0.022	0.013	25.74
Mn	Ni	Co	Mo	Ti	N	Cu	Cb
0.45	-	-	-	-	0.15	-	-
<u>Fe</u> Balance							

The chemical composition of the aqueous solution is not a unique constant since different coal gasification processes form somewhat different chemical combinations. The aqueous corrosion is normally due to some specific process in the coal gasification plant. The major factor influencing the aqueous corrosion of components is condensation forming during the start up and shut down procedures. The following selection of the ionic compounds for aqueous solution are arrived at based on condensate analysis from a pilot plant [25]. This analysis indicates that the harmful ions, in terms of corrosion, are chloride, sulfate and bicarbonate ions. The base solution composition was selected to reflect the relative ratios in reference [25] but concentrated somewhat. The chemical composition of the solution is given in table 4.12 and is the best

estimate to actual conditions from available information to date.

TABLE 4.12  
CHEMICAL COMPOSITION OF THE TEST SOLUTION

Constituent	gram/litre
$\text{Na}^+$	2.43
$\text{SO}_4^{--}$	2.00
$\text{HCO}_3^-$	0.80
$\text{Cl}^-$	2.00

The gas mixture was selected on the basis of pilot plant gas analysis [25]. In order to obtain a better understanding of the corrosion process and its effect on the alloying elements, the gas constituents were broken down as shown in the table 4.13. Each gas mixture was given a code name.

TABLE 4.13  
SIMULATED GAS MIXTURE TEST CONDITIONS

Gas composition	Code name
100% Air	A
100% N <sub>2</sub>	N <sub>2</sub>
100% H <sub>2</sub>	H <sub>2</sub>
26% H <sub>2</sub> + 74% N <sub>2</sub>	H26
45% CO <sub>2</sub> + 55% N <sub>2</sub>	CO <sub>2</sub>
23% CO + 77% N <sub>2</sub>	CO
45% CO <sub>2</sub> + 23% CO + 32% N <sub>2</sub>	32N <sub>2</sub>
1% H <sub>2</sub> S + 99% N <sub>2</sub>	H <sub>2</sub> S
1% NH <sub>3</sub> + 99% N <sub>2</sub>	NH <sub>3</sub>
23% CO+45% CO <sub>2</sub> +4% CH <sub>4</sub> +26% H <sub>2</sub> +1% H <sub>2</sub> S+1% NH <sub>3</sub>	U

Due to explosion hazards and chemical instability, the total gas mixture (U) was received in 3 separate bottles. The total gas composition was mixed in the cell. This was obtained by mixing the three bottled gases using different flow meter settings (table 4.14). The total gas mixture resulted in the overall desired composition.

TABLE 4.14  
TOTAL GAS MIXTURE

Received gas mixtures	Required percentage for total mixture	Flow meter reading
100% CO	23%	33
3.3%NH <sub>3</sub> +84%H <sub>2</sub> +13%CH <sub>4</sub>	31%	45
2.2%H <sub>2</sub> S + 97%CO <sub>2</sub>	46%	67

#### 4.3 Description of Experimental Set-Up

The equipment used in this study for potentiodynamic cathodic-anodic polarization measurements conforms to ASTM standard G5-82 [26]. The experimental set up is shown in figure 4.1. The principal components of this set up are as follows;

1. The potentiostat.
2. The standard polarization cell.
3. The salt bridge.
4. The reference saturated calomel electrode (SCE).
5. The auxiliary electrodes (platinum).
6. The working electrode.

##### 4.3.1 EG & G potentiostat (Model 273)

The potentiostat (figure 4.2) was interfaced with a Tandy 3000 HL personal computer system. This allowed automation in respect to data acquisition. The potential of the working electrode is capable of being controlled to  $\pm 10$  V. The electrode currents are measurable within the range  $10^{-1}$  to  $10^6 \mu\text{A}$ .

Due to some internal problems with this potentiostat only 26 tests were conducted using this unit. The remainder of the tests were done with a potentiostat designed and built at the University of Calgary.



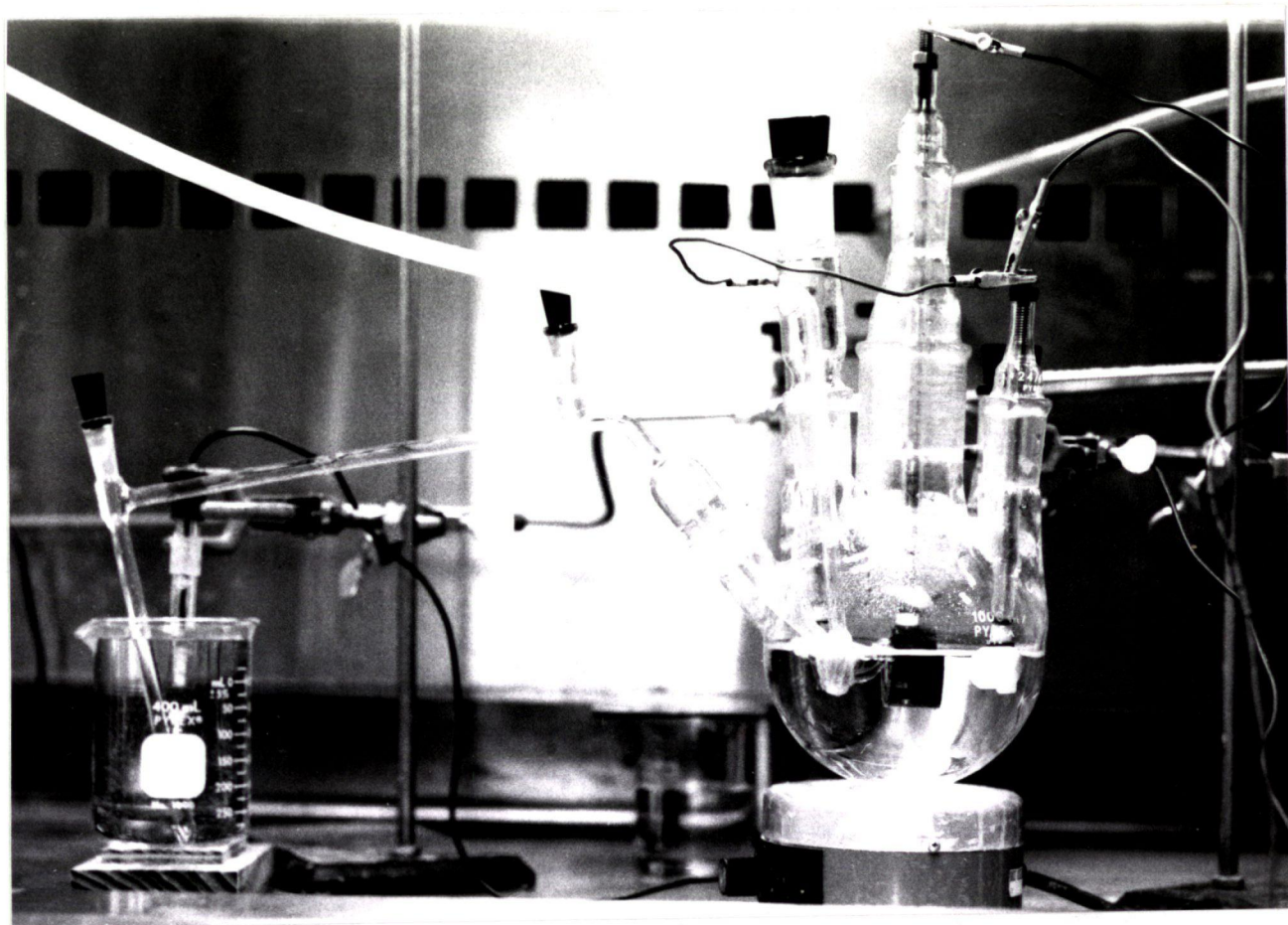


FIGURE 4.1 Experimental Set up.

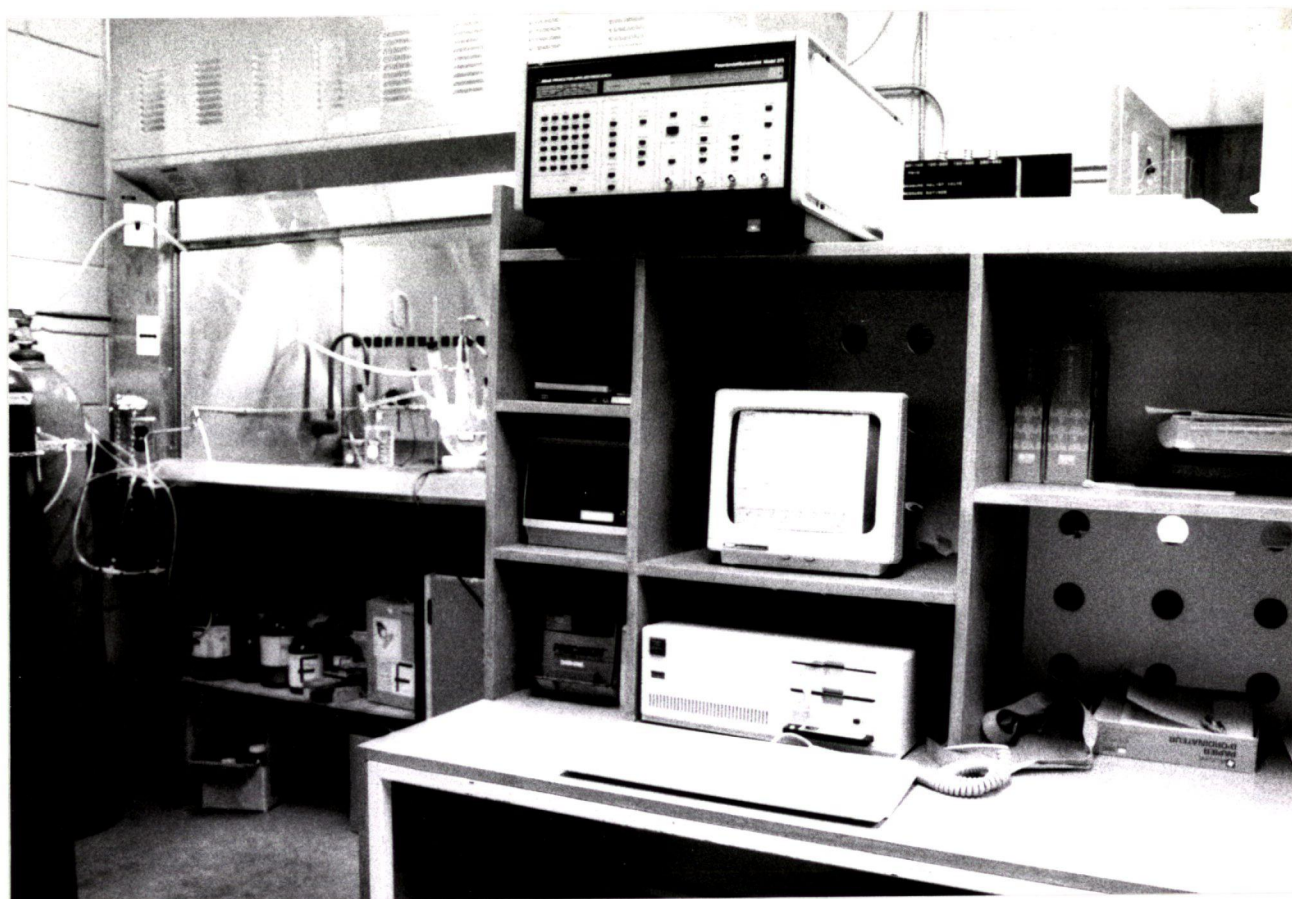


FIGURE 4.2 EG & G Potentiostat.

#### 4.3.2 The Old Potentiostat

This potentiostat was designed and built at the University of Calgary and has been used for many years [29]. It is capable of maintaining a potential change of  $\pm 2.0$  V with respect to SCE and current range of  $10^{-1}$  to  $10^6$   $\mu$ A. Potential and current are recorded on a chart recorder with the aid of a logarithmic amplifying circuit. The chart recorder is built into the potentiostat frame. This unit is a manual one and must be monitored continuously.

#### 4.3.3 The Standard Polarization Cell

The test cell used in this study is shown in figure 4.1. It is a 1-litre round bottom flask which has been modified by the addition of various necks. This was done to permit the introduction of electrodes, gas inlet and outlet tubes, and a thermometer.

#### 4.3.4 The Salt Bridge

The salt bridge used for this study was a Luggin probe. It has a fine porosity glass sinter plug. The salt bridge was mainly used to prevent contamination of test solution from the reference electrode.

#### 4.3.5 The Reference Electrode

A saturated calomel electrode, SCE, Fisher Model 13-639-51 was used to measure the potential of electrode solution interface. It was immersed in an open beaker of test solution and electrically linked to the test cell by means of the salt bridge.

#### 4.3.6 The Auxiliary Electrodes

Two platinum leaf electrodes were used as auxiliary electrodes. These were immersed in the test cell in a face to face position. Care was taken to install these electrodes so that the total area of each platinum leaf electrode was greater or equal to the exposed area of the working electrode. This was done to ensure that a restriction at the auxiliary electrode did not occur due to insufficient area.

### 4.4 General Experimental Techniques

#### 4.4.1 Preparation of the Working Electrode

The specimen was cut using a slow speed diamond saw (Buehler-Isomet) specially designed for sample preparation. This was done to avoid any work hardening of the specimen during preparation. The test specimens were then mounted in epomet with the cut face exposed (transverse direction).

The mounted samples were then drilled and tapped through the epomet from the top. This allowed for easy attachment to the standard electrode holder without exposing the holder to the aqueous solution. The mounted specimens were polished to 600 grit then rinsed in distilled water, sprayed with methanol and air dried prior to immersion into the corrosion cell.

#### 4.4.2 Solution Preparation

The test solution was prepared by dissolving the salts shown in table 4.15 in distilled water. The solution was prepared in batches of 15 litres.

TABLE 4.15  
CONCENTRATION OF THE TEST SOLUTION

Compound	gram/litre
NaCl	3.296
NaSO <sub>4</sub>	2.954
NaHCO <sub>3</sub>	1.108

#### 4.4.3 Experimental Procedure

The apparatus was set up as shown in figure 4.1. Prior to each test, auxiliary electrodes (platinum) were cleaned by immersing them in a 10% HCl solution and driving a

current between these electrodes by means of a 6V battery. Every 60 seconds the direction of the current flow was reversed by switching the battery polarity. The test cell was filled with the prepared solution and deaerated with the respective gas mixture for one half hour prior to the start of each test. During deaeration the flow rate of the gas mixture was maintained at 0.37 litres/min. While the solution deaerated the specimen was immersed in the solution and cathodically protected by using the potentiostat.

The potentiodynamic scans were conducted from -1200 to 0 mV (vs SCE) at a rate of 0.6V/hour. In the range of -200 mV to 0 mV the potentiodynamic scan direction was reversed to more active potentials. This was done to check on whether the material exhibited any tendency towards pitting. When the reverse sweep curve intersected the forward curve or when a value between -200 to -300 mV was achieved for a material that did not exhibit a positive hysteresis curve the cyclic polarization test was considered complete.

During the test the solution was maintained at room temperature and stirred at a rate of 1900 rpm using a 15mm stirrer. After deaerating the solution with the gas mixture

for one half hour the pH of the solution was measured (table 4.16). pH was measured before and after testing and no significant difference was found.

TABLE 4.16

pH VALUES OF THE SOLUTION WITH DIFFERENT GAS MIXTURES

Gas composition	pH value
100% N <sub>2</sub>	8.6
100% H <sub>2</sub>	8.5
26% H <sub>2</sub> + 74% N <sub>2</sub>	8.8
45% CO <sub>2</sub> + 55% N <sub>2</sub>	6.3
23% CO + 77% N <sub>2</sub>	8.4
45% CO <sub>2</sub> + 23% CO + 32% N <sub>2</sub>	6.4
1% H <sub>2</sub> S + 99% N <sub>2</sub>	7.65
1% NH <sub>3</sub> + 99% N <sub>2</sub>	9.4
23% CO+45% CO <sub>2</sub> +4% CH <sub>4</sub> +26% H <sub>2</sub> +1% H <sub>2</sub> S+1% NH <sub>3</sub>	6.2

TABLE 4.17ABBREVIATIONS FOR THE TEST MATERIALS

Material	Code name
Mild Steel	MS
Fe-Mn-Al Stainles Steel	PMS
316 Stainless Steel	316SS
Pyromet 31	P31
Pyromet 751	P751
Hastalloy C22	C22
Hastalloy C276	C276
Custom 450	C450
Ferralium 255	F255
Udimet 700	U700
446 Stainless Steel	446SS



## CHAPTER 5

### TEST RESULTS AND DISCUSSION

#### 5.1 Introduction

This section presents a comparison of the corrosion rates of 11 different alloy materials in ten different gas mixtures which can be found in the coal gasification environment. Results obtained by using two different techniques are presented.

#### 5.2 Techniques Used to Determine Tafel Slopes and Corrosion Current Density

##### 5.2.1 Linear Polarization Method

The linear polarization method has been used to determine the corrosion rate for many metals in a wide variety of environments. It can also be used to evaluate inhibitors and protective coatings, as well as for detecting changes of corrosion with time. The following equation was derived by Stern and Geary [28].

$$\frac{1}{R_p} = \left( \frac{\Delta i}{\Delta E} \right)_{E_{\text{corr}}} = 2.3 \left( \frac{\beta_a + \beta_c}{\beta_a \cdot \beta_c} \right) I_{\text{corr}} \quad (5.1)$$

where  $R_p$  is the polarization resistance determined at potentials close to  $E_{\text{corr}}$ . Other symbols are defined in

previous chapters. Equation (5.1) was derived assuming both anodic and cathodic reactions were charge-transfer controlled and IR drop was negligible. Several researchers have attempted to define a validity region for the above equation. According to Stern and Geary [28] the relationship was within 10 mV of the anodic or cathodic polarization. However, Oldham and Mansfeld [45] showed that linearity of the  $\Delta E - \Delta i$  curve is not essential and  $i_{\text{corr}}$  can be evaluated from the slopes of the tangents of the nonlinear curve determined at potentials of about 20-30 mV more positive or negative than  $E_{\text{corr}}$ . Limitations of using this method can be found in the references [17,22].

#### 5.2.2 Tafel Extrapolation Method

This method for determining corrosion rate was used by Wagner and Traud [44] to verify mixed potential theory. By plotting applied potential versus  $\log i$  a linear relationship between current density and applied potential can be developed. This region was referred to as the Tafel region and linearity was valid for 50 mV more negative or positive than the  $E_{\text{corr}}$  [21]. Extrapolation of the applied current density from anodic or cathodic Tafel region to the open-circuit potential ( $E_{\text{corr}}$ ) allows for the determination of the value of  $i_{\text{corr}}$ .

Up to the present time this method has been used to calculate the  $i_{\text{corr}}$  of normal materials in normal environments. However, dealing with exotic materials (as in this work) and in more complicated ionic solutions saturated with various gas mixtures a limitation to the use of this method has arisen. The major limitation is to identify the Tafel region in the anodic polarization curve. As in figures 5.1 and 5.2, the material started to passivate at fairly low current density. This did not allow for the identification of the linear Tafel region in the anodic polarization curve within the 50 mV from  $E_{\text{corr}}$ . Also, for the same reason, a distinct intersection of the cathodic and anodic Tafel slopes could not be found on the  $E_{\text{corr}}$ . Therefore, a computer program (CORRLOT) was designed to overcome this problem. This program was designed based on fundamental theories in electrochemistry. These are as follows;

1. The slopes that aligned with the anodic and cathodic polarization curves were theoretical Tafel slopes based on the equation (3.23).
2. These slopes were calculated based upon how many charge transfers were occurring in the rate

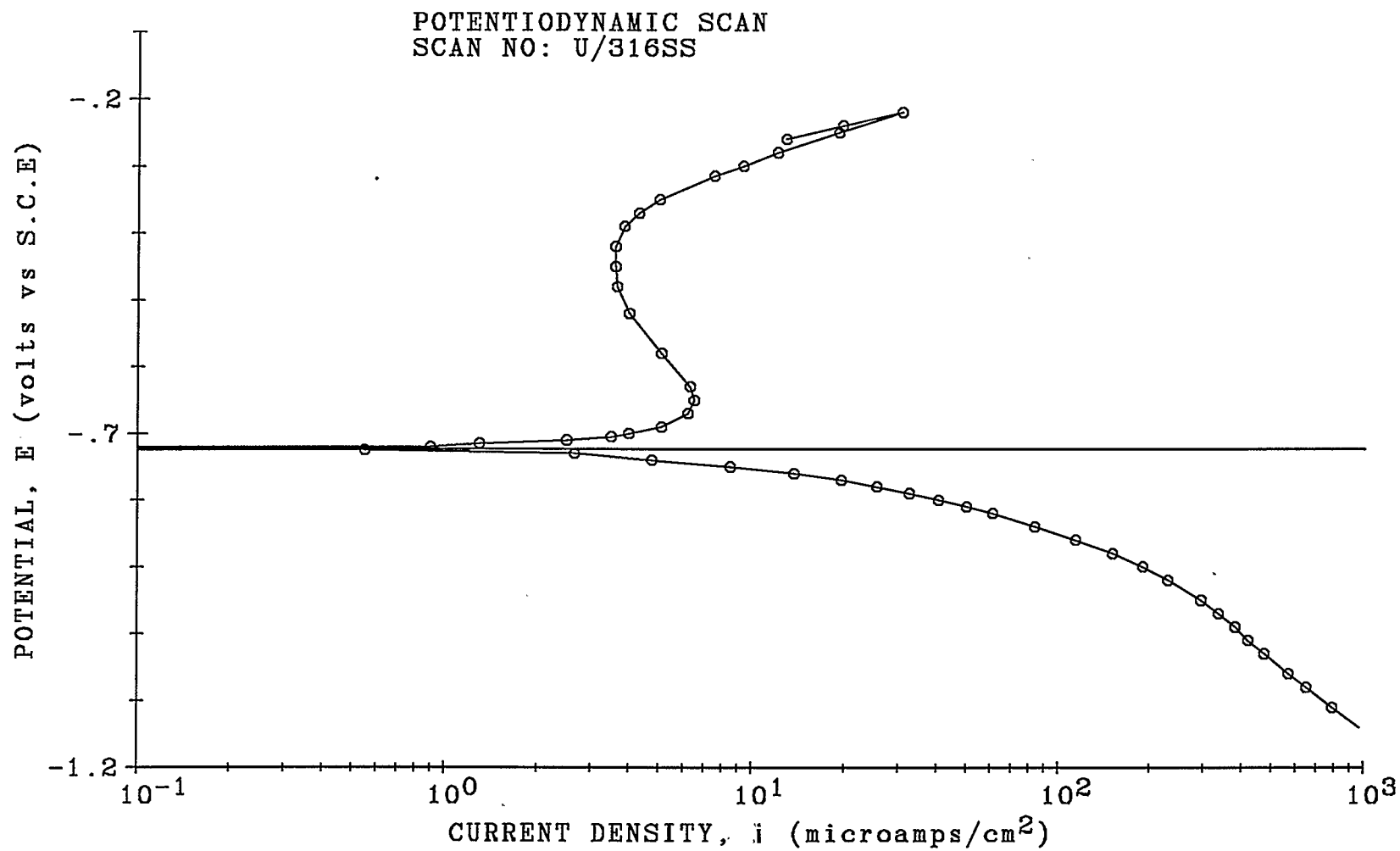


FIGURE 5.1 Potentiodynamic Scan of 316 Stainless Steel in Total Gas Mixture.

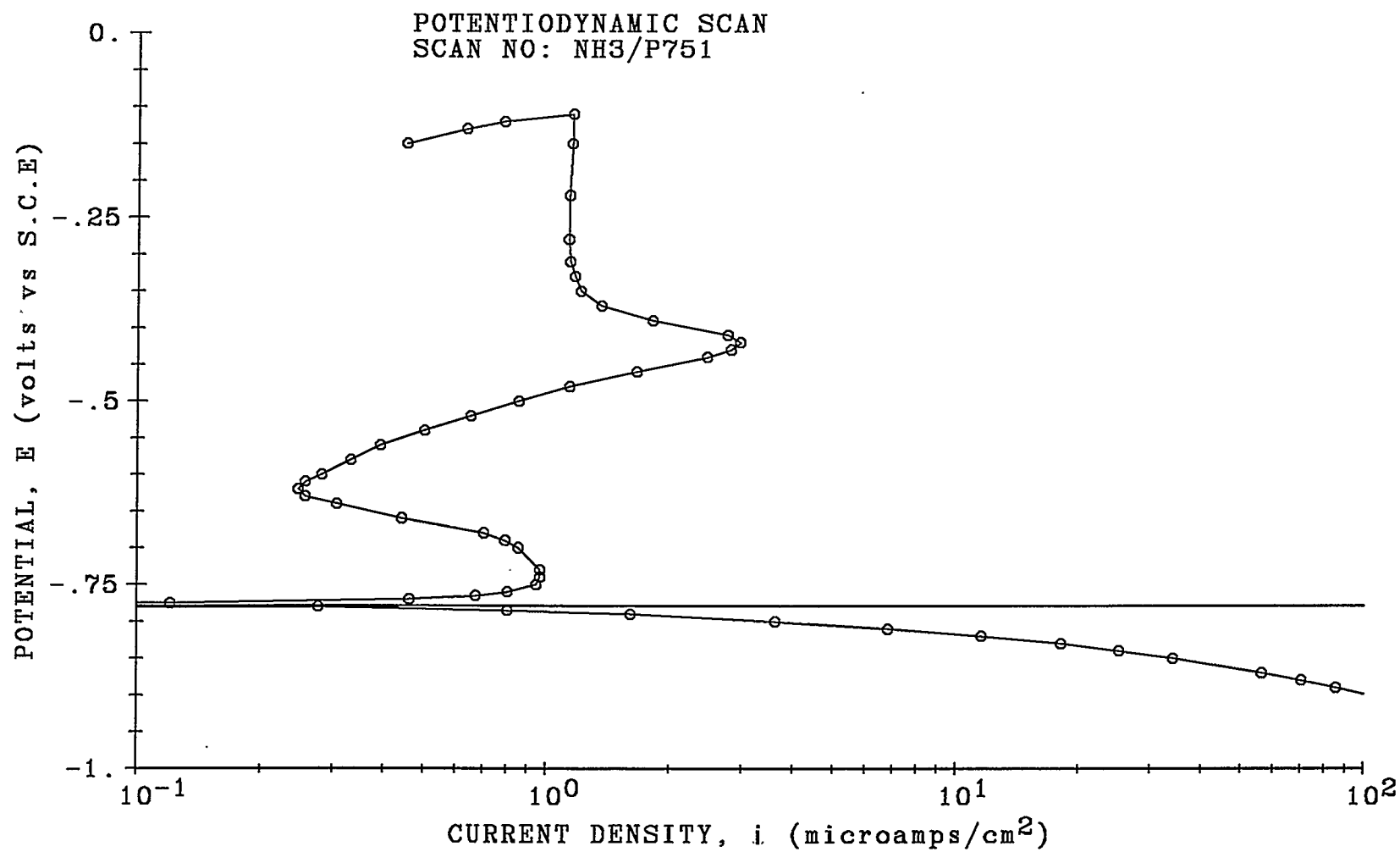


FIGURE 5.2 Potentiodynamic Scan of Pyromet 751 in Ammonia Environment.

determining step of the anodic or cathodic reactions.

3. Depending on the charge transfer, Tafel slopes were assumed from a minimum value of 30 mV/decade to a maximum value of 240 mV/decade.

When CORR PLOT was used to calculate corrosion current density ( $i_{\text{corr}}$ ) it was decided that;

- (a)  $i_{\text{corr}}$  is the corresponding current density at the intersection of the best matching pair of cathodic and anodic Tafel slopes at the corrosion potential.
- (b) If the intersection of two Tafel slopes could not be found on the  $E_{\text{corr}}$ , then  $i_{\text{corr}}$  was taken from the midpoint value of the  $E_{\text{corr}}$  given by the two closest matching Tafel slopes.

In this way  $i_{\text{corr}}$  for all of the materials was found on a consistent basis. The type of control for the corrosion process is governed by anodic control when the value of the anodic Tafel slope is greater than twice the value of the cathodic Tafel slope. Similarly, the process

is governed by cathodic control when the value of the cathodic Tafel slope is greater than twice the value of anodic Tafel slope. Mixed control is defined as a process which is governed by either anodic or cathodic control, both contributing approximately equally.

### 5.3 Comparison of Linear Polarization Method with Tafel Extrapolation

TABLE 5.1

LINEAR POLARIZATION VERSUS TAFEL EXTRAPOLATION

Material	Gas Mixture	$i_{\text{corr}}, \mu\text{A}/\text{cm}^2$	
		Linear pol.	Tafel extra.
Mild Steel	CO	2.27	2.39
Mild Steel	32N <sub>2</sub>	2.41	2.49
316 Stainless	CO	4.52	2.31
316 Stainless	32N <sub>2</sub>	3.02	1.61

As shown in the table 5.1, the corrosion rates of the mild steel calculated by using the two different techniques were very close to each other. However, when the material was changed, corrosion rates calculated by using the two different techniques varied greatly. The linear polarization technique does not give good accuracy in determining corrosion rate for different materials. Since

the Tafel method is the most accurate method of the two all future corrosion rates were calculated using the Tafel method.

Figure 5.3 shows the determination of the corrosion current density by the Tafel extrapolation method using the computer program CORRLOT for mild steel in the total gas mixture U environment. Also shown is the corrosion current density at the intersection of the best matching pair of cathodic and anodic Tafel slopes on the corrosion potential line. Figure 5.4 shows the determination of  $i_{\text{corr}}$  using the same method for 316SS material in a CO environment. As shown in this figure the material started to passivate at a fairly low current density. In figure 5.5 it shows that F255 material starts to passivate at low current density in a combination of gas mixtures  $\text{CO}_2/\text{CO}$ . Again the best matching intersection of Tafel slopes can be found on the corrosion potential line.

#### 5.4 Comparison of Material Corrosiveness under Different Gaseous Environments

A summary of electrochemical corrosion test results for all the materials in the corrosive environments is



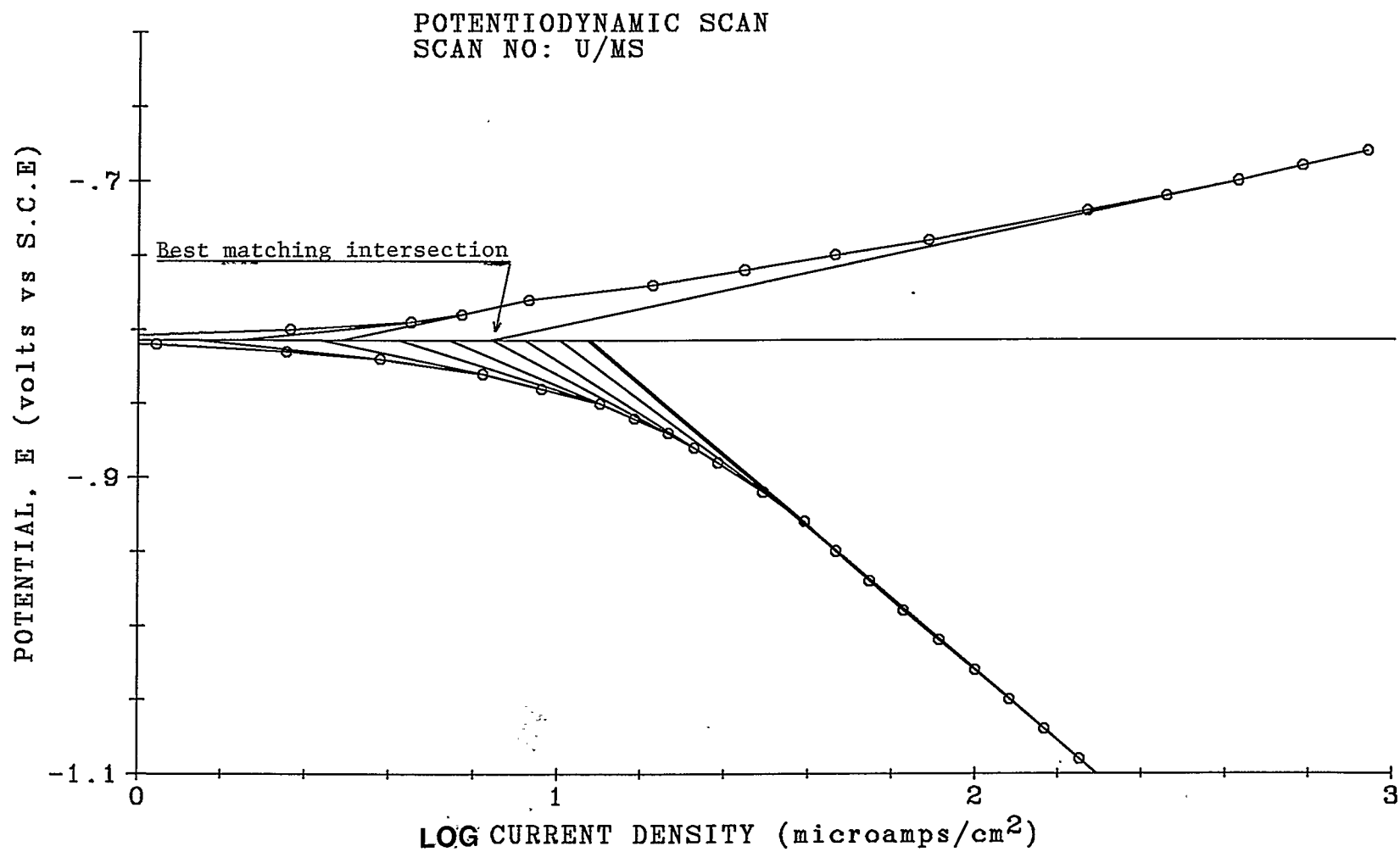


FIGURE 5.3 Determination of Corrosion Current Density of Mild Steel in Total Gas Mixture.

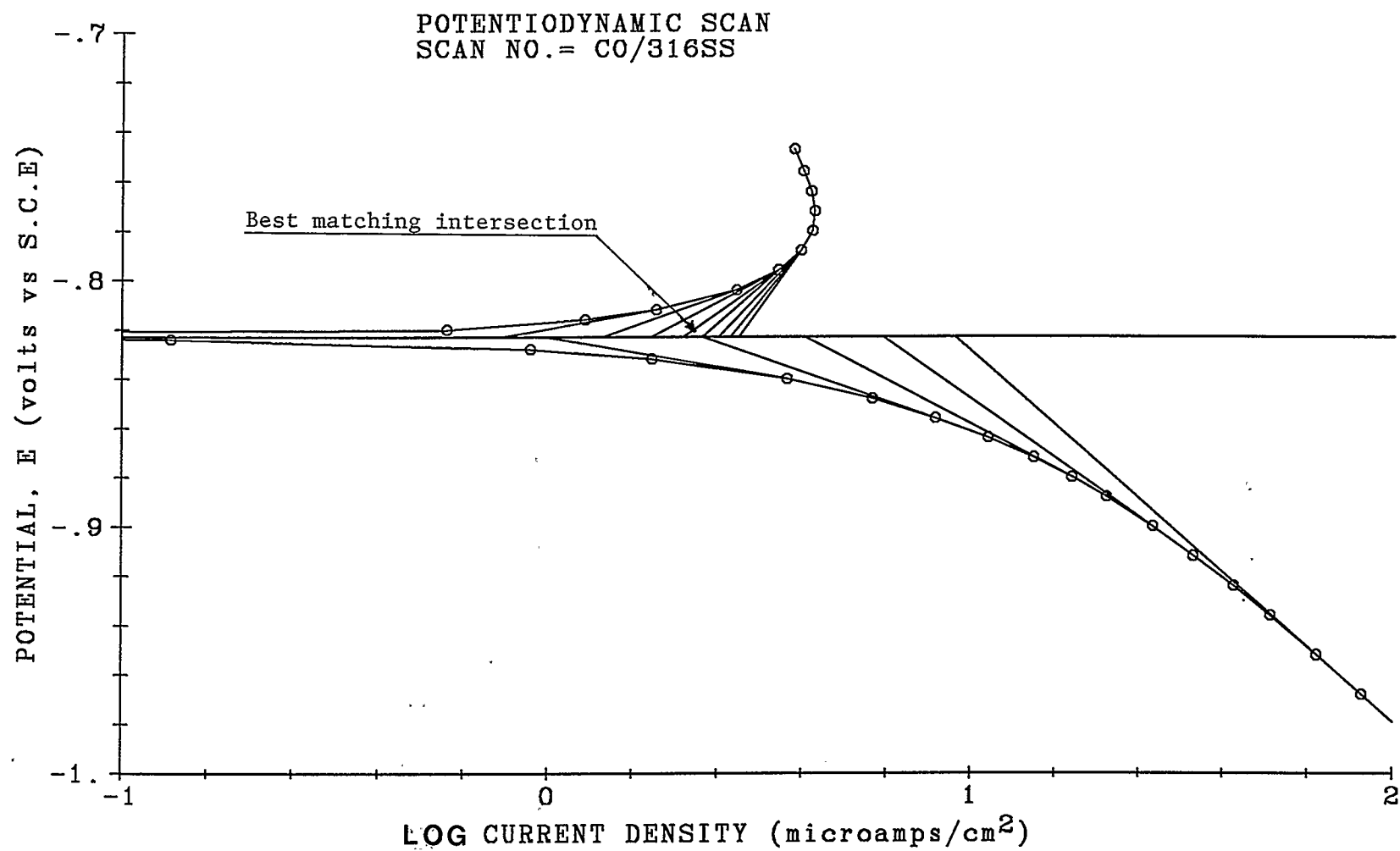


FIGURE 5.4 Determination of Corrosion Current Density of 316 Stainless Steel in Carbon Monoxide Environment.

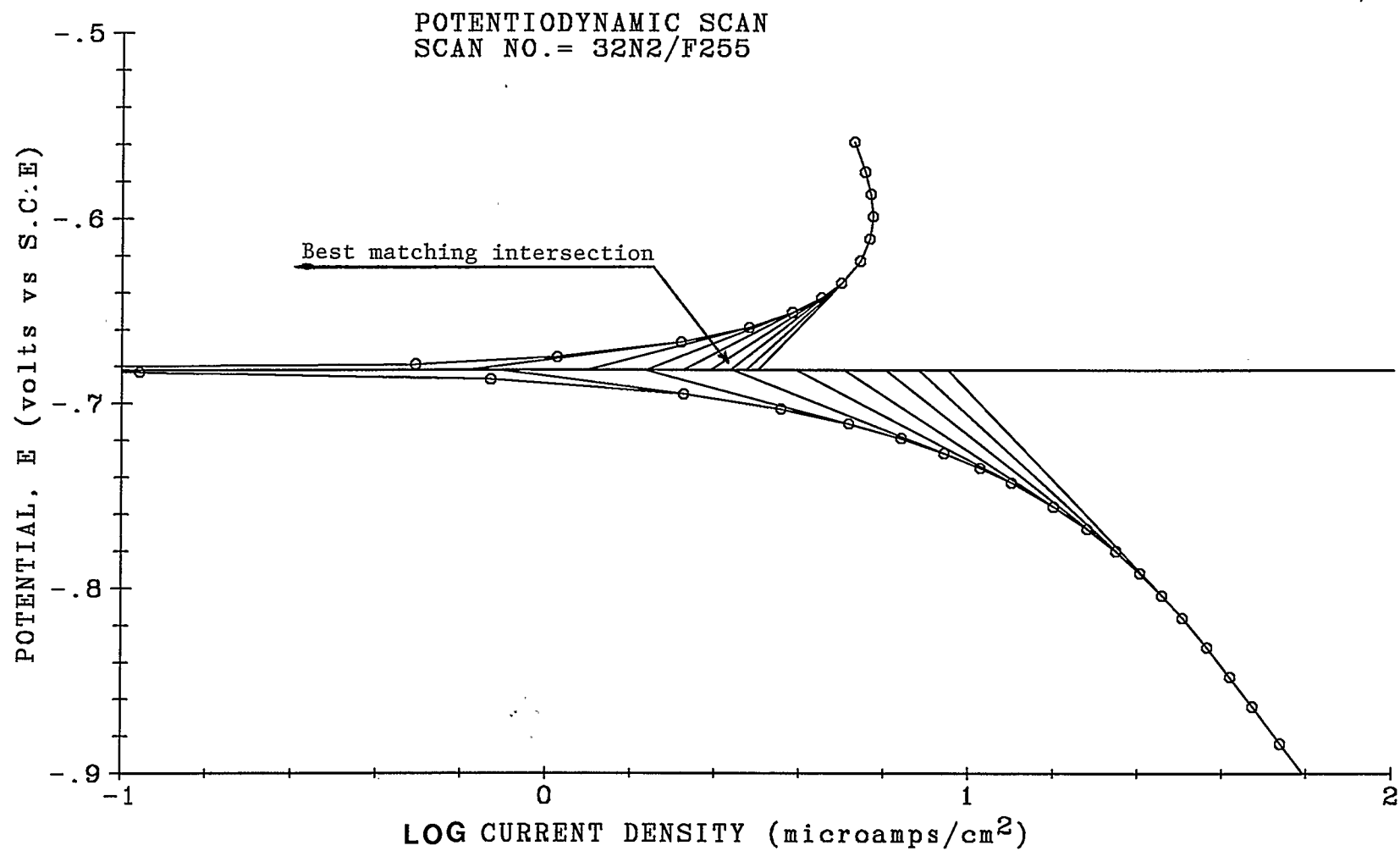


FIGURE 5.5 Determination of Corrosion Current Density of Ferralium 255 in Carbon Dioxide/Carbon Monoxide Environment.

found in table 5.2. The corrosion current densities of these materials in deaerated, aerated conditions and Hydrogen environments are shown in the table 5.3. Table 5.4 lists the electrochemical data for PMS material in the various environments. These tables list the corrosion current density which is a measure of the corrosion rate of the material. Errors which could be associated with calculation of  $i_{\text{corr}}$  are as follows;

1. When choosing Tafel slopes for the CORR PLOT program a value of  $1/2$  was assumed for the symmetry factor ( $\beta$ ) and this value was used in calculating the transfer coefficient ( $\alpha$ ). However, this symmetry factor ( $\beta$ ) is likely some other unique value and could change from material to material.
2. The apparent surface area of the each material was taken as exactly  $1 \text{ cm}^2$ . However, the true surface area will change somewhat due to the inability to obtain a perfectly flat surface when using the polishing procedure.

3. The rate determining steps can vary as dependent upon the test conditions. The rate determining steps chosen for this analysis are based on work by others and were obtained for different environmental conditions than those tested here.

TABLE 5.2  
CORROSION BEHAVIOUR OF MATERIALS IN DIFFERENT  
GASEOUS ENVIRONMENTS

Material	Corrosion rate, $\mu\text{A}/\text{cm}^2$					
	$\text{CO}_2$	CO	$32\text{N}_2$	$\text{H}_2\text{S}$	U	$\text{NH}_3$
MS	11.6	2.4	2.5	2.6	6.8	2.8
PMS	1.4	2.3	0.2	1.7	2.5	1.4
316SS	10.6	2.3	1.6	0.4	3.4	0.4
P31	1.8	2.3	1.8	1.5	4.0	0.3
P751	0.8	3.4	2.1	1.1	4.6	0.7
C22	0.2	5.6	3.8	0.6	5.8	1.1
C276	0.6	4.4	3.4	1.4	5.7	0.7
C450	2.1	6.5	5.1	1.6	5.5	0.8
F255	0.6	0.4	1.7	3.2	2.9	0.4
U700	0.3	5.7	3.9	5.2	5.6	0.6
446SS	0.2	2.8	1.8	0.6	3.9	0.4

TABLE 5.3

CORROSION BEHAVIOUR OF MATERIALS IN AERATED, DEAERATED  
AND HYDROGEN ENVIRONMENTS

Material	Corrosion rate, $\mu\text{A}/\text{cm}^2$			
	A	N <sub>2</sub>	H <sub>2</sub>	H26
MS	1.5	8.8	2.1	6.8
PMS	1.4	4.7	1.9	2.1
316SS	1.2	0.7	1.2	0.5
P31	0.1	0.6	0.9	1.3
P751	0.9	0.3	4.6	7.4
C22	0.7	0.3	3.4	3.6
C276	0.6	1.9	8.3	4.1
C450	0.1	0.5	9.3	3.2
F255	0.2	1.8	0.3	0.7
U700	0.4	0.2	4.1	8.1
446SS	0.2	0.3	1.5	0.9

TABLE 5.4  
ELECTROCHEMICAL CORROSION DATA FOR PMS  
MATERIAL IN DIFFERENT GASEOUS ENVIRONMENTS

GAS MIXTURE	$I_{\text{corr}}$ $\mu\text{A}/\text{cm}^2$	$E_{\text{corr}}$ mV S.H.E.	TAFEL SLOPES mV/decade		TYPE OF CONTROL	PITTING POSSIBLE *
			$\beta_a$	$\beta_c$		
A	1.4	-431	30	90	Cathodic	No
N <sub>2</sub>	4.7	-859	60	150	Cathodic	Yes
CO <sub>2</sub>	1.4	-784	60	60	Mixed	Yes
H <sub>2</sub> S	1.7	-852	30	60	Cathodic	Yes
32N <sub>2</sub>	0.2	-653	30	90	Cathodic	Yes
CO	2.3	-801	60	210	Cathodic	Yes
H <sub>2</sub>	1.9	-874	30	60	Cathodic	Yes
H <sub>2</sub> 6	2.1	-862	30	60	Cathodic	Yes
NH <sub>3</sub>	1.4	-901	30	60	Cathodic	No
U	2.5	-788	30	90	Cathodic	Yes

\* Pitting corrosion did not occur under the conditions which this material was tested. However if the working condition changes (increasing electrode potential) in the field condition then this material could experience possible pitting attack.

Corrosion rates and Tafel slopes in tables 5.2, 5.3 and 5.4 were calculated by using the program CORRLOT. It

should be noted that the values in these tables are for a only one test except for the total gas mixture where duplicate testing was conducted and the average values reported. Therefore the discussion that follows is possibly subject to considerable error.

It can be seen in table 5.2 that mild steel has the highest corrosion rate in the  $\text{CO}_2$  environment. When the  $\text{CO}_2$  and CO gas mixtures are combined ( $32\text{N}_2$ ) the corrosion rate of the mild steel is much closer to the CO environment than the  $\text{CO}_2$  environment. In the  $\text{H}_2\text{S}$  environment the corrosion rate of mild steel did not change much as compared to the CO environment. However, in the total gas mixture (U), which represents the simulated coal gasification environment, mild steel has the highest corrosion rate compared of all the materials tested in this environment. Also in  $\text{NH}_3$  environment, mild steel shows the highest corrosion rate among all the materials tested and its corrosion behaviour is similar to the CO,  $32\text{N}_2$  and  $\text{H}_2\text{S}$  environments. From the table 5.3 it can be seen that mild steel shows the highest corrosion rate in deaerated condition among all the materials tested.

The corrosion rate of PMS does not change much in the different gaseous environments. Furthermore, it gives the



lowest overall corrosion rate in the simulated coal gasification environment, of all the materials tested. From the table 5.4 it can be seen this material has small Tafel slopes and the corrosion process is governed by cathodic control in all the gaseous environments except in the  $\text{CO}_2$  environment. Moreover it shows, the highest corrosion rate in the deaerated condition (table 5.3) and its magnitude is one and a half times lower than the mild steel in the same condition. Looking at the  $\text{CO}_2$  gaseous condition it is found that this material has a low corrosion rate. Again if it is examined, in CO gas, the corrosion rate has been elevated somewhat. However the combination of two of these gases together ( $32\text{N}_2$ ) gives even lower corrosion rate than what would be expected (table 5.2). In  $\text{H}_2\text{S}$  gas condition this material shows moderate corrosion rate compared to the other materials. Hydrogen and Hydrogen combination gas conditions ( $\text{H}_2$  and  $\text{H}_2\text{S}$ ) did not show much effect on the corrosion rate of this material (table 5.3). A unique characteristic of this material is that it tends towards pitting corrosion if the working conditions change (increasing electrode potential) relative to the environment in which this material was tested (table 5.4).

316SS material shows its highest corrosion rate in  $\text{CO}_2$  environment and lowest in  $\text{H}_2\text{S}$  environment (table 5.2). Its

corrosion behaviour in  $\text{CO}_2$ , CO and  $32\text{N}_2$  gas conditions is similar to the PMS material however elevated somewhat in corrosion rate. In the  $\text{H}_2\text{S}$  environment its corrosion rate is lowest among all the materials and 5 times lower than the PMS in the same environment. In deaerated condition this material shows a very low corrosion rate which is seven times lower than the PMS in the same condition (table 5.3). Again in  $\text{NH}_3$  environment, 316SS shows very low corrosion rate compared to the other materials. If this material is examined in either the aerated condition or the  $\text{H}_2$  environment the corrosion rate is very close to the PMS material (table 5.3). However in  $\text{H}_2\text{S}$  gas combination, it shows a very low corrosion rate (table 5.3). Finally in total, gas mixture (U), 316SS has a corrosion rate slightly greater than PMS.

The corrosion rate of P31 in  $\text{CO}_2$ , CO and  $\text{H}_2\text{S}$  environments is close to PMS in these environments (table 5.2). However its corrosion rate is elevated in  $32\text{N}_2$  gas condition and U environment but lowered in  $\text{NH}_3$  environment compared to the PMS in these conditions. In the aerated condition, P31 shows a very low corrosion rate (table 5.3). In the deaerated condition and  $\text{H}_2$  environment its corrosion rates are close to the 316SS material, but become lower in

the H26 environment. In the total gas mixture (U), P31 shows a higher corrosion rate than PMS (table 5.2).

Corrosion rates of P751 in  $\text{CO}_2$ , CO,  $32\text{N}_2$ ,  $\text{H}_2\text{S}$ , U and  $\text{NH}_3$  environments are not changed significantly compared to the P31 in same gas mixtures (table 5.2). In comparison to PMS, the corrosion rate of this material in the total gas mixture (U) is increased somewhat. In the aerated condition the corrosion rate of this material is close to the PMS, but is sixteen times lower than the PMS in the deaerated condition (table 5.3). If it is examined in the  $\text{H}_2$  and H26 gas conditions corrosion rates increase to a considerable amount compared to the PMS in the same environments (table 5.3).

Hastalloy C22 shows a vast difference of corrosion rates in different gaseous environments. For instance, its corrosion rate in the CO environment is 33 times higher than in the  $\text{CO}_2$  environment and only 3 times higher in the  $\text{H}_2\text{S}$  environment than in the  $\text{CO}_2$  environment (table 5.2). In the total gas mixture (U) this material has the highest corrosion rate among all the alloy materials. Compared with materials P31 and P751, the corrosion rate of this material has not changed significantly in the total gas mixture (U). In the aerated condition, C22 shows a corrosion rate two

times higher than in the deaerated condition (table 5.3) and does not show any marginal differences in  $H_2$  and  $H_2S$  environments (table 5.3)

Hastalloy C276 behavior with respect to the different environments is similar to the Hastalloy C22 except in  $H_2$  and  $N_2$  environments (table 5.3). These two materials are very close in chemical compositions (tables 4.6 and 4.7) and their corrosion rates in the total gas mixture are similar. The corrosion rate of this material in  $H_2$  environment increased to a high value and it is almost two and half times, in comparison to the C22 in the same environment. In the aerated condition C276 shows a similar corrosion rate to C22. However in the, deaerated condition the corrosion rate of C276 has been elevated five and half times compared to the C22 in the same condition. Compared with PMS material, alloy C276 shows a much higher corrosion rate in  $CO$ ,  $32N_2$  and  $U$  environments (table 5.2). However in aerated, and deaerated conditions it shows a lower corrosion rate compared to the PMS alloy (table 5.3).

C450 shows similar corrosion rates to the C22 and U700 in the  $CO$  environment (table 5.2). It does not show large differences of corrosion rate in different gaseous environments. Furthermore in aerated conditions this

material shows, similar corrosion rates to the P31, F255 and 446SS (table 5.3). In the total gas mixture C450 shows similar corrosion rates to C22 and C276 (table 5.2).

The other materials listed in table 5.2 show different corrosion rates in these various combinations and it can be seen that a synergistic effect occurs when the various gas constituents are combined. For example, Ferralium 255 (duplex alloy) in the  $\text{CO}_2$  environment shows a very low corrosion rate. If it is examined in the CO environment the corrosion rate is somewhat lower. However the combination, of these two gas mixtures gives a higher corrosion rate than what would be expected. F255 material in the total gas mixture shows fairly low corrosion rate compared to the other materials and is very close to the PMS alloy (table 5.2). In  $\text{H}_2$  and H26 environments this material has the lowest corrosion rate among all the materials (table 5.3).

U700 shows a fairly high corrosion rate in the total gas mixture (U), CO and  $\text{H}_2\text{S}$  environments. However it shows, very low corrosion rates in the  $\text{CO}_2$  and  $\text{NH}_3$  environments (table 5.2). If this material is examined in the deaerated condition it is found that it has a very low corrosion rate (table 5.3). Again if it is, examined in the  $\text{H}_2$  environment its corrosion rate has accelerated to a high value. However

a combination, of the two of these gases together gives a higher corrosion rate than what would be expected (table 5.3).

446SS material compared to U700 gives low corrosion rates in the most of gaseous environments (table 5.2 and 5.3). This is likely due to the absence of molybdenum and cobalt in the 446SS alloy (table 4.17).

It can be seen from the table 5.2 that small changes in gas constituents can drastically alter the corrosion rate. This means that it is not straight forward in analyzing or predicting the effect of aqueous corrosion for the various environmental conditions.

Typical potentiodynamic scans for three different materials in three different gaseous environments can be found in figures 5.6 to 5.8. Figure 5.6 shows the polarization behaviour of PMS in  $\text{NH}_3$  environment. Figure 5.7 describes the polarization behaviour of F255 in  $\text{H}_2\text{S}$  environment. Potentiodynamic scan of P751 in  $\text{H}_2\text{S}$  gaseous condition can be found in figure 5.8. Results of the other tests conducted for this project can be found in the reference 43.

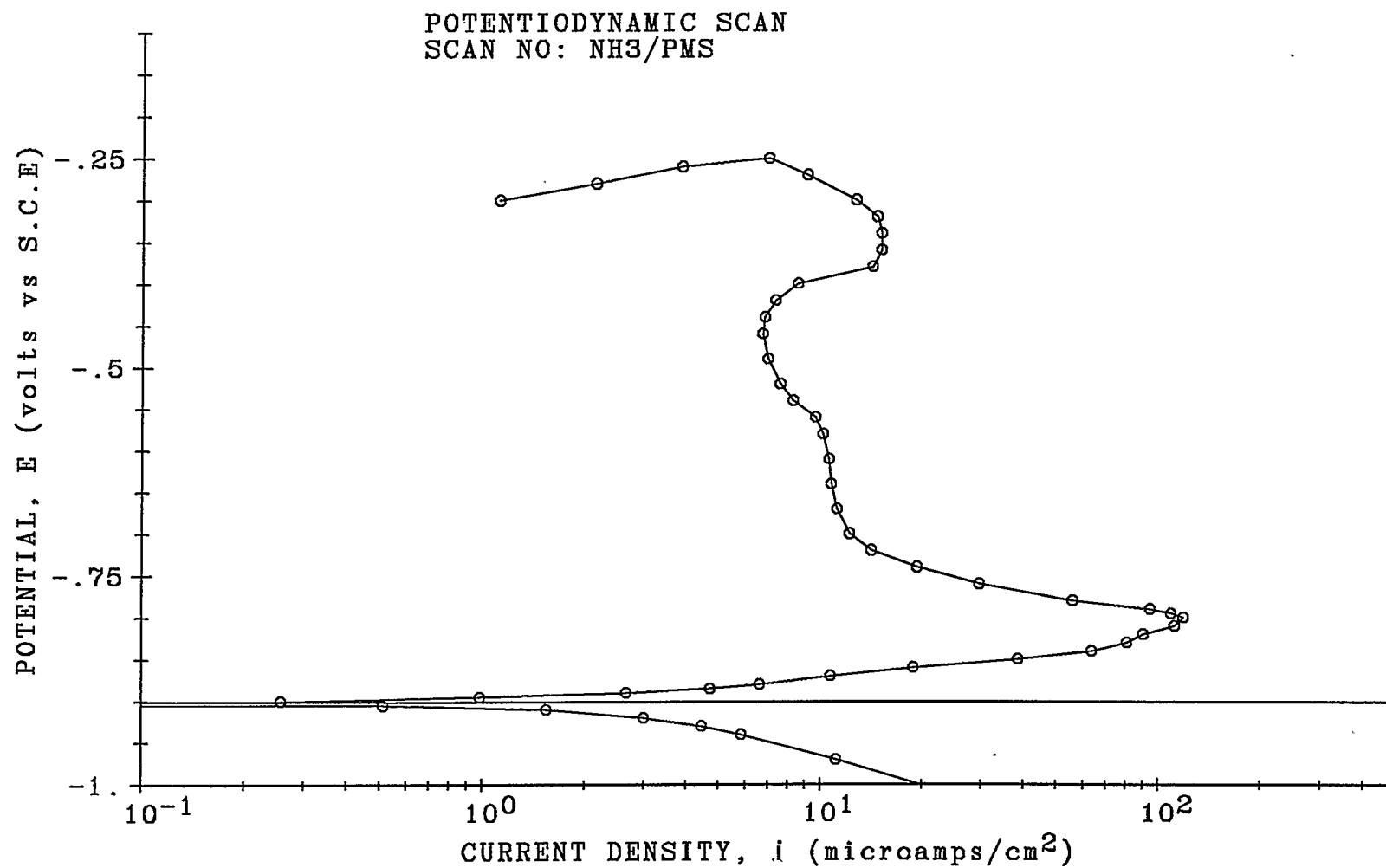


FIGURE 5.6 Potentiodynamic Scan of Fe-Mn-Al Stainless Steel in Ammonia Environment.

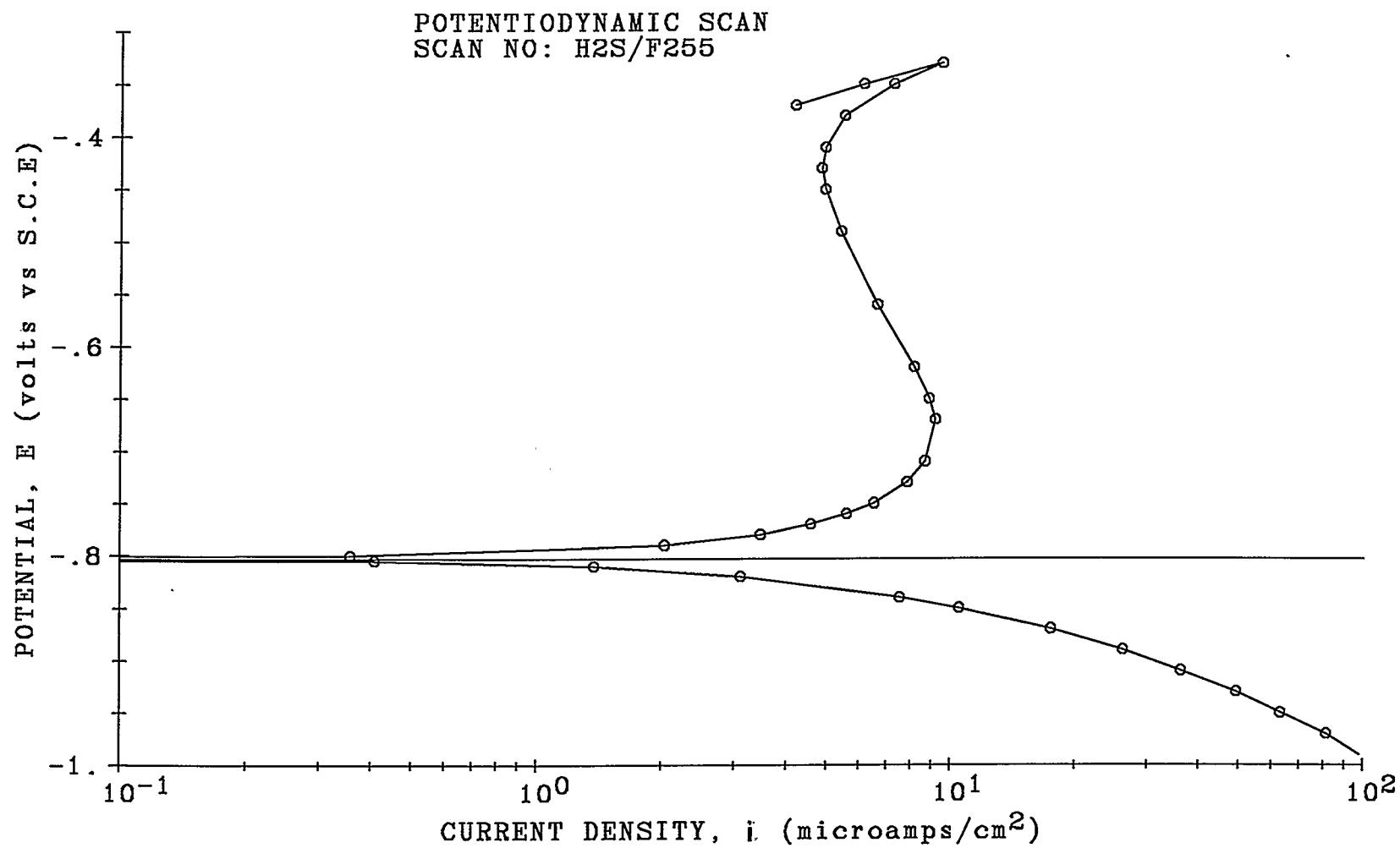


FIGURE 5.7 Potentiodynamic Scan of Ferralium 255 in Hydrogen Sulfide Environment.



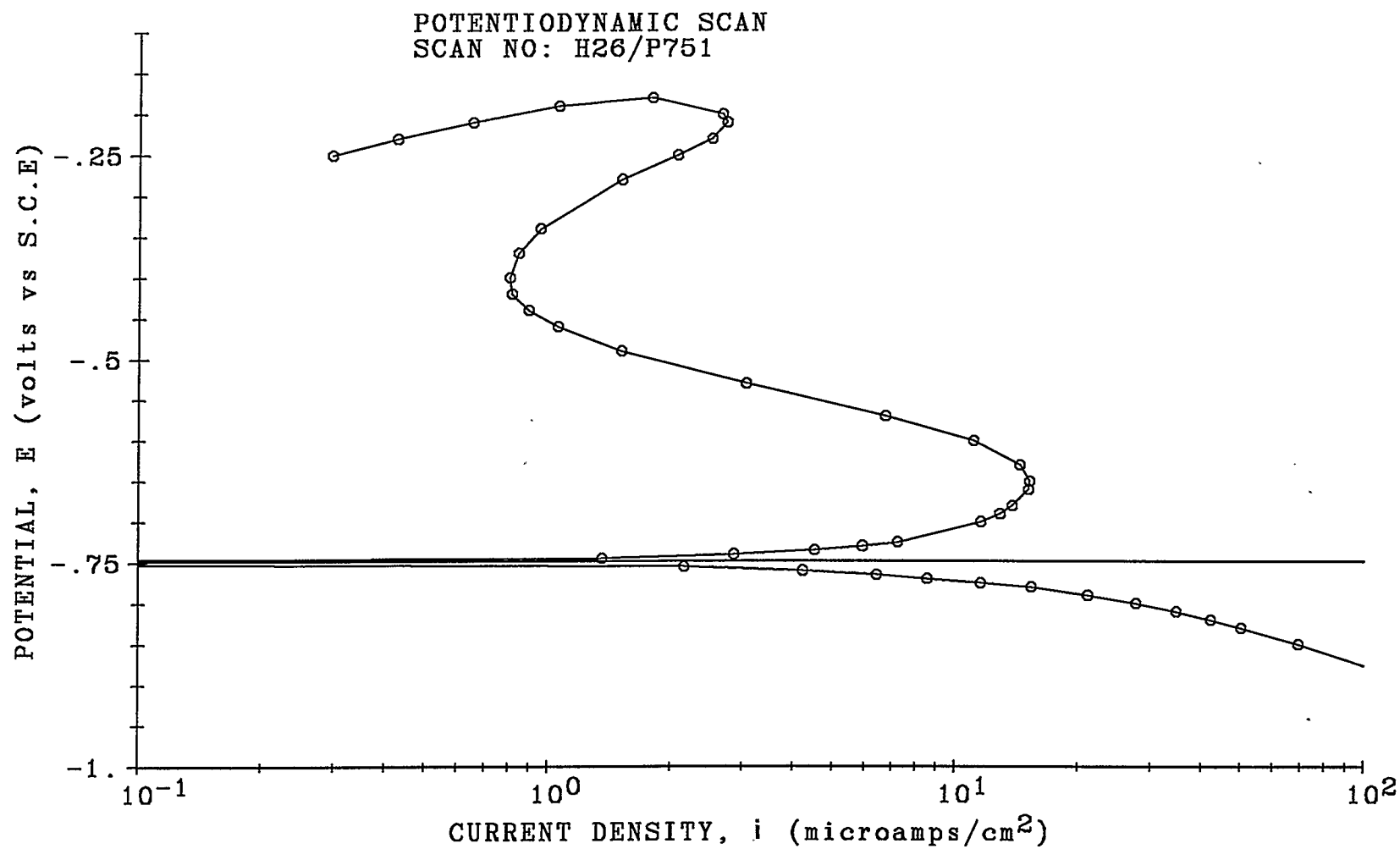


FIGURE 5.8 Potentiodynamic Scan of Pyromet 751 in Hydrogen Gas Combination Environment.

## CHAPTER 6

### GENERAL DISCUSSION AND ANALYSIS

#### 6.1 Introduction

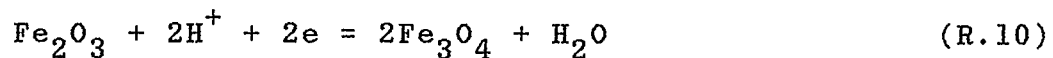
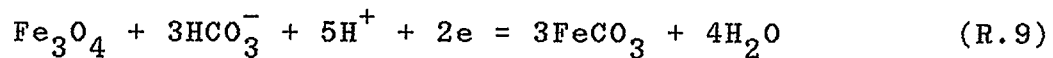
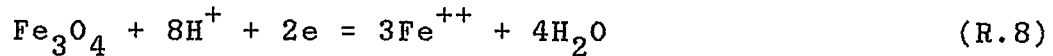
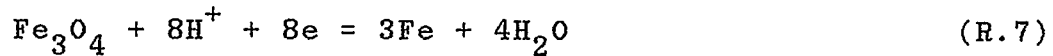
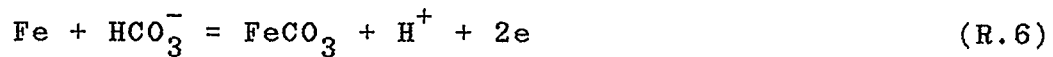
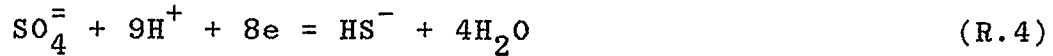
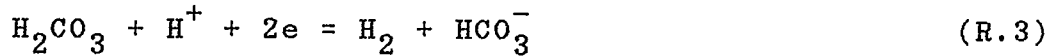
This chapter covers identification of theoretical electrochemical reactions which are most likely to support the corrosion process. These reactions are derived on the basis of thermodynamic equilibrium. This chapter also includes a discussion of the best corrosion resistant material that can be used in the coal gasification environment. Furthermore, pitting tendencies of the materials is also discussed.

#### 6.2 Kinetics of the Corrosion Process

In this section the potentiodynamic results obtained from the experimental studies for mild steel in a deaerated gaseous environment are examined. Analyses of the reactions which represent the total corrosion behavior are also presented here.

##### 6.2.1 Corrosion kinetics in the Nitrogen Environment

Under this environment the following possible reactions are considered for supporting the corrosion process:



The above electrochemical reactions are obtained from the Pourbaix diagrams in [30,31] by considering the solution pH and corrosion potential for N<sub>2</sub>/Mild steel system.

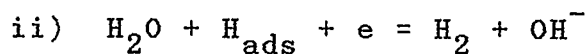
#### (A) Cathodic Partial Reaction Kinetics

##### 1. The Hydrogen Reduction Reaction:



(R.1) can occur with the following step sequences as,

i)  $\text{H}_2\text{O} + \text{e} \xrightarrow{\text{r.d.s.}} \text{H}_{\text{ads}} + \text{OH}^-$ , being the rate determining step, r.d.s,

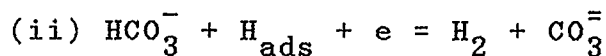
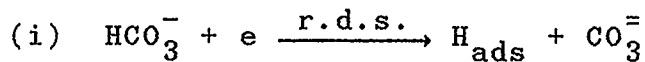


Using step i) as r.d.s.,  $\vec{\alpha}$  (transfer coefficient) can be found as 1/2. The Cathodic Tafel slope can be derived from the eq.(3.20) to be  $\beta_c = 118 \text{ mV/decade}$ . There is not any information of exchange current densities available in the present literature for this specific solution/gas environment. Therefore from here on, all the values of exchange current densities will be assumed. For reaction (R.1)  $i_o = 10^{-7} \text{ A/cm}^2$ . Calculated reversible potential ( $E_r$ ) for this reaction is  $-0.751 \text{ V vs. S.C.E.}$

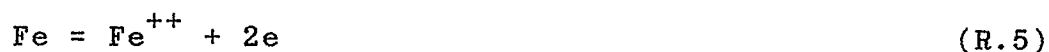
## 2. The Bicarbonate Reduction Reaction:



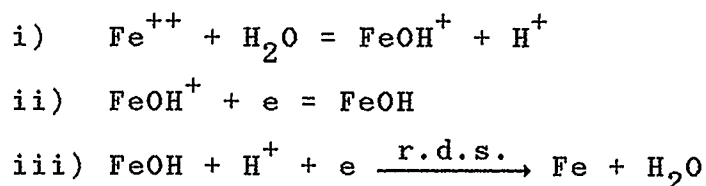
(R.2) can occur with the following step sequences:



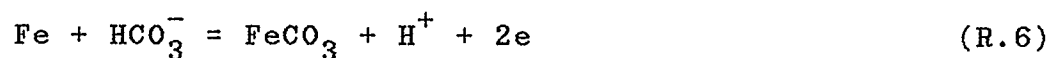
Using step i) as the r.d.s.,  $\vec{\alpha} = 1/2$ ,  $\beta = 118 \text{ mV/decade}$  and  $E_r = -0.615 \text{ V vs. S.C.E.}$ . Assume that  $i_o = 1.5 \times 10^{-7} \text{ A/cm}^2$ .

(B) Anodic Partial Reaction Kinetics1. Iron Oxidation Reaction:

The following step sequence for reaction R.5 was suggested by Schwable et al. [33] and Condit [34]:



Using step iii) as the r.d.s., the transfer coefficient for the anodic Tafel slope can be found as,  $\bar{\alpha} = 1/2$ . Hence,  $\beta_a = 118 \text{ mV/decade}$  and calculated  $E_r = -0.994 \text{ V vs.S.C.E.}$  Exchange current density,  $i_o$ , is assumed to be  $10^{-7} \text{ A/cm}^2$ .

2. Formation of  $\text{FeCO}_3$  through  $\text{HCO}_3^-$ :

The following step sequences can occur for the reaction (R.6).

- i)  $\text{FeCO}_3 + \text{H}^+ = \text{Fe}^{++} + \text{HCO}_3^-$
- ii)  $\text{Fe}^{++} + \text{H}_2\text{O} = \text{FeOH}^+ + \text{H}^+$
- iii)  $\text{FeOH}^+ + \text{e} = \text{FeOH}$
- iv)  $\text{FeOH} + \text{H}^+ + \text{e} \xrightarrow{\text{r.d.s.}} \text{Fe} + \text{H}_2\text{O}$

Using step iv) as the r.d.s., the appropriate transfer coefficient for anodic Tafel slope can be found as  $\bar{\alpha} = 1/2$ . Hence,  $\beta_a = 118 \text{ mV/decade}$  and calculated  $E_r = -0.766 \text{ vs. S.C.E.}$  Exchange current density,  $i_o$ , is assumed to be  $6 \times 10^{-7} \text{ A/cm}^2$ .

#### 6.2.2 Total Cathodic and Anodic Polarization Curves

The polarization characteristics of cathodic and anodic reactions which were given in the preceding subsections are shown as in the figure 6.1. Figure 6.2 represents the total polarization behaviour (theoretical and experimental) of mild steel in deaerated conditions. It can be seen from the figure 6.2 that experimental polarization characteristics closely match the theoretical values.

After comparing the Tafel slopes and reversible potentials for the reactions listed under section 6.2.1 to the experimental data, only a few reactions were found to be close to the measured information. These were reactions

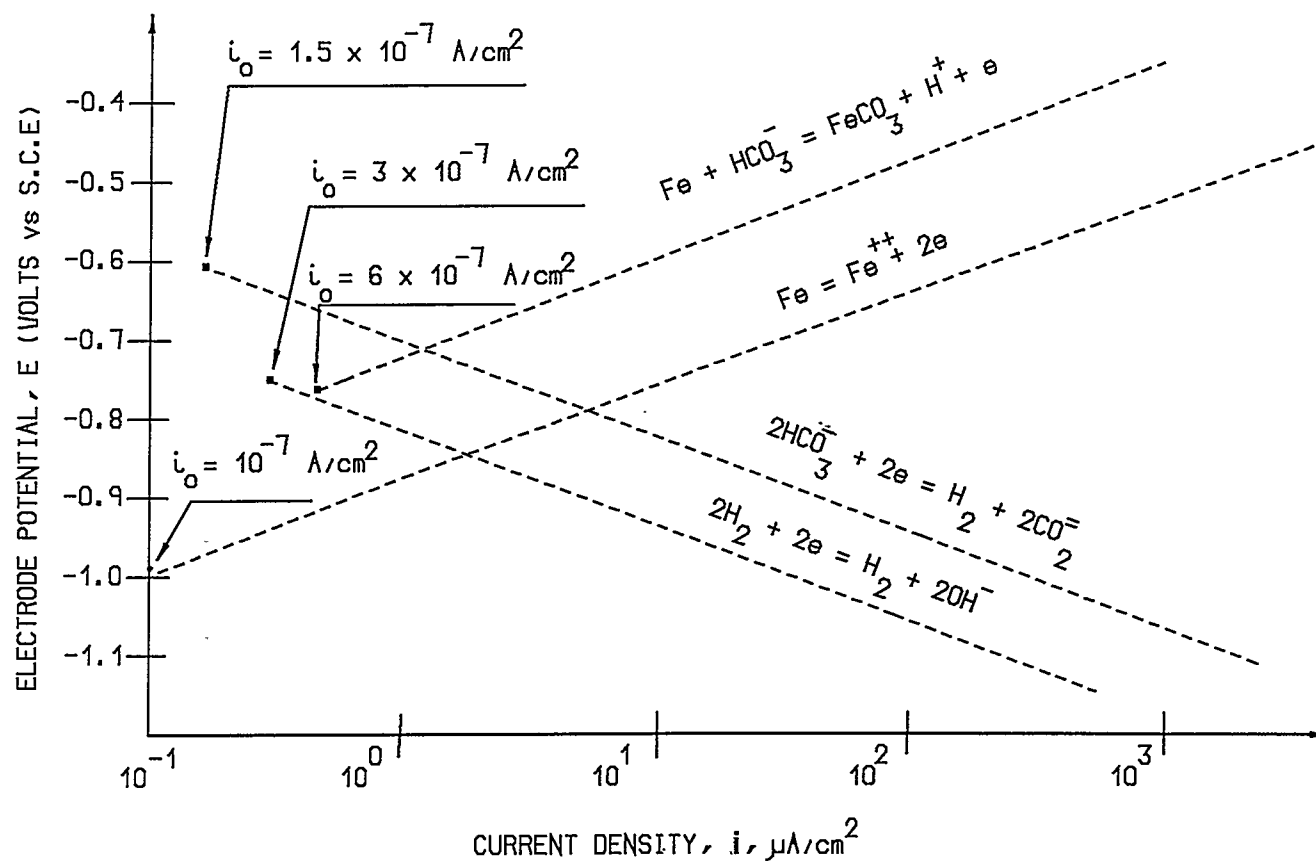


FIGURE 6.1 THEORETICAL ANODIC AND CATHODIC POLARIZATION CHARACTERISTICS FOR MILD STEEL IN NITROGEN SATURATED SOLUTION

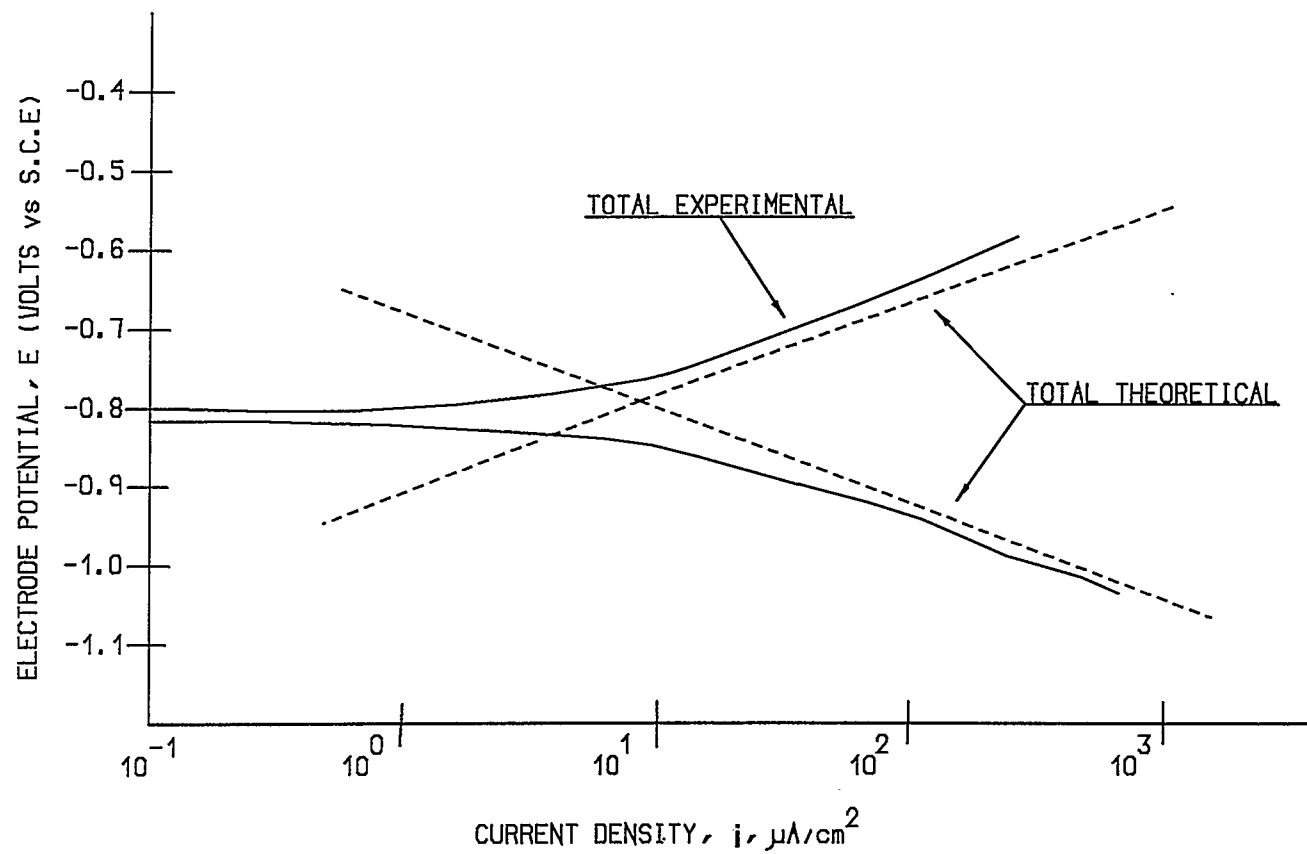


FIGURE 6.2 THEORETICAL AND EXPERIMENTAL POLARIZATION CURVES FOR MILD STEEL IN NITROGEN SATURATED SOLUTION



(R.1), (R.2), (R.5) and (R.6). The other reactions were found to be far removed from experimental values and therefore could be discounted as contributing to the corrosion processes.

### 6.3 Corrosion Resistance of Materials Under Variable Concentration of Gas Composition in Coal Gasification Environment

PMS shows the lowest corrosion rate for a condition which is close to the simulated coal gasification environment (table 5.2). However, for other environments with a very high  $\text{CO}_2$  content, then Hastalloy C22 would be the best corrosion resistant material. The PMS material has an acceptable corrosion rate in the  $\text{CO}_2$  environment and on a cost comparison would then be preferable over Hastalloy C22.

If the CO environment is predominant, then Ferralium 255 would be the best corrosion resistant material to be used in that environment (table 5.2). Again considering, the cost factor, PMS material can still be used since the corrosion rate of this material ( $i_c = 1.74 \mu\text{A}/\text{cm}^2$ ) results in an acceptable value.

316 stainless steel shows the lowest corrosion rate ( $i_c = 0.35 \mu\text{A}/\text{cm}^2$ ) compared to all the materials tested in

the  $H_2S$  environment. If the  $H_2S$  content increases in the simulated coal gasification environment such that it dominates, then 316 stainless steel would be the best corrosion resistant material in that environment. However, considering the cost factor, PMS material can still be used in an environment which has a high content of  $H_2S$ . This is because the corrosion rate ( $i_c = 1.74 \mu A/cm^2$ ) of the PMS material in the  $H_2S$  environment exhibits an acceptable value.

In a high Ammonia concentration environment Pyromet 31 would be the best corrosion resistant material to use. This is due to the lowest corrosion rate ( $i_c = 0.31 \mu A/cm^2$ ) of Pyromet 31 in  $NH_3$  environment. By considering the cost factor, PMS material can still be used in a high content of  $NH_3$  condition since it shows a corrosion rate of only  $1.42 \mu A/cm^2$ .

#### 6.4 Effect of Anion Concentration on the Corrosion Rate in Coal Gasification Environment

All the tests were done based upon the solution composition given in table 4.15. This composition is the best estimate of actual conditions from available information to date. However, if the anion concentration or ratio changed somewhat in the actual field condition, then

the corrosion rate of those materials could be changed significantly.

For example, Condit [34] showed that increasing  $\text{Cl}^-$  concentration caused the rapid increase of corrosion rate of Fe-25 Ni alloy. In general, depending on the  $\text{Cl}^-$  ion concentrations, pitting corrosion can be found in most of the steel alloys. Therefore, increasing  $\text{Cl}^-$  ion concentrations in the field environment would give different corrosion rates than what has been measured in this investigation. Unexpected pitting attack may also occur.

Ogundele [31] noted that the variation of  $\text{SO}_4^{=}$  ion concentration did not have much effect on the corrosion rate of the API-5AC-L-80 steel. However, if the  $\text{SO}_4^{=}$  ion concentration changes considerably in the actual field environment then the corrosion rate of the materials tested could behave differently. The reason for this is that the chromium content in the material has a greater influence on corrosion in the presence of  $\text{SO}_4^{=}$  ions [17]. Increasing  $\text{HCO}_3^-$  ion concentration has the effect of increasing the corrosion rate of iron. This was noted by Ogundele [31] and Davies, et al. [35]. Therefore, it is possible to have a higher corrosion rate in an environment which contains a

higher concentration of various ions than those examined in this investigation.

#### 6.5 Pitting Tendency of the Materials

All of the materials tested here did not show pitting corrosion in this work. However, if the working condition changes (increasing electrode potential,  $\text{Cl}^-$  ion concentration or temperature) in an actual coal gasification environment, then PMS material may show possible pitting attack. This is because the PMS material showed a critical pitting potential,  $E_{pr}$ , above the open circuit potential. If the electrode potential,  $\text{Cl}^-$  ion concentration or temperature increases, then  $E_{pr}$  will be lowered to more active potentials and pitting corrosion can occur. This is an important aspect that needs to be looked at for use of this material.

## CHAPTER 7

### EFFECT OF ALLOY COMPOSITION ON CORROSION

#### 7.1 Introduction

In this chapter factors influencing the corrosion resistance of materials will be discussed. In addition to this, the effect of the metallurgical constituents on corrosion are also presented.

#### 7.2 Methods for Developing Corrosion Resistant Alloys

In chapter 3, factors  $E_{pp}$ ,  $E_p$ ,  $i_p$  and  $E_b$  relevant to passivity were discussed in detail. There are two general methods for developing new, corrosion-resistant alloys by means of anodic polarization methods:

Method 1. Increasing ease of passivation of the given metal is accomplished by reducing its critical anodic current density ( $i_c$ ) or shifting its primary passive potential ( $E_{pp}$ ) to more active potentials. This can be achieved by changing anodic dissolution behaviour by alloying.

Method 2. Increasing passivation tendency by increasing the rate of the cathodic reaction.

Effectively, this technique changes the system from either case 1 or 2 to case 3 as shown in Figure 3.8. This can be accomplished by coupling to, or alloying with, a noble metal having a high exchange current density for the reduction process.

### 7.3 Effects of Alloying on the Corrosion Resistance of Materials

Considering anodic polarization curves which were obtained from all the materials tested in the total gas mixture (U) the characteristics of passivity are tabulated as shown in the table 7.1. Mild steel did not passivate under this environment.

TABLE 7.1  
CHARACTERISTIC PASSIVATION VALUES OF MATERIALS TESTED IN  
THE TOTAL GAS MIXTURE (U)

Alloy	Composition	$i_c$ $\mu\text{A}/\text{cm}^2$	$E_p$ Volts	$i_p$ $\mu\text{A}/\text{cm}^2$
446SS	26 Cr, 0.45 Mo, 0.15 N	12.0	-0.33	9.5
F255	27 Cr, 6 Ni, 3.5 Mo	11.0	-0.36	7.0
C450	15 Cr, 7 Ni, 1.5 Cu	16.5	-0.42	4.8
	Ferritic ↑			
	Austenitic ↓			
316SS	19 Cr, 11 Ni	6.6	-0.44	3.7
P31	57 Ni, 23 Cr, 2.3 Ti, 2 Mo	8.4	-0.4	7.5
P751	71 Ni, 15 Cr, 2.4 Ti,	13.0	-0.43	3.9
U700	55 Ni, 15 Cr, 17 Co, 5 Mo	13.5	-0.39	5.2
C22	58 Ni, 14 Cr, 17 Mo, 4 W	15.0	-0.41	5.3
C276	56 Ni, 15 Cr, 17 Mo, 4 W	11.0	-0.43	3.5
PMS	30 Mn, 8 Al, 1.5 Si	90.0	-0.63	17.5

By considering the corrosion resistance of the ferritic alloys there is not much difference between steel type 446SS and F255. It can be seen from the table 7.1 that critical anodic current densities ( $i_c$ ) and passivation potential ( $E_p$ ) for those materials are close to each other (figures 7.1 and 7.2). Therefore, the tendency to passivation of both materials is the same. The similarity in the  $i_c$  values is because the chromium content in the



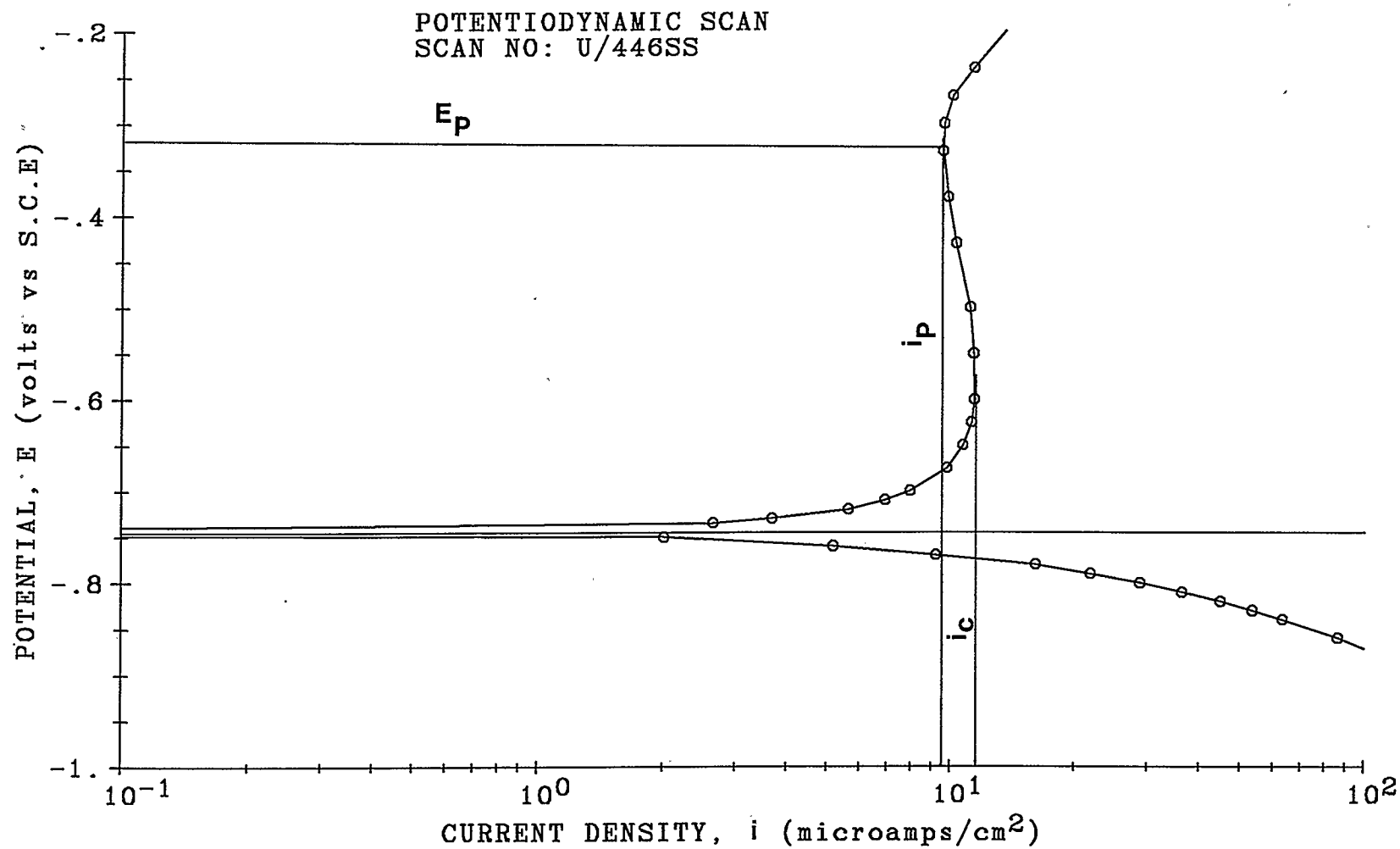


FIGURE 7.1 Passivation Characteristics of 446 Stainless Steel in Total Gas Mixture.

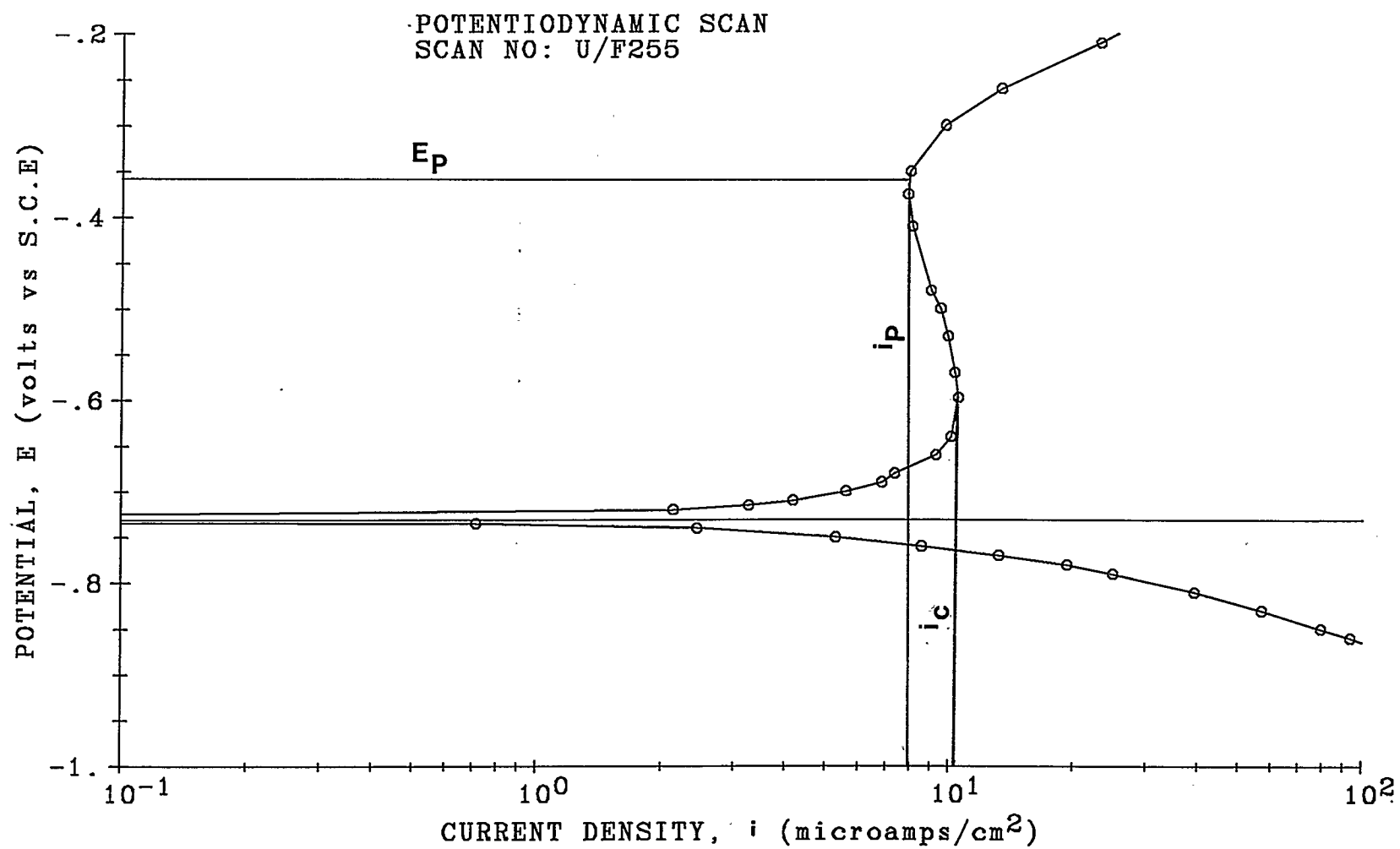


FIGURE 7.2 Passivation Characteristics of Ferralium 255 in Total Gas Mixture.

composition does not change much between both alloys and the nickel content is too low to have much effect. When the chromium content decreases a considerable amount as in the alloy C450, then  $i_c$  increased to  $16.5 \mu\text{A}/\text{cm}^2$  from  $11 \mu\text{A}/\text{cm}^2$  (F255) and  $E_p$  also decreased from  $-0.36 \text{ V}$  (F255) to  $-0.42 \text{ V}$  (C450) (figure 7.3). In addition to this, the lowest corrosion current in the passive state ( $i_p = 4.8 \mu\text{A}/\text{cm}^2$ ) can be found in the alloy which contains the lowest amount of chromium content (C450).

Considering the austenitic steels, 316SS shows a lower value of  $i_c$ , from  $16.5 \mu\text{A}/\text{cm}^2$  (C450) to  $6.6 \mu\text{A}/\text{cm}^2$  (figure 7.4). This can be due to the increase in nickel content. This relationship between composition and  $i_c$  was noted by Prazak [36]. Also, 316SS shows the lower value of  $E_p = -0.44 \text{ V}$  and  $i_p = 3.7 \mu\text{A}/\text{cm}^2$ .

The characteristics of steel type P31 include  $i_c$  and  $E_p$  values (figure 7.5) that are greater than for the 316SS alloy. Although one would expect that the high content of chromium and Nickel in the composition of P31 would have given a low value of  $i_c$  compared to the 316SS, the value of  $i_c = 8.4 \mu\text{A}/\text{cm}^2$  in P31 is probably attributed to the presence of the other alloys, possibly titanium or aluminum. High corrosion current in the transpassive area

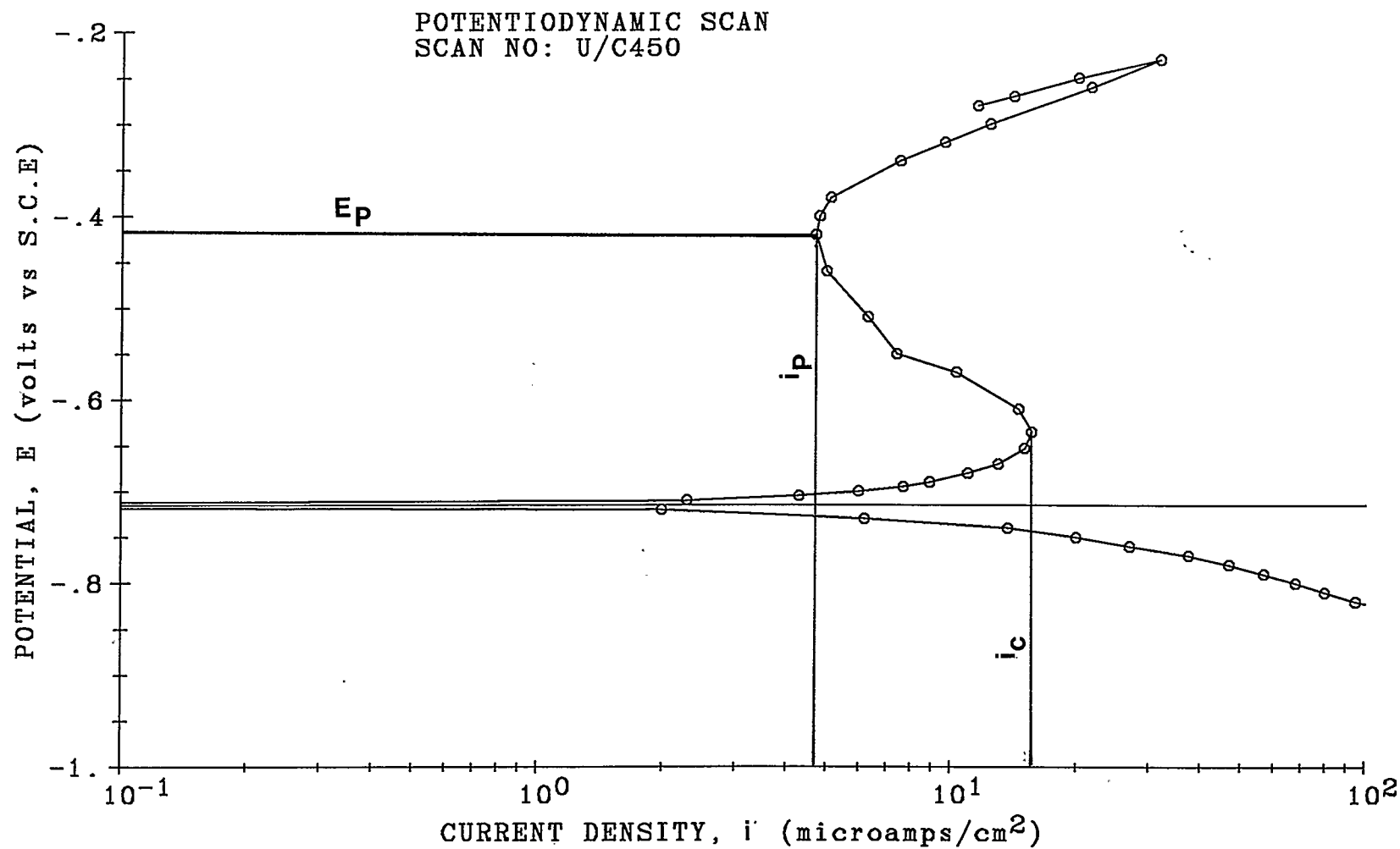


FIGURE 7.3 Passivation Characteristics of Custom 450 in Total Gas Mixture.

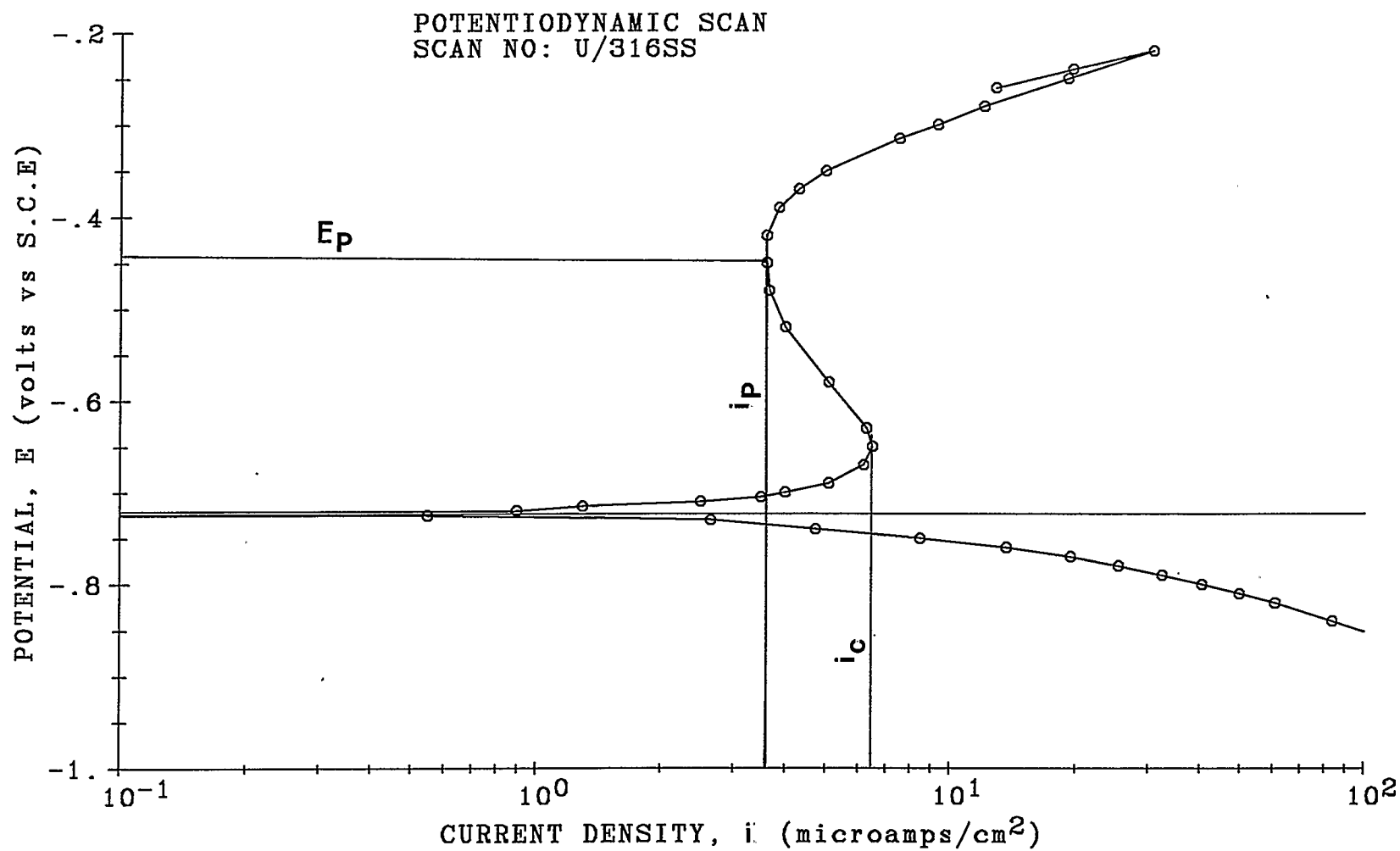


FIGURE 7.4 Passivation characteristics of 316 Stainless Steel in Total Gas Mixture.

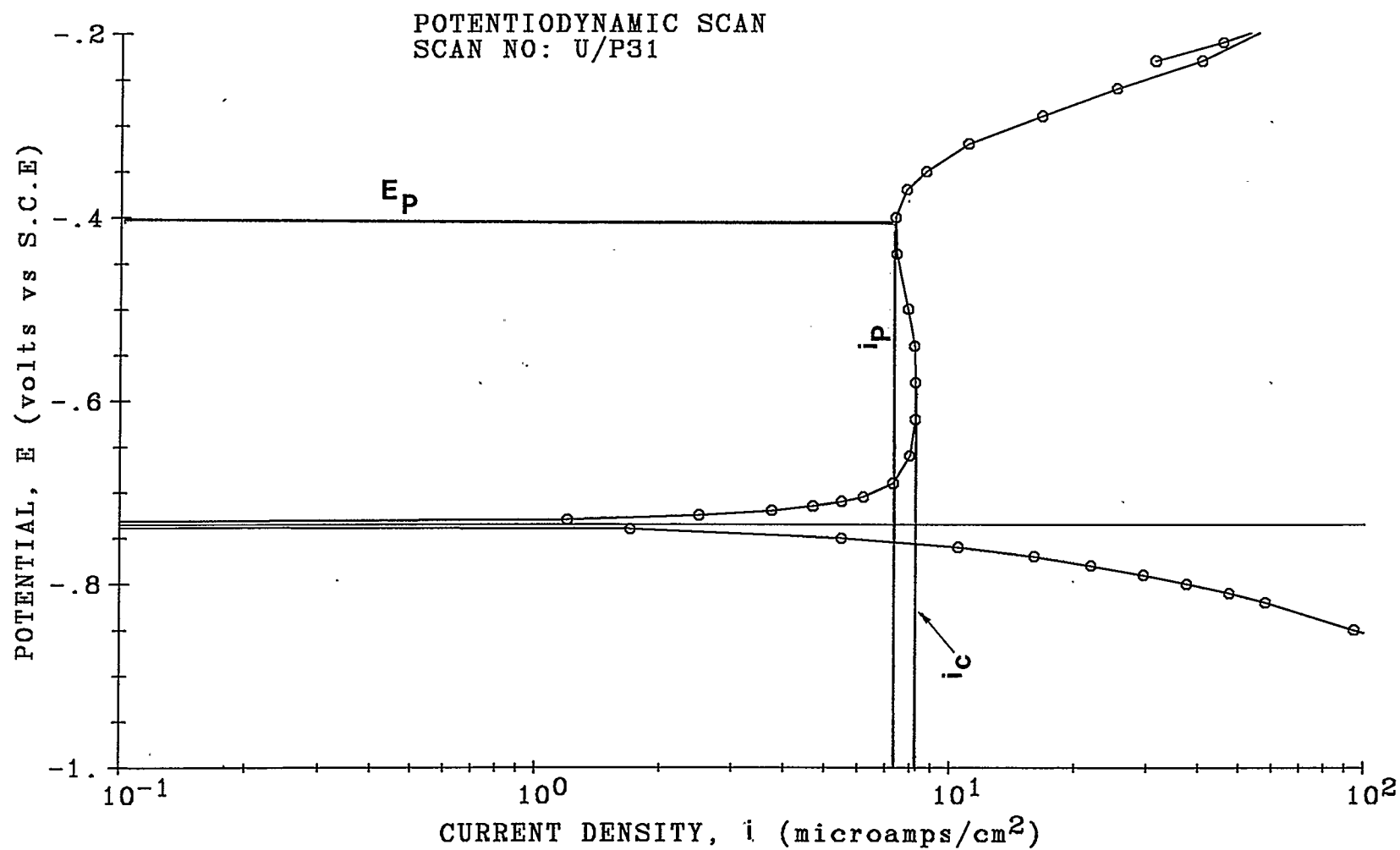


FIGURE 7.5 Passivation Characteristics of Pyromet 31 in Total Gas Mixture.

(figure 7.5) shows that molybdenum in the composition influences this increment of the current. On the other hand, this high current in the transpassive area can be the cause of lower corrosion resistance of such a material in a highly oxidizing medium [36]. Furthermore, low differences between values of  $i_c$  and  $i_p$  (table 7.1) of the P31 material reflects that a limiting anodic diffusion current exists.

When comparing the corrosion resistance of the alloy P751 against alloy P31, alloy P751 shows higher anodic critical current density of  $i_c = 13.0 \mu\text{A}/\text{cm}^2$ . This is due to the higher content of nickel in the alloy P751. Large differences between  $i_c$  and  $i_p$  in alloy P751 (figure 7.6) results because of the absence of molybdenum. Since chromium and nickel in the compositions of U700 and C22 are not much different from each other,  $i_c$ ,  $i_p$  and  $E_p$  (figures 7.7, 7.8 and table 7.1) values of these materials are comparatively close to each other. Although alloy C276 is very similar to the C22 in chemical composition,  $i_c$  (figure 7.9) values of these materials show considerable differences. It could be either due to differences of nickel content in the composition or metal processing or heat treatment of the two alloys.

The PMS alloy (figure 7.10) shows the highest critical anodic current density ( $i_c = 90 \mu\text{A}/\text{cm}^2$ ) among all the

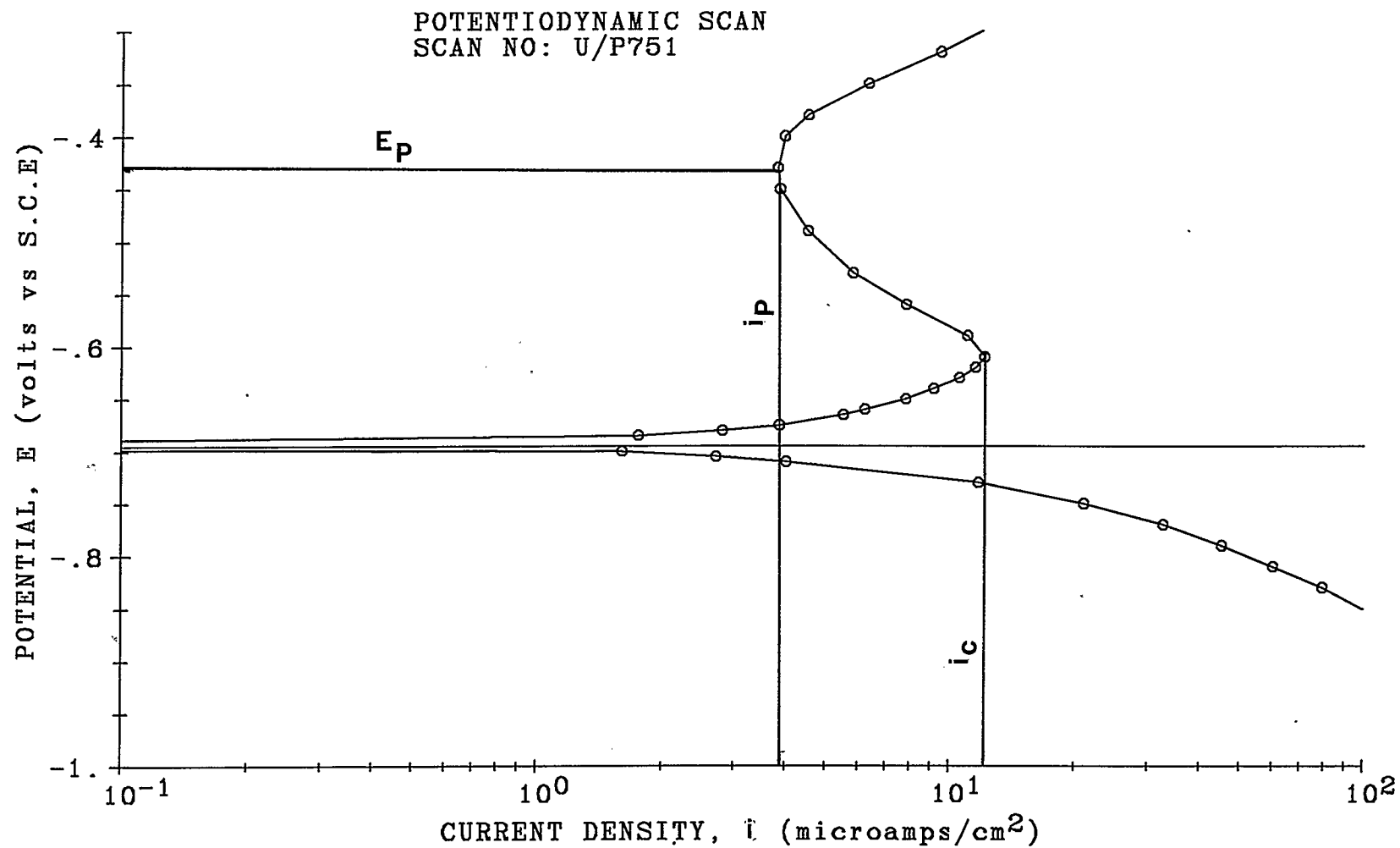


FIGURE 7.6 Passivation Characteristics of Pyromet 751 in Total Gas Mixture.



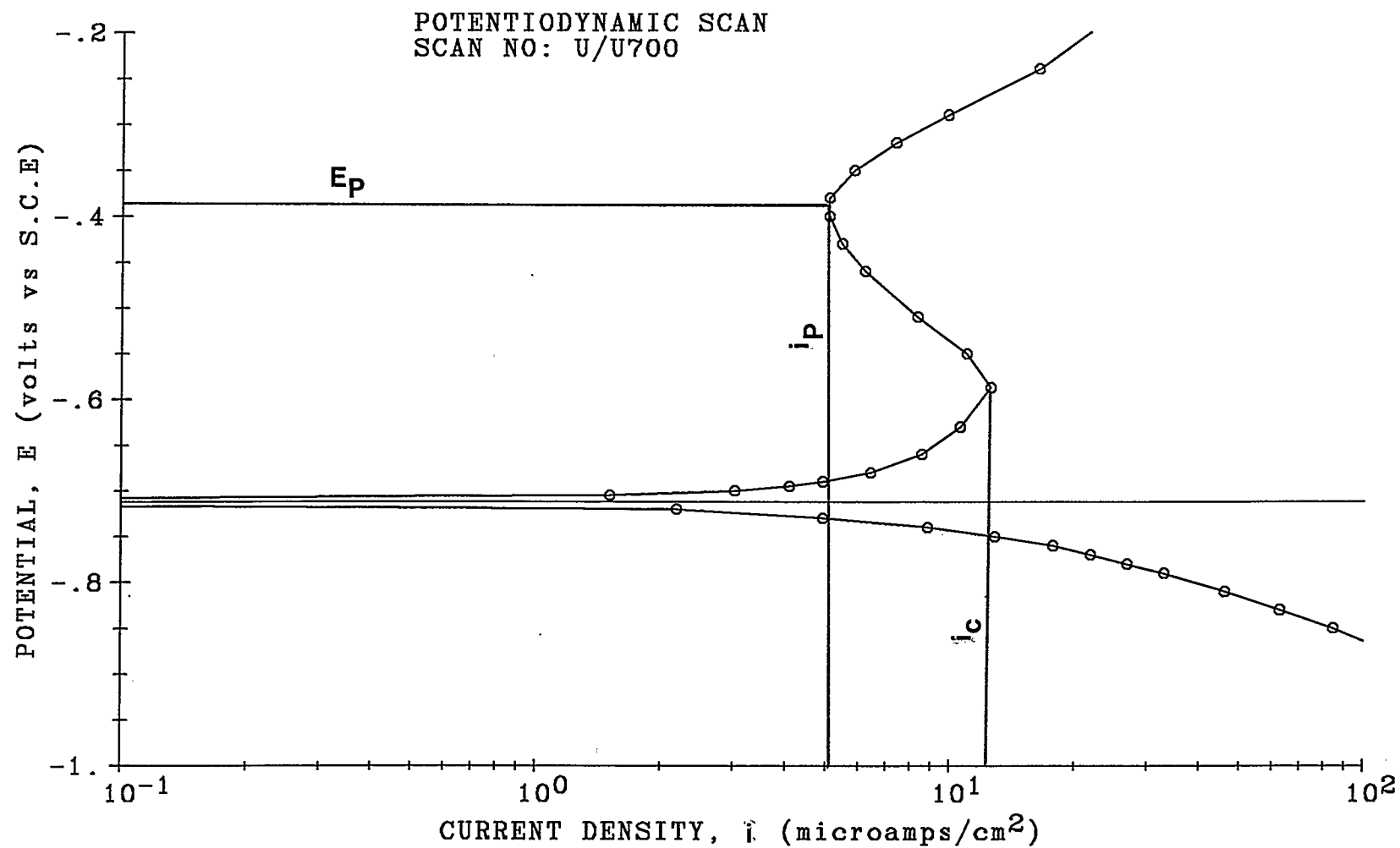


FIGURE 7.7 Passivation Characteristics of Udimet 700 in Total Gas Mixture.

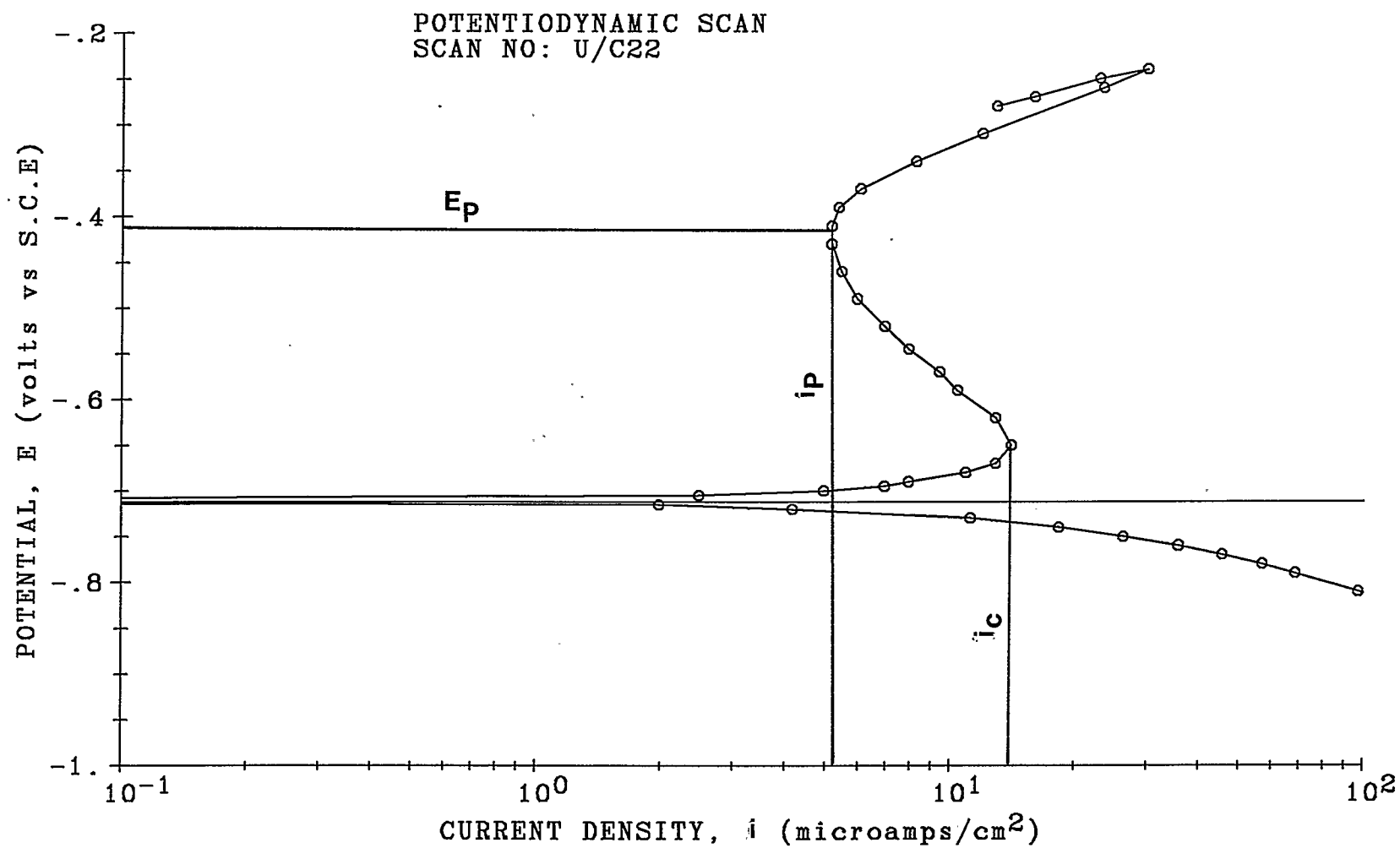


FIGURE 7.8 Passivation Characteristics of Hastalloy C22 in Total Gas Mixture.

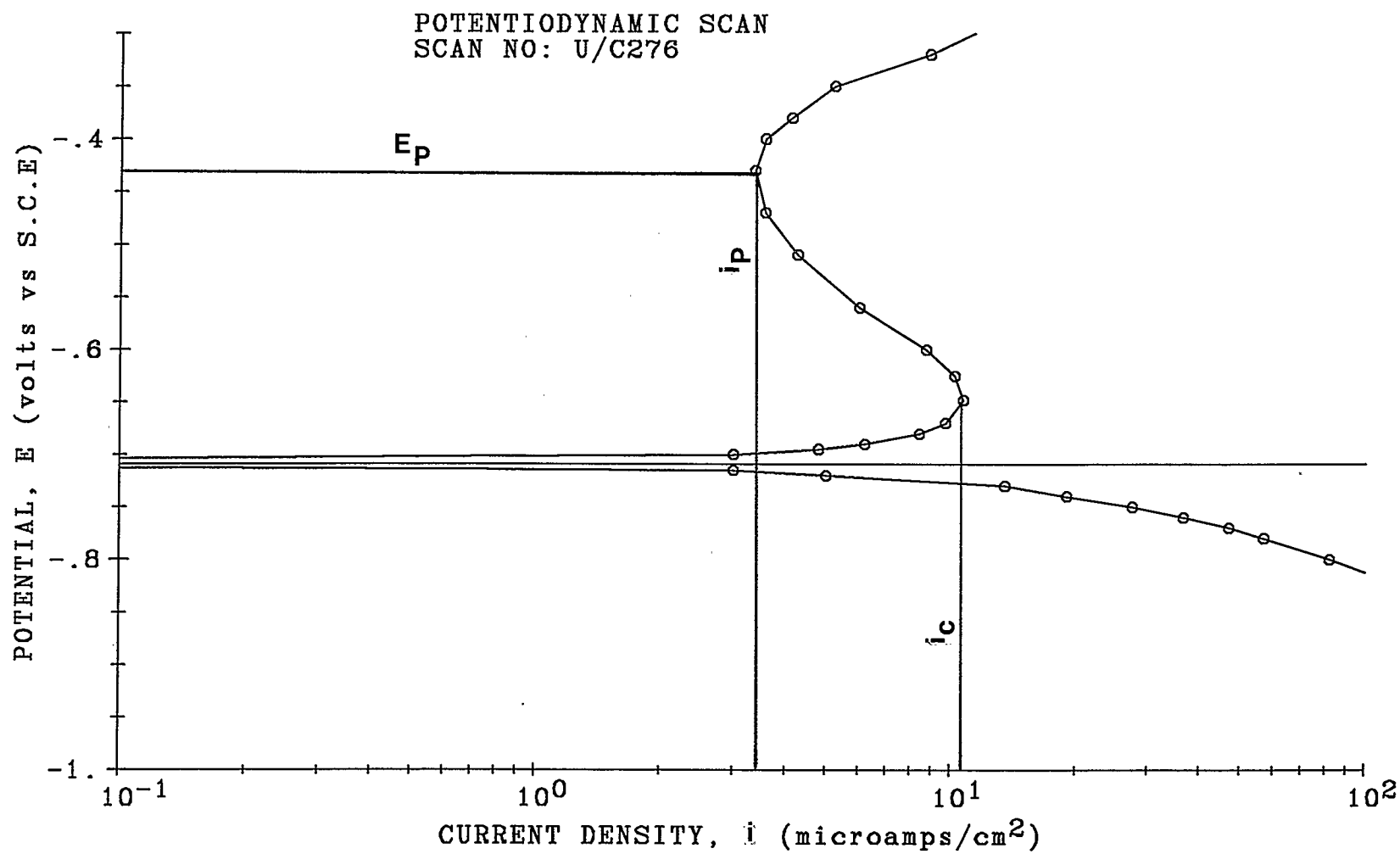


FIGURE 7.9 Passivation Characteristics of Hastalloy C276 in Total Gas Mixture.

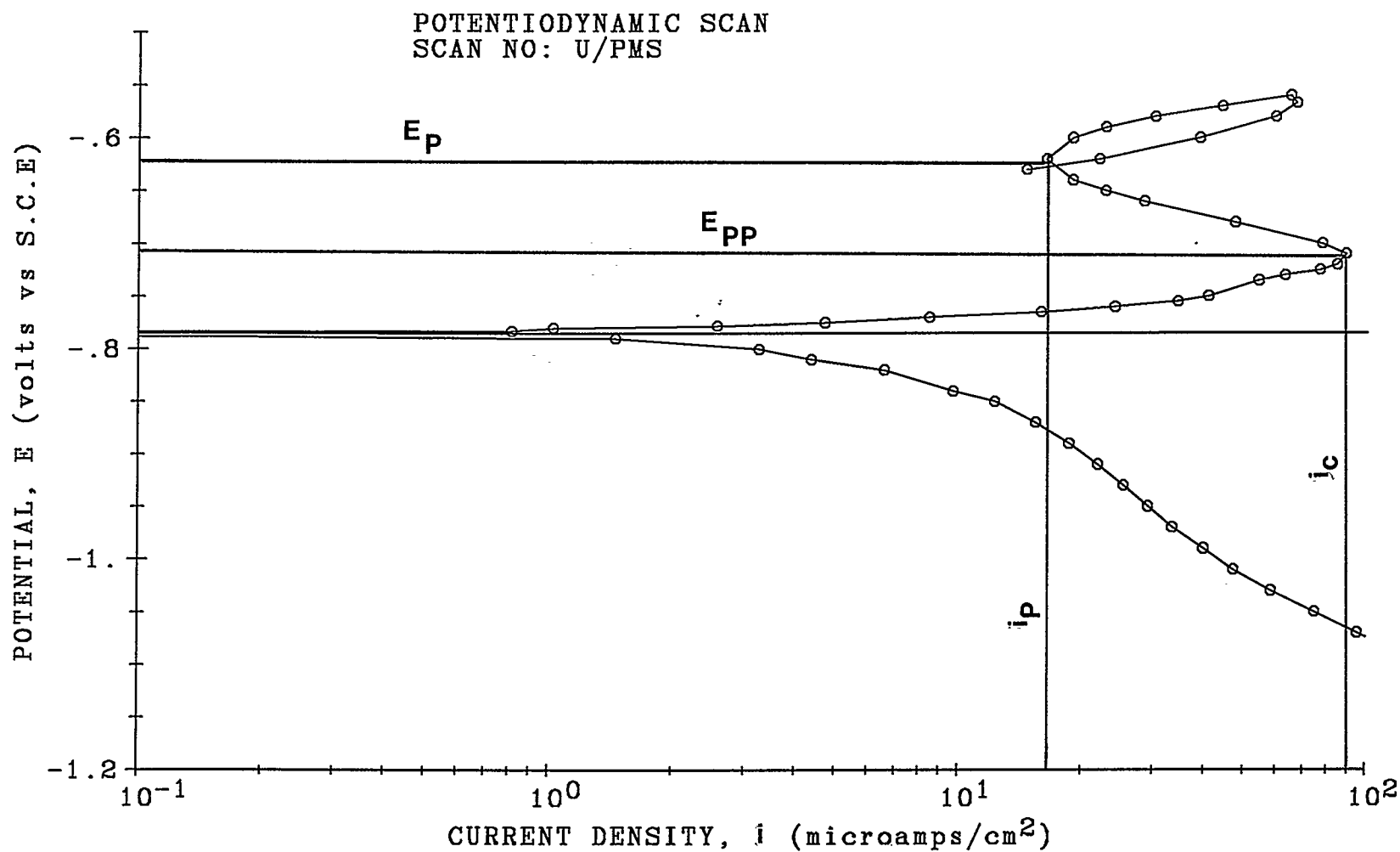


FIGURE 7.10 Passivation Characteristics of Fe-Mn-Al Stainless Steel in Total Gas Mixture.

materials. This is due to the absence of chromium and nickel content in the alloy composition. Since all the materials were exposed to an environment which contains an activation controlled reduction process, the best approach to selecting a corrosion resistant alloy is to find the material with the lowest primary passive potential ( $E_{pp}$ ). Obviously PMS alloy is the best corrosion resistant material under this environment, since it shows the lowest value of  $E_{pp} = -0.71$  V (figure 7.10).

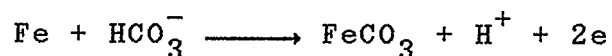
If any effort is made to develop a new alloy based on the above mentioned characteristics, one should be cautioned about certain limitations. These are as follows:

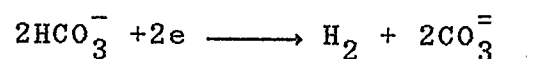
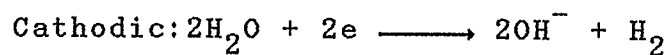
1. The above mentioned principles apply only to metals which demonstrate active-passive transition.
2. The noble metal additions normally decrease the corrosion resistance of active-passive metals in a highly oxidizing environment.
3. The addition of noble metals to non-passivating metals tends to increase the corrosion rate.

CHAPTER 8  
CONCLUSIONS

1. The calculation of corrosion current density ( $i_{\text{corr}}$ ) for the different materials using the linear polarization technique did not give good results except for mild steel.
2. Fe-Mn-Al stainless steel showed the lowest corrosion rate among all the materials tested when exposed to a condition which attempted to simulate the coal gasification environment. Mild steel showed the highest corrosion rate under the same condition.
3. Except for mild steel and 316 stainless steel, all the other materials showed low corrosion rate in the CO<sub>2</sub> environment.
4. In the CO environment all the materials showed moderate corrosion rate except Ferralium 255.
5. Combination of CO<sub>2</sub> and CO gaseous environment drastically changed corrosion rates of some of the materials.

6. Except Udimet 700, most of the materials in the H<sub>2</sub>S environment showed low corrosion rates.
7. The NH<sub>3</sub> environment and aerated condition did not show any significant changes in corrosion rate of most the materials.
8. It was observed that small changes of gas constituents drastically altered the corrosion rate some materials.
9. None of the materials showed any possible pitting corrosion under the environment in which they were tested. However, the material with the highest tendency towards pitting attack is the Fe-Mn-Al stainless steel.
10. The kinetic analysis of the polarization curve (Fig. 6.1) showed that the reactions listed below were responsible for the corrosion of the mild steel in the deaerated condition:





11. Examining the effect of alloy content shows that chromium content has the greatest influence on the critical anodic current density ( $i_c$ ).
12. Under activation controlled reduction processes, Fe-Mn-Al stainless steel showed the lowest primary passive potential and hence proved to be the best corrosion resistant alloy among the select materials tested in the simulated coal gasification environment.



## CHAPTER 9

### RECOMMENDATIONS FOR FUTURE WORK

1. Further corrosion behaviour of the materials should be studied by changing the concentration and the temperature of the test solution.
2. Since CO, CO<sub>2</sub> and H<sub>2</sub>S gas constituents have a large effect on the corrosion behaviour of materials tested, attempts should be made to do more extensive tests with different concentrations of the above mentioned gases.
3. There is a lack of information available on exchange current densities in the current literature. Therefore attempts should be made to determine this information by experimentation for specific solution/gas environments.
4. During the start up and shut down procedures in the coal gasification plant there may be low concentrations of moist air in the environment. Further corrosion studies with air in the total gas mixture should be carried out.

5. Since Fe-Mn-Al material has the highest tendency towards the pitting attack, more investigation should be carried out on this material.

REFERENCES

1. Arnold, J.M., "An Overview of Metal Properties Council Materials Studies in Gasification Pilots Plants", The Properties and Performance of Materials in the Coal Gasification Environment, Ed. V.L. Hill and H.L. Black, ASM, 1985, pp. 39-63.
2. MacNab, A.J., Schultz, C.A. and Black, H.L., "Materials for Gasification, MPC Program and Priorities", The Properties and Performance of Materials in the Coal Gasification Environment, Ed. V.L. Hill and H.L. Black ASM, 1981, pp.7-24.
3. Hebsur, M.G., "A Brief Survey of Attempts to Develop Corrosion/Erosion Resistant Materials for Coal Gasification", Applied Energy, Vol.15, 1983, pp.99-126.
4. Baylor, V.B. and Keiser, J.R., "Corrosion and Stress Corrosion Cracking in Coal Liquefaction Processes", Materials to Supply the Energy Demand, Ed. E.B. Hawbolt and A. Mitchell, ASM, 1981, pp. 271-310.
5. Bakker, W.T., Perkins, R.A. and Van Lierre, J., "Corrosion of Syngas Coolers of Coal Gasification, Combined Cycle Power Plants", Materials Performance, Vol.24, 1985, pp. 9-17.

6. Keiser, R.J. and Olsen, A.R., "Corrosion Studies in Coal Liquefaction Plants", Microstructure Science, Vol. 12, 1985, pp. 173-186.
7. Bhattacharyya, S., Hales, C. and Hill. V. "Erosion/Corrosion of Materials in Coal Gasifier Environment", Corrosion-Erosion Behaviour of Materials, Ed. K. Natesan, AIME:1980, pp. 244-267.
8. Baxter, D.J. and Natesan, K. "The Corrosion Behaviour of Fe-Cr-Ni-Zr Alloys in Coal Gasification Environments at High Temperatures", Corrosion Science, Vol. 26, No. 2, pp. 153-172.
9. Natesan, K., "High-Temperature Corrosion in Coal Gasification System, Corrosion, Vol. 41, No. 11, 1985, pp. 646-655.
10. Jones, J.P., Buchheim, G.M., Lendvai-Lintner, E. and Sorell, G., "Materials Performance in the EDS Coal Liquefaction Pilot Plant", Materials Performance, Vol. 24, May 1985, pp. 18-24.
11. Kane, R.H., "Corrosion of Commercial High Temperature Alloys in Simulated Coal Gasification Environments", Materials Performance, Vol. 23, No. 10, 1984, pp.9-19.
12. Block, F.R. and Mueller, W. "On the Corrosion of Externally Heated Coal-Gasification Tubes", paper from seminar in the Institute of Central for Heat and Mass Transver, Dubrovnik, Yugoslavia, 1979, pp. 711-719.

13. MacNab, A.J., "Report on Corrosion and Erosion of High Btu Gasifier Components", Metal Progress, November 1977, pp. 44-48.
14. Green, B.N., "Materials Experience at the Synthane Coal Gasification Plant", Corrosion, Paper No. 83, 1979, pp. 83.1-83.15.
15. Barkalow, R.H., Goebel, J.A. and Pettit, F.S., "Design of Materials for Erosion-Hot Corrosion Conditions in Coal Gasification and Coal Combustion Systems", Annual Conference on Mater for Coal Conversion and Utility, published by DOE Washington, D.C., 1978, pp. V.34-V.39.
16. Hill, V.L., "High Temperature Problems in Coal Gasification System", Journal of Metals, Vol. 36, No.8, 1984, pp. 8.
17. Metals Hand Book, "Corrosion", Vol. 13, 9th Ed., 1987.
18. Uhlig, H.H. and Revie, R.W., Corrosion and Corrosion Control, John Wiley & Sons, U.S.A, 1985.
19. Pourbaix, M., Atlas of Electrochemical Equilibria in Aqueous Solutions, Edited. NACE, Pergamon Press, 1974.
20. Pourbaix, M., Lectures on Electrochemical Corrosion, Plenum Press, 1973.
21. Fontana, M.G. and Green, N.D., Corrosion Engineering 2nd edition, McGraw-Hill Book Company, 1978.
22. Sheir, L.L., Corrosion, Vol. 1, 2nd edition, Newnes-Butterworths, London, 1976.

23. Scully, J.C. The Fundamentals of Corrosion, 2nd edition, Pergamon Press, 1975.
24. Green, N.D. "Predicting Behaviour of Corrosion Resistant Alloys by Potentiostatic Polarization Methods", Corrosion, Vol. 18, No. 4, 1962, pp. 136t-142t.
25. Hansen, L.D. and Phillips, L.R. "Analytical Study of the Effluents from a High Temperature Entrained Flow Gasifier", Fuel, Vol. 59, No. 5, 1980, pp. 323-330.
26. "Standard Reference Method for Making Potentiostatic and Potentiodynamic Anodic Polarization Measurements", ASTM Standard G5-82, 1985.
27. Ogundele, G.I., M.Sc. Thesis, "A Study of Some of the Environmental Factors Affecting the Corrosion and Failure of Metallic Orthopaedic Implant Materials", Department of Mechanical Engineering, The University of Calgary, 1980.
28. Stern, M. and Geary, A.L., "Electrochemical Polarization, A Theoretical Analysis of the Shape of Polarization Curves", J. of Electrochem. Soc., Vol. 104, No. 1, 1957, pp. 56-63.
29. Thom, R.M., M.Sc. Thesis, "An Investigation into the Effect of Cathodic Overpotential on Low Strength Steel", Department of Mechanical Engineering, University of Calgary, 1985.

30. Gosta W., An Introduction to Corrosion and Protection of Metals, Butler & Tanner Ltd., London, 1972.
31. Ogundele, G.I., Ph.D. Thesis, "An Electrochemical Study of Corrosion of Carbon Steel in Aqueous Sour Gas Media", Department of Mechanical Engineering, University of Calgary, 1984.
32. West, J.M., Electrodeposition and Corrosion Processes, 2nd ed., Van Nostrand Reinhold Company, London, 1970.
33. Schwabe, K. and Voight, C., Electrochimica Acta, Vol. 14, 1969, pp. 853-869.
34. Condit, D.O., "Effect of the Chloride Ion Concentration the Polarization Behaviour of an Fe-25Ni Alloy", Corrosion, Vol. 28, No. 3, 1972, pp. 95-100.
35. Davies, D.H. and Burstein G.T., "The Effects of Bicarbonate on the Corrosion and Passivation of Iron", Corrosion, Vol. 36, No. 8, 1980, pp. 416-422.
36. Prazak, M., "Evaluation of Corrosion-Resistant Steels Using Potentiostatic Polarization Curves", Corrosion, Vol. 19, No. 3. 1963, pp. 75t-80t.
37. Sheir, L.L., Corrosion, Vol. 2, 2nd edition, Newnes-Butterworths, London, 1976.
38. Vader Voort, G. F., Metallography Principles and Practice, McGraw-Hill Book Company, 1984.
39. Tomashov, N.D., Theory of Corrosion and Protection of Metals, The Macmillan Company, N.Y., 1966.

40. Bockris, J. O'M. and Drazic, D.M., Electrochemical Science, Taylor & Francis Ltd., London, 1972.
41. Petrucci, R.H., "Principles and Modern Applications" General Chemistry, 4th ed., Macmillan Publishing Company, 1985.
42. Bockris, J. O'M., and Reddy, A.K.N., Modern Electrochemistry, Vol. 1, Plenum/Rosetta, N.Y., 1977.
43. Shaw W.J.D., "Electrochemical Corrosion Behaviour of Materials in Simulated Aqueous Coal Gasification Environments"., Final report for Alberta Energy and National Resources Office of Coal Research and Technology, 1988.
44. Wagner, V.C. and Traud, W., Z. Electrochem., Vol. 44, 1938, pp. 391-402.
45. Oldham, K.B. and Mansfeld, F., Corrosion, Vol. 13, 1973, pp. 811.
46. Bockris, J. O'M., and Reddy, A.K.N., Modern Electrochemistry, Vol. 2, Plenum/Rosetta, N.Y., 1977.